Dynamics and Morphological Evolution of Ferrofluid Droplet under the Influence of Magnetic Field

by

Abrar Ahmed

A thesis submitted in partial fulfillment of the requirements for the degree of

Master of Science

Department of Mechanical Engineering

University of Alberta

Abstract

Owing to the spectacular adaptability and unique but non-intuitive shape evolution ability, ferrofluid is leveraged as an alternative for many applications ranging from sealing in bearing to manufacturing and droplet based microfluidics. However, there are numerous unanswered questions and unexplored phenomena in case of ferrofluid droplet dynamics, which are attempted to be addressed in this study. In this thesis, several aspects of drop impact dynamics, maneuvering and an essence of the coalescence behavior of ferrofluid droplet under the influence of magnetic field has been analyzed both theoretically and experimentally. Firstly, we explained the transient variation in morphology of an impinging droplet before and after the impact, which was studied with the presence of magnetic field with various strengths and directions. Through extensive experimental investigation a new phenomenological evidence was observed, where ratio of drop shape parameters before the impact and after the impact with minimal impacting energy remain constant regardless of magnetic field strength and magnetic field direction. We also gave a careful attention on the effect of magnetic field on the generation of satellite droplet during the drop deposition process and its final destination and travel path. Then we identified critical vertically oriented magnetic field, which would govern whether the satellite droplet would merge with the already deposited droplet or not, however under radial magnetic field satellite droplet always retract back to the needle. We also proposed a theoretical model for drop impact dynamics for a magnetically actuated ferrofluid droplet on a solid substrate. We developed a generalized mathematical formulation where the maximum spreading ratio (maximum spreading diameter/initial diameter of the droplet) is a function of numerous nondimensional parameters dictating the inertia, viscous, capillary and magnetic effects which are represented in the form of Weber number, Reynolds number and magnetic Bond number. We also validated this theoretical

statement with comprehensive experimental investigations. Finally, we gave an explanation on the ferrofluid droplet coalescence under the effect of magnetic field, which will give us a complete insight on the application of ferrofluid as a potential element for 3D printing.

Preface

This thesis is an original work by Abrar Ahmed under the supervision of Dr. Prashant Waghmare and co-supervision of Dr. Brian Fleck. A version of the chapter 2 presented in this thesis has been prepared for submission to a peer-reviewed journal (Langmuir) for publication as, "Abrar, A; Brian, A, F; Qureshi, A; Waghmare, P., Dynamics of magneto-wetting with ferrofluids." A version of the chapter 3 of this thesis has been prepared for submission to another peer-reviewed journal (Physics of Fluids) for publication as, "Abrar, A; Brian, A, F; Waghmare, P., Maximum spreading of a ferrofluid droplet under the effect of magnetic field." Abrar Ahmed was responsible for concept formulation, model development, theoretical analysis, experiments, data analysis, results evaluation and the composition of manuscripts. Dr. Waghmare was the primary supervisory author of all the works presented here by Abrar Ahmed and was involved with the concept formulation, theoretical analysis, evaluation and assessment of results, manuscript composition and providing necessary funds. Dr. Fleck was the co-supervisor and associated with the necessary revisions of works, general discussions and providing necessary funds for all the works presented in this thesis by Abrar Ahmed. Dr. Qureshi was associated with the works presented in chapter 2 only through general discussion and providing experimental assistance.

Acknowledgement

First, I want to thank to the one and only Almighty as I am blessed with so many kind hearted and wise people around me, without whom I could not reach this point of my master thesis. Two of the most important people who have done the most to help me get here are my supervisors –Dr. Prashant Waghmare and Dr. Brian Fleck. I show my sincere gratitude and appreciation to Dr. Waghmare for his guidance throughout my entire project – from the development of the experimental setup to the writing of this manuscript. All the knowledge of science, professionalism and punctuality that I gained from him throughout this master program has been invaluable. Dr. Waghmare's excellent cooperation and valuable guidance provided me all the tools that I needed to finish my thesis successfully. I believe that I am fortunate enough to get a chance to work with Dr. Fleck. It is not only for that he is a renowned professor but also for the mental and financial support and inspiration, I got from him. I greatly appreciate both of my supervisors for their wisdom, patience and benevolence.

I would also like to thank all the other members of the interfacial Science and Surface Engineering Lab. I must have to specially thank Dr. Aleksey Baldygin for all of his training and assistance in performing the experiments. Without his assistance, I would not have operated single machine in the lab. I also want to thank Farhad Ismail for his initial guidance and assistance. I am also grateful to the post doctoral fellow Dr Ravi Kant Upadhyay for so many useful discussion during my research. Last but not the least I want to thank Muhammad Rizwanur Rahman for being such a great company in the lab and his valuable comments throughout my research.

I could not have measured the magnetic field without the gaussmeter provided by 'The Shack', a lab in the CCIS. I really appreciate all the generous support and help provided by professor Dr. Mark Freeman and Clayton B. Coutu in the shack. Special thanks go to professor Dr Qureshi, for providing oil based ferrofluid samples. I am also grateful to Dr. Marc Secanell, Dr. Tian Tang, Dr. Ben Jar, Dr. Amit Kumar, Dr. Ru and Dr. Peter Schiavone , as I have gained a lot of knowledge by attending their lectures during my coursework in master. I also want to give a special thanks to my thesis defense committee examiner, Dr. Alexandra Komrakova and the committee chair Dr. Marc Secanell for generously allocating a time slot from their busy schedule for my master defense. I also thank Dr. Chun Il kim for his initial guidance and suggestions.

A special thanks goes out to the support staffs of the department office for all their administrative and technical support throughout my graduate program. They made it easy for me to stay motivated by making cordial interactions almost every day.

To my family, words cannot express how grateful I am to have such wonderful people. I want to give my heartfelt thanks to my parents Selina Ahmed and Tarek Uddin Ahmed; my brother Sabbir Ahmed, sister in law Shaila Ahmed, my niece Anila Nazmi Ahmed (Kashfia) and Sanjana Ferdous, a special one in my life. Their support and encouragement have allowed me to aim high, knowing there is someone to catch me if I fall.

Table of Contents

List of Figures

List of Tables

1 Introduction

Ferrofluid, a complex fluid, is extremely popular in state of the art research due to its unique non intuitive response under the effect of magnetic field. For centuries, it was believed that magnetism is a property of solid materials [1]. However, that longer lasting belief was proved to be wrong when ferrofluid was first synthesized in 1965 at NASA's Lewis Research Center patented by Papell[2]. Owing to the definition given by Rosenweig[3], Ferrofluid mainly consists of ferromagnetic particles with a mean diameter of 10 nm where particles are suspended in a carrier liquid and undergoes translational and rotational motion due to the thermal Brownian motion. In order to stabilize and prevent agglomeration under magnetic field, the ferrous nano-particles are coated with surfactant or dispersing agent. Generally, the suspended ferrous particles in ferrfofluids can be considered as an ensemble of individual atoms with its own magnetic moment[3,4]. These atomic-scale magnets are placed arbitrarily in the suspension and inherent thermal energy, which is sufficient to randomize their orientation. Hence, without the application of magnetic field the ferrofluid droplet behaves as a regular droplet with no magnetization. However, when an external magnetic field is applied, the atomic magnetic moments reorient themselves along the magnetic field direction, resulting in a small net magnetization and susceptibility. As the applied field is increased, the net magnetization increases in-line with the external field which results in bulk motion of fluid towards or opposite to the magnetic field, resulting the deformation of interface or bulk fluid drop. Depending on the carrier liquid, ferrofluids are of two types; water-based ferrofluids which are diamagnetic in nature and oil based ferrofluids which are paramagnetic in nature. When an external magnetic field is applied, some of the atomic magnetic moments inside the paramagnetic fluid

rotate and align themselves along the field direction whereas for diamagnetic fluids the atomic moments are aligned themselves opposite to the magnetic field direction[5].

1.1 Application

The precise control of ferrofluid with unique response under the effect of magnetic field allowed to be considered for numerous application. An earlier application of ferrofluid was the sealing of rotating shaft for a dust free operations[6]. In case of in machine tool industry, ferrofluidic seal can maintain longer bearing life by providing a barrier between cutting fluid containing machined particulate debris and the circulating lubricating oil inside the bearing[7]. Viscoelastic ferrofluid [8] can work as an inertia damper by which it can improve the dynamic response of a system by suppressing the unwanted oscillation. Another common application of ferrofluid is in lubrication[9], due the low cost manufacturing, less noise and self-sealing ability.

At microscale, interesting application of ferrofluid is in the form of pumps and actuators. By manipulating the temperature and magnetic field gradients ferrofluid can be driven in a microfluidic channel without the application of any passive actuation [10, 11] .Thus the contamination during the handling of microfluidic sample can be minimized[10] as well as the fluid flow under microgravity can be obtained [11]. Paper impregnated with ferrofluid is used for the excitation of cantilever through DC or AC magnetic field which has a potential applications in manipulations of soft biological samples.[12].

Due to the significant transparency of ferrofluid, ferrofluidic sensor can be used to measure the intensity of magnetic field with great sensitivity[13]. Capillary tube filled with magnetic fluid can also be used as a magnetic field sensing device which lays a solid foundation for photonic sensing device[14]. With the ferrofluid an ultrasensitive optical sensor has already been developed which

produces visually perceptible color images to detect the presence of ammonia in parts per million level[15]. With proper manipulation of ferrofluid by magnetic field, ferrofluid immersed in a non magnetic fluid can be separated from that fluid. This technique has been proposed for oil spill clean-up from the ocean[16]. Most recently, ferrofluids have been used in the development of digital electronics as well as lab-on-a-chip platforms, with AND, OR, XOR, NOT and NAND logic gates operations by merely coupling magnetic and hydrodynamic forces on the droplets[17]. This ferrofluid-based lab on a chip platform, influenced by rotating magnetic field poses an error free physical computation due to synchronous propagation of ferrofluid through logic gates, which was previously not possible with a low-Reynolds-number driven droplet hydrodynamics.

Another potential, perhaps one of the most novel applications of ferrofluid is in the field of biomedical science. Owing to the dynamic response of ferrofluid under the effect of magnetic field, the drug delivery system has revolutionized alternatives. Lubbe et al. [18] first reported on the application of ferrofluids in tumor healing where anticancer drug tagged with ferrofluid is guided to the locally advanced tumor. Later on Alexiou et al.[19] successfully delivered an anticancer agents bounded by biocompatible ferrofluids in the area of hind limb of a tumor bearing rabbit without any negative side effects, for example leukocytopenia or gastrointestinal disorders. .

1.2 Aim of the Present Work

So far minimal attention has been given to the use of ferrofluid for the 3D printing based application. Ferrofluid might be a potential source for 3D printing of metal objects which can also resolve some issues regarding metal based 3D printing. For instance, during the fabrication of complex 3D structures through laser induced forward transfer (LIFT) method, the undesired

droplet spreading results in the shape distortion i.e., both the excessive or insufficient spreading of the droplet may produce distorted or porous object [20]. It was also observed that the printing quality was reduced due to the formation of shape irregularities caused by larger droplet spreading, in case of LIFT 3D printing method[21,22]. In addition, Delft Lohse et al.[23] also reported the contamination of impact surface due to the deposition of satellite droplet around the main droplet. In this study we have presented a detailed study on the role of magnetic field on the formation of a satellite droplet and its trajectory as it lands on the substrate. Therefore, in case of metal 3D printing with ferrofluid, a comprehensive investigation of spreading dynamics and manipulation of ferrofluids under the effect of magnetic field is of great importance to solve the issues regarding shape distortion due to droplet spreading. However, according to our best knowledge a comprehensive study on the shape morphology and transient evolution of an impinging ferrofluid droplet is yet to be performed which have investigated in the present study.

It is also crucial to realize that impinging phenomenon is influenced by magnetic field. During 3D printing of metal object through LIFT process researchers have already encountered various metal droplet shape such as, sphere, ellipsoid, disk and toroid (at maximum spread) which corresponds to whole droplet impact scenario. The knowledge of those droplet shapes is of greater importance while solidifying droplet for metal 3D printing since manipulating droplets with different shapes ultimately facilitate to optimize the drop-to-drop contact area and adhesion. Therefore, investigation of maximum spreading of a magnetic fluid droplet under the influence of magnetic field is one of the priority for understanding the basic physics of the 3-D printing of the magnetic material. Despite being abundance of modelling approaches in the field of maximum droplet interestingly the detailed theoretical modeling for ferrofluid droplet impact scenario in the presence of magnetic field where droplet is missing from the literature. In this work, we have

also proposed a detailed generalized modelling approach that not only characterize the maximum spread but also suggest the optimized parameters for maximum spread. The detailed experimental study is performed to validate and tune the theoretical model. Finally, the obtained knowledge from drop impact studies is implemented to study the realistic 3-D printing sensation by studying the preliminary droplet coalescence studies.

1.3 Literature Review

In this thesis, our primary concern is the ferrofluid droplet impact phenomena under the effect of magnetic field. That is why the whole literature review is divided into two sections: droplet impact phenomenon and effect of magnetic field on the ferrofluid droplet.

1.3.1 Droplet Impact Phenomenon

This section will summarize the available literatures related to impact dynamics of an impinging droplet. Many researchers studied drop impact phenomenon from all three aspects of research: theoretical[24-36], numerical[37-43] and experimental[24-36]. The underlying foundation of the dynamics of droplet impact process was first proposed by Worthington[24] who showed deformation of a large milk droplet falling vertically on a horizontal plate (carbon soot coated). In impact dynamics most of the focus is concentrated on a dimensionless parameter, maximum spreading factor denoted as $\xi_{max} = \frac{D_{max}}{D_0}$ [25]; where D_{max} is the measured maximum spreading diameter and D_0 is the initial droplet diameter before impact . In general, the mathematical expression of ξ_{max} is a function of Weber number (We), Reunolds number (Re) and Ohnesorge number(Oh) which can be defined as ; $\mathrm{Re} = \frac{\text{Inertial force}}{\text{Viscous force}} = \frac{\rho v D}{\mu}$; $\mathrm{We} = \frac{\text{Inertial force}}{\text{Interfacial tension}} = \frac{\rho D v^2}{\gamma}$ and $\mathrm{Oh} = \frac{\sqrt{We}}{Re}$; where ρ, v, D, μ, γ denote the density, velocity, characteristics length, viscosity and the surface tension of the liquid, respectively. However, most of the approaches are based upon the energy balance between kinetic

energy, surface energy and viscous dissipation during spreading. Adopting the concept of energy balance, Chandra et al[26] proposed that $\xi_{max} = \sqrt{\frac{1}{3}We + 4}$ for large Re (≥2300) with an laminar flow viscous dissipation. Pasandideh-Fard et al. presented a comprehensive theoretical model based on droplet impacting on a solid surface where they obtained a simple expression for maximum spreading factor, $\xi_{max} = \sqrt{\frac{We+12}{3(1-\cos\theta)+4(We/\sqrt{Re})}}$. It was also reported that if $We \gg \sqrt{Re}$, the capillary can be considered negligible. In that study they experimentally observed that though the shape of a droplet fused with surfactant did not change during the initial stages of impact, the maximum spreading diameter and the recoiling height of the droplet increasing and decreasing, respectively. Later on, Mao et al.[27] amended the mathematical modelling proposed by Pasandideh et al. in order to minimize the error from the experimental measurement and developed a semi empirical droplet impact model where a theoretical expression for viscous dissipation was proposed for high viscous and low viscous fluids. Besides developing model for maximum spreading Mao et al. also developed a rebound model which could successfully predict the tendency of a droplet to rebound. Clanet et al.[28] reported two different scaling law for two different regime where $\xi_{max} \propto \sqrt{We}$ in the capillary region and $\xi_{max} \propto Re^{\frac{1}{5}}$ in the viscous regime. Most recently, Yonemoto and Kunugi[29] presented a theoretical model which can predict the transition point from capillary regime to viscous regime. So far, this theoretical model shows the better agreement with the experimental results regardless of low or high We. In this model instead of considering either static or dynamic contact angle, authors have considered the average of static and dynamic contact angle instead. Surface properties significantly affect the droplet impact dynamics, which includes overall spreading, rebound or splashing. Renardy et al.[30] observed that on a superhydrophobic surface the water droplet can experience bouncing even at very low (We<1)

impact speed. In case of textured surface, the overall impact dynamics of the droplet can be controlled by varying the wettability of the solid surface. Maximum spreading diameter or the recoiling stage of the droplet upon impact depend whether the liquid droplet penetrates the textured surface (the Wenzel state) or slides over the structures (the Cassie-Baxter state)[31,32,33]. Antkowiak et al. [34] and Piroird et al.[35] reported complex rebound phenomenon on elastic membranes and fibers respectively. Shen et al.[36] observed the rapid bouncing off a droplet on a dome convex superhydrophobic surface with a 28.5% reduction in contact time compared with that on conventional flat superhydrophobic surface. Besides, theoretical and experimental investigation a considerable amount of efforts are devoted to numerical studies for same purpose i.e., to quantify maximal deformation of droplet. Detailed studies have been performed on maximum droplet spreading through several numerical schemes such as; finite difference[37 38 39], finite element [40] and volume of fluid method [40, 41 42 43].

1.3.2 Magnetic Fluids and Droplet Dynamics

In this section of literature review we will discuss about the available literature on the maneuvering and deformation of ferrofluid droplet under the effect of magnetic field. Droplet shape deformation and controlled manipulation of liquid droplet is of greater importance in terms of droplet-based microfluidics. Egatz et al.[44] demonstrated a method to control the movement of a water drop containing fractions of paramagnetic particles on a superhydrophobic surface using a permanent magnet where the role of particle concentration, in relation with magnetic field, while controlling the drop motion is studied in details. Later on, the similar concept of drop actuation was implemented detecting H5N1 virus in a throat swab sample by using magnetic forces [45]. Several numerical studies have already been conducted for ferrofluid droplet shape deformation under the effect of magnetic field. Korlie et al.[46] adopted a volume of fluid scheme to numerically model a

falling ferrofluid droplet inside a nonmagnetic liquid medium at uniform magnetic field. Afkhami et al. [47] also developed a volume of fluid scheme to investigate the deformation of a PDMS ferrofluid droplet suspended in a glycerol medium and compared with experimental data. However, at higher magnetic field their computed drop shape does not agree with experimental observation when surface tension is assumed constant.

Nguyen et al. [48] experimentally investigated the controlled motion of a sessile water based ferrofluid droplets under the effect of vertical magnetic field created by a permanent magnet as shown in figure 1-1. In another study, they have also showed a comparison between experimental and numerical results where both models confirmed with the nonlinear deformation of a water based sessile ferrofluid droplet in a uniform magnetic field [49]. Recently Selin and Marius[4] have compared the wetting behavior of oil based ferrofluid and water based magnetic paint in terms of change of geometrical parameter with respect to magnetic field on a hydrophobic flat surface. Further Rigoni et al. [50] also studied the morphological evolution of water based sessile ferrofluid droplet base and height with respect to magnetic field at various droplet concentration and magnets of various size and strengths. Very recently Zhou et al. [51] developed a mathematical model to predict the maximum spreading of liquid metal drops when impacting onto dry surfaces under the influence of a vertical magnetic field. This model covers a wide range of impact speeds, contact angles and magnetic strengths in terms of numerical analysis; however, no experimental investigation has been presented to demonstrate the validation of the theoretical modelling.. Chen and Cheng [52] experimentally investigated on Rosenweig instabilities [3] where the breaking pattern of subscale droplets can be characterized by a dimensionless magnetic Bond number [53]. Timonen et al. [54] reported about the breakup of a sessile parent droplet into two sister droplets and also demonstrated the break up droplet occurs under oscillating magnetic field as shown in figure 1-2.

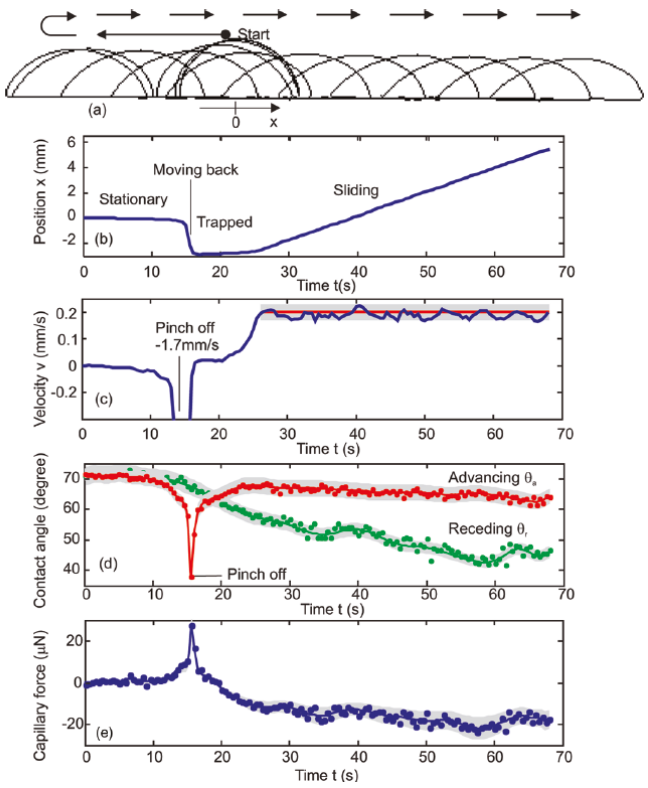

Figure 1-1.sliding of a sessile ferrofluid droplet in the presence of a moving permanent magnet (H = 2 mm, D = 3 mm, B = 64 mT, v = 0.2 mm/s, and a ≈ 2.22 mm): (a) Evolution of the tracked droplet (every 10 frames). (b) Displacement of the droplet centroid versus time. (c) Velocity of the droplet versus time. The constant velocity of 0.2 mm/s is plotted as the redline (d) Contact angles versus time. The confidence interval is (4%. (e) Capillary force versus p time. "Reprinted (adapted) with permission from (Nguyen, N. T.; Zhu, G.; Chua, Y. C.; Phan, V. N.; Tan, S. H. Magnetowetting and sliding motion of a sessile ferrofluid droplet in the presence of a permanent magnet. **Langmuir 2010, 26 (15), 12553–12559.). Copyright (2010) American Chemical Society."**

Korovin[55] mathematically represented that in the presence of a horizontal magnetic field , a much stronger external vertical magnetic field is required for the emergence of the Rosensweig instability[3] of the free surface of the nonlinearly magnetizable ferrofluid than in the case of a strictly vertical field. Many researchers also address formation of satellite droplets during drop detachment from the needle. R. Li [56] in his thesis work discussed about the formation of satellite droplet under electric field where at the role of higher working voltage on satellite droplet

formation during inkjet printing is studied. Xiao et al. [57] experimentally investigated the dynamics of satellite droplets under vertical upward and vertical downward magnetic field. They showed the shape evolution of satellite droplet of an oil based ferrofluid under vertical magnetic field.

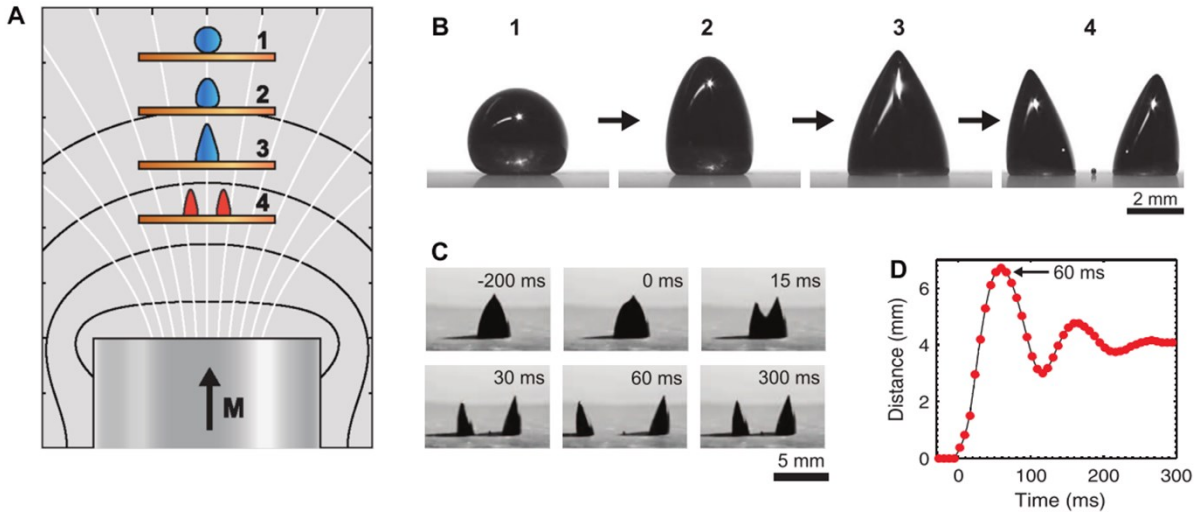

Figure 1-2. Magnetically triggered ferrofluid droplet division on a superhydrophobic surface. (A) Schematic side-view of the magnetic field geometry of a cylindrical permanent magnet (white lines, magnetic field; black lines, constant field contours). State of the droplet is indicated as follows: 1, near-zero field (nearly spherical droplet); 2, weak field (slightly deformed droplet); 3, strong field (conical spiked droplet); and 4, above critical field (two daughter droplets). (B) Photographs of a 20-ml ferrofluid droplet upon increasing the field from 80 Oe (dH/dz 3.5 Oe/mm) to 680 Oe (dH/dz 66 Oe/mm). Notice the small asymmetry in daughter droplet sizes and the small satellite droplet between the two . (C)Frames of a high-speed video of the division)and (D) the corresponding distance between the daughter droplets as a function of time, approaching the distance determined by static self-assembly. **"From Reference 50 and Reprinted with permission from AAAS."**

1.4 Thesis Outline

In this section, the thesis structure and topics covered in the subsequent chapters are discussed

This thesis is focused on the fundamental physics underlying 3D printing using ferrofluid liquids

which involves the study of droplet formation, deposition, spreading, coalescing and solidification. Therefore, in this thesis we tried to explain the effect of magnetic field on the droplet shape deformation and droplet impact both mathematically and experimentally. However, for the sake of completeness we also shed a light on the coalescence behavior of ferrofluid droplet under the effect of magnetic field.

In chapter 2, we have presented a comprehensive experimental investigation of the dynamics of a paramagnetic oil based ferrofluid which included the droplet shape deformation before and after the impingement over time while the droplet is under the influence of magnetic field. We also showed a comparative study between the ferrofluid droplet deformation under vertical and radial magnetic field. Subsequently, a new phenomenological evidence is presented that the ratio of the drop shape parameters before an impact and after the impact remains constant. At the later section of this chapter we also presented the influence of magnetic field on the satellite droplet formation during the droplet deposition from the needle.

In chapter 3, theoretical model for ferrofluid droplet impingement under the influence of magnetic field is developed. Here we presented the maximum spreading ratio as function of three dimensionless numbers such as; magnetic Bond number, Weber number and Reynold's number. The proposed model is also validated with experiments that are performed for wide range of nondimensional parameters.

The final chapter draws the conclusion of the whole thesis work with a brief discussion about the merging of ferrofluid droplet under the effect of magnetic field, which is next natural choice to extend this study in relation with the 3D printing application. However, this concept of ferrofluid droplet coalesce has been kept as a future recommendations as it is one of the inevitable stages of 3D printing.

References

(1) Speight, J. G. A Review of:"Magnetic Fluids Guidebook: Properties and Applications" By VE Fertman Hemisphere Publishing Corporation Bristol, PA 19007-1598 1990, xi+ 146 pp. Fuel Sci. Technol. Int. **1991**, 9 (3), 399.

(2) Papell, S. S.; Otto, C. F. J. Influience of nouniform magnetic fields on ferromagntic colloidal sols. J. Chem. Inf. Model. **1968**, 53 (9), 1689–1699.

(3) Rosensweig, R. E. Ferrohydrodynamics; 1997; Vol. 1.

(4) Manukyan, S.; Schneider, M. Experimental Investigation of Wetting with Magnetic Fluids. Langmuir **2016**.

(5) Krishnan, K. M. Fundamentals and applications of magnetic materials; Oxford University Press, 2016.

(6) Raj, K.; Moskowitz, R. Commercial applications of ferrofluids. J. Magn. Magn. Mater. **1990**, 85, 233–245.

(7) Raj, K.; Moskowitz, R. Commercial applications of ferrofluids. J. Magn. Magn. Mater. **1990**, 85 (1–3), 233–245.

(8) Schlaich, J.; Bergermann, R.; Schiel, W.; Weinrebe, G. Design of Commercial Solar Updraft Tower Systems – Utilization of Solar Induced Convective Flows for Power Generation. 49 (711), 1–9.

(9) Ochonski, W. The attraction of ferrofluid bearinos. Mach. Des. **2005**, 77 (21), 96–102.

(10) Pal, S.; Datta, A.; Sen, S.; Mukhopdhyay, A.; Bandopadhyay, K.; Ganguly, R. Characterization of a ferrofluid-based thermomagnetic pump for microfluidic applications. J. Magn. Magn. Mater. **2011**, 323 (21), 2701–2709.

(11) Odenbach, S. Microgravity experiments on thermomagnetic convection in magnetic fluids. J. Magn. Magn. Mater. **1995**, 149 (1–2), 155–157.

(12) Ding, Z.; Wei, P.; Chitnis, G.; Ziaie, B. Ferrofluid-impregnated paper actuators. J. Microelectromechanical Syst. **2011**, 20 (1), 59–64.

(13) Nair, S. S.; Rajesh, S.; Abraham, V. S.; Anantharaman, M. R. Ferrofluid thin films as optical gaussmeters proposed for field and magnetic moment sensing. Bull. Mater. Sci. **2011**, 34 (2), 245–249.

(14) Ji, H.; Pu, S.; Wang, X.; Yu, G.; Wang, N.; Wang, H. Magnetic field sensing based on capillary filled with magnetic fluids. Appl. Opt. **2012**, 51 (27), 6528–6538.

(15) Mahendran, V.; Philip, J. An optical technique for fast and ultrasensitive detection of ammonia using magnetic nanofluids. Appl. Phys. Lett. **2013**, 102 (6), 63107.

(16) Khushrushahi, S.; Zahn, M.; Hatton, T. A. Magnetic separation method for oil spill cleanup. Magnetohydrodyn. **2013**, 49.

(17) Katsikis, G.; Cybulski, J. S.; Prakash, M. Synchronous universal droplet logic and control. Nat. Phys. **2015**, 11 (7), 588–596.

(18) Lübbe, A. S.; Bergemann, C.; Riess, H.; Lãbbe, A. S.; Schriever, F.; Reichardt, P.; Possinger, K.; Matthias, M.; Dã, B.; Herrinann, F.; et al. Clinical Experiences with Magnetic Drug Targeting: A Phase I Study with 4′-Epidoxorubicin in 14 Patients with Advanced Solid

Tumors in 14 Patients with Advanced Solid Tumors. Cancer Res. **1996**, 56, 4686–4693.

(19) Alexiou, C.; Schmid, R.; Jurgons, R.; Bergemann, C. Targeted Tumor Therapy with " Magnetic Drug Targeting ": Therapeutic Efficacy of Ferrofluid Bound Mitoxantrone. Lect. Notes Phys. **2002**, 594, 233–251.

(20) Visser, C. W.; Pohl, R.; Sun, C.; Römer, G.-W.; in't Veld, B.; Lohse, D. Toward 3D printing of pure metals by laser-induced forward transfer. Adv. Mater. **2015**, 27 (27), 4087–4092.

(21) Zenou, M.; Sa'ar, A.; Kotler, Z. Digital laser printing of aluminum micro-structure on thermally sensitive substrates. J. Phys. D. Appl. Phys. **2015**, 48 (20), 205303.

(22) Zenou, M.; Sa'Ar, A.; Kotler, Z. Supersonic laser-induced jetting of aluminum micro-droplets. Appl. Phys. Lett. **2015**, 106 (18).

(23) Visser, C. W.; Pohl, R.; Sun, C.; Römer, G. W.; Huis In 'T Veld, B.; Lohse, D. Toward 3D Printing of Pure Metals by Laser-Induced Forward Transfer. Adv. Mater. **2015**, 27 (27), 4087–4092.

(24) Worthington, A. M. A Second Paper on the Forms Assumed by Drops of Liquids Falling Vertically on a Horizontal Plate. Proc. R. Soc. London **1876**, 25 (171–178), 498–503.

(25) Pasandideh-fard, M.; Qiao, Y. M.; Chandra, S.; Mostaghimi, J. Capillary effects during droplet impact on a solid surface. Cit. Phys. Fluids **1996**, 8.

(26) Chandra, S.; Avedisian, C. T. The collision of a droplet with a solid surface. Phys. Fluids A Fluid Dyn. **1990**, 2 (9), 1525.

(27) Mao, T.; Kuhn, D. C. S.; Tran, H. Spread and Rebound of Liquid Droplets upon Impact on Flat Surfaces. **1997**, 4 (9), 2169–2179.

(28) Clanet, C.; Béguin, C.; Richard, D.; Quéré, D. Maximal deformation of an impacting drop. J. Fluid Mech. **2004**, 517, 199–208.

(29) Yonemoto, Y.; Kunugi, T. Analytical consideration of liquid droplet impingement on solid surfaces. Sci. Rep. **2017**, 7.

(30) Renardy, Y.; Popinet, S.; Duchemin, L.; Renardy, M.; Zaleski, S.; Josserand, C.; Drumright-Clarke, M. A.; Richard, D.; Clanet, C.; Quéré, D. Pyramidal and toroidal water drops after impact on a solid surface. J. Fluid Mech. **2003**, 484, 69–83.

(31) Bartolo, D.; Bouamrirene, F.; Verneuil, E.; Buguin, A.; Silberzan, P.; Moulinet, S. Bouncing or sticky droplets: Impalement transitions on superhydrophobic micropatterned surfaces. EPL (Europhysics Lett. **2006**, 74 (2), 299.

(32) Kwon, D. H.; Huh, H. K.; Lee, S. J. Wetting state and maximum spreading factor of microdroplets impacting on superhydrophobic textured surfaces with anisotropic arrays of pillars. Exp. Fluids **2013**, 54 (7), 1576.

(33) Maitra, T.; Tiwari, M. K.; Antonini, C.; Schoch, P.; Jung, S.; Eberle, P.; Poulikakos, D. On the nanoengineering of superhydrophobic and impalement resistant surface textures below the freezing temperature. Nano Lett. **2013**, 14 (1), 172–182.

(34) Antkowiak, A.; Audoly, B.; Josserand, C.; Neukirch, S.; Rivetti, M. Instant fabrication and selection of folded structures using drop impact. Proc. Natl. Acad. Sci. **2011**, 108 (26), 10400–10404.

(35) Piroird, K.; Clanet, C.; Lorenceau, É.; Quéré, D. Drops impacting inclined fibers. J. Colloid Interface Sci. **2009**, 334 (1), 70–74.

(36) Shen, Y.; Liu, S.; Zhu, C.; Tao, J.; Chen, Z.; Tao, H.; Pan, L.; Wang, G.; Wang, T. Bouncing dynamics of impact droplets on the convex superhydrophobic surfaces. Appl. Phys. Lett. **2017**, 110 (22), 221601.

(37) Harlow, F. H.; Shannon, J. P. The splash of a liquid drop. J. Appl. Phys. **1967**, 38 (10), 3855–3866.

(38) Tsurutani, K.; Yao, M.; Senda, J.; Fujimoto, H. Numerical analysis of the deformation process of a droplet impinging upon a wall. JSME Int. journal. Ser. 2, Fluids Eng. heat Transf. power, Combust. Thermophys. Prop. **1990**, 33 (3), 555–561.

(39) Watanabe, T.; Kuribayashi, I.; Honda, T.; Kanzawa, A. Deformation and solidification of a droplet on a cold substrate. Chem. Eng. Sci. **1992**, 47 (12), 3059–3065.

(40) Fukai, J.; Zhao, Z.; Poulikakos, D.; Megaridis, C. M.; Miyatake, O. Modeling of the deformation of a liquid droplet impinging upon a flat surface. Phys. Fluids A Fluid Dyn. **1993**, 5 (11), 2588–2599.

(41) Pasandideh-Fard, M.; Mostaghimi, J. Deformation and solidification of molten particles on a substrate in thermal plasma spraying; 1994.

(42) Trapaga, G.; Szekely, J. Mathematical modeling of the isothermal impingement of liquid droplets in spraying processes. Metall. Mater. Trans. B **1991**, 22 (6), 901–914.

(43) Trapaga, G.; Matthys, E. F.; Valencia, J. J.; Szekely, J. Fluid flow, heat transfer, and solidification of molten metal droplets impinging on substrates: comparison of numerical and experimental results. Metall. Trans. B **1992**, 23 (6), 701–718.

(44) Egatz-Gómez, A.; Melle, S.; García, A. A.; Lindsay, S. A.; MárquezP Domínguez-García,

M.; RubioS T Picraux, M. A.; Taraci, J. L.; Clement, T.; YangMark Hayes, D. A.; Gust, D.; et al. Discrete magnetic microfluidics. Cit. Appl. Phys. Lett **2006**, 89 (34106).

(45) Pipper, J.; Inoue, M.; Ng, L. F.-P.; Neuzil, P.; Zhang, Y.; Novak, L. Catching bird flu in a droplet. Nat. Med. **2007**, 13 (10), 1259–1263.

(46) Korlie, M. S.; Mukherjee, A.; Nita, B. G.; Stevens, J. G.; Trubatch, A. D.; Yecko, P. Modeling bubbles and droplets in magnetic fluids. J. Phys. Condens. Matter **2008**, 20 (20), 204143.

(47) Afkhami, S.; Tyler, A. J.; Renardy, Y.; Renardy, M.; St. Pierre, T. G.; Woodward, R. C.; Riffle, J. S. Deformation of a hydrophobic ferrofluid droplet suspended in a viscous medium under uniform magnetic fields. J. Fluid Mech. **2010**, 663, 358–384.

(48) Nguyen, N. T.; Zhu, G.; Chua, Y. C.; Phan, V. N.; Tan, S. H. Magnetowetting and sliding motion of a sessile ferrofluid droplet in the presence of a permanent magnet. Langmuir **2010**, 26 (15), 12553–12559.

(49) Zhu, G. P.; Nguyen, N. T.; Ramanujan, R. V.; Huang, X. Y. Nonlinear deformation of a ferrofluid droplet in a uniform magnetic field. Langmuir **2011**.

(50) Rigoni, C.; Pierno, M.; Mistura, G.; Talbot, D.; Massart, R.; Bacri, J. C.; Abou-Hassan, A. Static Magnetowetting of Ferrofluid Drops. Langmuir **2016**.

(51) Zhang, J.; Han, T.-Y.; Yang, J.-C.; Ni, M.-J. On the spreading of impacting drops under the influence of a vertical magnetic field. J. Fluid Mech **2016**, 809.

(52) Chen, C.-Y.; Cheng, Z.-Y. An experimental study on Rosensweig instability of a ferrofluid droplet. Cit. Phys. Fluids **2008**, 20.

(53) Chen, C. Y.; Cheng, Z. Y. An experimental study on Rosensweig instability of a ferrofluid droplet. Phys. Fluids **2008**, 20 (5).

(54) Timonen, J. V. I.; Latikka, M.; Leibler, L.; Ras, Robin H A; Ikkala, O. Switchable Static and Dynamic Self-Assembly of Magnetic Droplets on Superhydrophobic Surfaces. Science (80-.). **2009**, 325 (5939), 419–422.

(55) Korovin, V. M. On the influence of a horizontal magnetic field on the Rosensweig instability of a nonlinear magnetizable ferrofluid. Tech. Phys. **2014**, 59 (11), 1577–1584.

(56) Li, R. I. Droplet deposition in solid Ink. **2008**, 249.

(57) Jiang, X. F.; Wu, Y. N.; Ma, Y.; Li, H. Z. Formation and breakup dynamics of ferrofluid drops. Chem. Eng. Res. Des. **2016**, 115, 262–269.

2 Dynamics of Magnetowetting with Ferrofluids

2.1 Abstract

This chapter reports on a comprehensive experimental study of the effects of vertically and radially applied magnetic fields on the dynamics of magnetowetting and the formation of satellite droplet. Besides explaining the physics of the transient variation of different drop shape parameters, the role of a magnetic field on controlling the dynamics of spreading is also presented. Ultimately, the magnetic field maneuvers the droplet spreading without altering the surface chemistry. The morphological evolution and dynamics of an impacting ferrofluid droplet has also been briefly studied. By observing the spreading at an appropriate time scale, the contrary spreading behavior of the paramagnetic ferrofluid under the effect of vertically and radially oriented magnetic field, is noticed. Special attention has been given to the droplet break-up and satellite droplet formation. New phenomenological evidence is presented that the ratio of the drop shape parameters before an impact and after the impact remains constant. The destination and travel path of the satellite droplet is analyzed in a critical vertically-oriented magnetic field, which governs the satellite droplet merging with the already deposited parent droplet. On the other hand, under a radial magnetic field, the satellite droplet always returns to the dosing unit.

2.2 Introduction

Ferrofluid is a smart fluid, increasingly popular since it was first synthesized in 1965[1]. The unique, non-intuitive response of these fluids, to magnetic field has been leveraged for numerous applications from sealing rotating shafts for dust-free operation[2] to isolating or delivering biomolecules at targeted locations[3, 4, 5]. Ferrofluid is renowned for its application in cancer treatment; an anticancer drug tagged with ferrofluid is guided to the locally advanced tumor[3].

Ferrofluids are also promising alternatives to restrict undesirable vibrations and to reduce the size of heat exchangers[6]. Most recently, ferrofluids have been used in the development of digital electronics as well as lab-on-a-chip platforms, with AND, OR, XOR, NOT and NAND logic gates operations by merely coupling magnetic and hydrodynamic forces on the droplets[7]. Another potential application of ferrofluid can be in 3D printing which has become burgeoning area of research due to its simplicity and adaptability to numerous complex shape requirements[8]. In 3D printing of metal, shape distortion of metal object is dictated by the droplet spreading dynamics during the laser induced curing[9]. It was concluded that both excessive and insufficient spreading of droplets would produce distorted or porous objects. Metal droplet spreading is one of the key parameters in the lateral resolution in 3D printing[10]. Droplet spreading during 3D printing therefore requires careful attention. Larger droplet spreading due to supersonic velocity in laser-induced forward transfer 3D printing allows the formation of shape irregularities that reduce the printing quality[11]. Therefore, during the metal 3D printing process, if the droplet spreading can be controlled through the application of an external force, the shape distortion can be resolved. In case of 3D printing with ferrofluids in presence of magnetic field, it is paramount to investigate the spreading of the deposited fluid in the presence of a magnetic field. Therefore, this chapter reports on three processes: 1. the dynamics of magnetowetting with ferrofluids while focusing on the control of ferrofluid droplet spreading; 2. the satellite droplet formation and 3.the morphological evolution of ferrofluid droplets under a magnetic field, which is an inevitable process in 3D printing application.

The generation, deformation and interaction of these droplets, on a given substrate, under magnetic fields, are intriguing phenomena. While investigating such aspects, considerable efforts are devoted to magnetowetting[8, 12, 13, 14], droplet spreading[15] and the manipulation of droplet

movement[12, 16, 17]. Egatz et al.[16] demonstrated a method to control the movement of a water drop containing fractions of paramagnetic particles on a superhydrophobic surface using a permanent magnet. In that same literature, the role of particle concentration, in relation to the magnetic field, while controlling the drop motion is studied in greater details. A similar method was borrowed to detect the H5N1 virus in a throat swab sample by using magnetic forces[18]. Nguyen et al.[12] experimentally investigated the magnetowetting characteristics of water-based sessile ferrofluid droplets under a vertical magnetic field created by a permanent magnet for sliding droplet motion. Recently, Selin and Marius[8] compared the wetting behavior of oil-based ferrofluid and water-based magnetic paint in terms of the change in geometrical parameters with respect to magnetic field on a hydrophobic flat surface.

To the best of our knowledge, although many studies are devoted to the equilibrium wettability of sessile ferrofluid droplet, the dynamics of droplet spreading while impinging on a substrate, in the presence of magnetic field, have not been published yet. This dynamic spreading is crucial to the final configuration of a drop and will decide the optimum operating parameters to obtain a desirable drop shape for a designed outcome. We studied the dynamics of a paramagnetic ferrofluid droplet under radial and vertical magnetic field. This study is not limited to the spreading of sessile ferrofluid droplet but investigates the droplet deposition and detachment of a drop from the needle, particularly the formation of satellite droplets and the consequences of this formation. First, we compared oil-based ferrofluid droplet spreading under both vertical and radial magnetic field. The dynamics of spreading is represented in terms of transient variations in the droplet base diameter, height and contact angle with respect to magnetic fields of various strengths. The morphological evolution of droplets before impingement in terms of direction of magnetic field is discussed to comment on the importance of the wetting and interfacial forces. Based on this

preliminary understanding, the control parameters for desired spreading and drop shape are proposed in terms of empirical relationships. For the sake of completeness, the entire cycle is discussed, from drop detachment to the attainment of equilibrium and the formation of satellite droplets during the drop pinched off from the needle or nozzle. Finally, the role of the magnetic field on the formation of a satellite droplet and its trajectory as it lands on the substrate are also investigated.

2.3 Materials and Methods

2.3.1 Ferrofluid

The ferrofluid used in this work is an oil-based ferrofluid (EFH-1 type ferrofluid) purchased from Ferrotec (USA Corp.), which is a colloidal suspension of magnetite particles (Fe_3O_4, 3-15% by volume) of 10nm in diameter in light hydro carbon oil (55-91 % by volume) with oil soluble dispersant (6-30% by volume). The saturation magnetization and initial magnetic susceptibility of that fluid is 6mT (mili - Tesla) and 2.64, respectively whereas viscosity and density of that fluid is 6 mPa. s (mili-pascal-second) and $1.21 \times 10^3 \frac{\text{kg}}{\text{m}^3}$, respectively. The surface tension of the EFH-1 ferrofluid was found to be 24.56 ± 0.04 mN/m, measured with a force tensiometer (K-100 from KRÜSS GmbH). Considering these thermo-physical properties, the capillary length, l, of the ferrofluid is ~1.5mm, which can be considered the critical radius with the critical Bond number, $\text{Bo}_{\text{cr}} = \frac{\rho g R_{\text{cr}}^2}{\gamma}$ [19], where $\rho, g, \gamma \; and \; R_{cr}$ imply the density , gravitational acceleration, interfacial tension and critical length of the ferrofluid droplet respectively. In order to maintain the Bo_{cr} below unity, the diameter for the ferrofluid droplet was chosen appropriately to circumvent unwarranted effects. It is to be noted that all the properties given in this section was measured in the absence of magnetic field.

2.3.2 Substrate

A tempered glass surface with oleophobic coating (purchased from ZAGG) was used as a substrate for oil based ferrofluid droplet spreading with equilibrium contact angle 59.5±0.5˚ (measured by DSA100E , KRÜSS GmbH). The surface was rectangular with a thickness of 0.6 mm and size of 120×30 mm^2, which accommodated at least four droplets before being reused for another set of experiments. Prior to each set of experiments, the substrate was cleaned with deionized (DI) water followed by anhydrous ethyl alcohol.

2.3.3 Magnets

Cube shape (9.5 mm × 9.5 mm × 9.5 mm) NdFeB Grade-N35 permanent magnet with Ni-Cu-Ni finish was used for the experiment. A homogeneous magnetic field was desired during the experiment. To keep the field homogenous, two magnets facing each other with opposite poles were used in case of horizontal magnetic field. A single magnet was used for the vertical magnetic field because it is difficult to keep the droplet aligned with the magnet if the deposition unit is between two moveable permanent magnets. To ensure that the magnetic field was homogenous in the horizontal plane, the diameter of the ferrofluid droplet was kept much smaller than the frontal area of the magnets [13]. A gaussmeter (H.S. Martin & Co.) was used to measure the magnetic field, (B – magnetic flux density) as a function of the distance between the magnets and the bottom of the droplets. The magnetic field as a function of distance between the magnet and the substrate is presented in Figure 2-1.

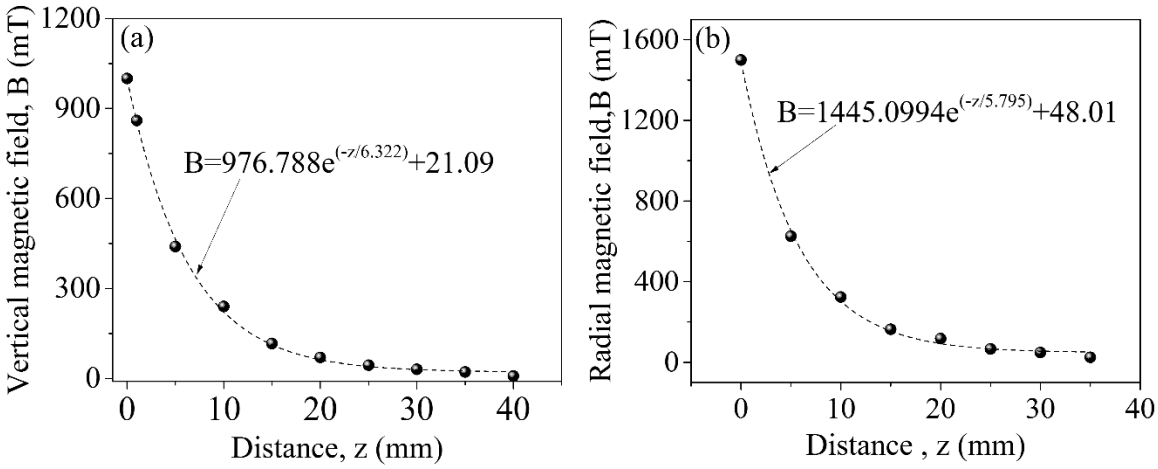

Figure 2-1. Magnetic field strength as a function of the distance from the surface of the magnets: (a) vertical magnetic field (b) radial magnetic field. An exponential decay fitting is used for obtaining the curve fitted expression. For vertical magnetic field, distance is measured from the top surface of the magnet to the bottom of the droplet and for horizontal magnetic field distance is equal to the half of the distance between two magnets.

The relation between distance from the magnet's surface versus the magnetic flux density for the vertical and horizontal magnetic field is presented in Figure 2-1 (a) and (b), respectively. It is evident that the magnetic field in vertical and horizontal or radial directions decays monotonically as the distance between the substrate and magnet is increased.

2.3.4 Optical Setup

The spreading of ferrofluid droplets was recorded with a CMOS high-speed camera (Vision research, Phantom V711) fitted with an extended macro lens assembly. For this experimental arrangement, attempts were made to keep the frame capturing frequency within the same order of spreading time scale. Here the maximum spreading speed was assumed to be around 1m/s, with a capillary length scale limit; the required time scale is in the order of ~10ms. Hence, for all experiments the frequency was more than 5000 fps at 30 μs exposure time for a resolution of 800 × 800 pixels. The camera was mounted on a tripod (Manfrotto, Italy) in such a way that the

substrate and camera sensor were aligned perfectly. The front view of the droplet was recorded with optimized magnification where more than two-thirds of the sensor was occupied by the drop image. A small portion of the needle (used for the drop deposition- KRÜSS GmbH), with a known diameter, was always in the frame and used as a reference for the calibration. A backlight illumination technique was employed using a 150Watt, 60 Hz fiber optics light source (Type MO150, JH TECHNOLOGIES INC). Due to the light source, no significant temperature rise was detected in the surrounding medium. To maintain smooth and homogeneous illumination, a 70 mm × 70 mm square glass diffuser (Thorlab, Inc.) was used between the camera and the light source. All the captured videos were further processed by in-built ADVANCE software with DSA 100E (KRÜSS GmbH) and other commercial image processing software (Image – Pro Premiere V. 9.2, MEDIA CYBERNATICS and ADVANCE, KRÜSS GmbH) were used to quantify the drop height, shape, contact angle and satellite drop volume.

2.3.5 Experimental Setup

The overall arrangement of the experimental setup, as shown in Figure **2-2**, was devised to obtain spreading dynamics and droplet generation. For the vertical magnetic field, a permanent magnet was attached to a 3D-printed base with a magnet holder. The base was attached to the linear movable stage (Z-axis) of the drop shape analyzer (DSA 100, KRÜSS GmbH) that enabled us to vary the magnetic field by altering the distance between the magnet and stage. To ascertain the appropriate distance and magnetic field, the substrate was fixed on another customized holder (Thorlab, Inc.). In the case of the radial or horizontal magnetic field the magnet was fixed on the substrate in such a way that the directions of spreading and the magnetic field were parallel to each other. In this case, two permanent magnets were placed with opposite poles facing each other. A droplet of the desired volume was formed and deposited with a flat tip needle of inner and outer

diameter of 0.50 mm and 0.52 mm, respectively. The distance between the tip of the needle and the substrate was maintained at approximately two times the drop diameter to avoid any additional kinetic energy implication during the drop deposition on the substrate.

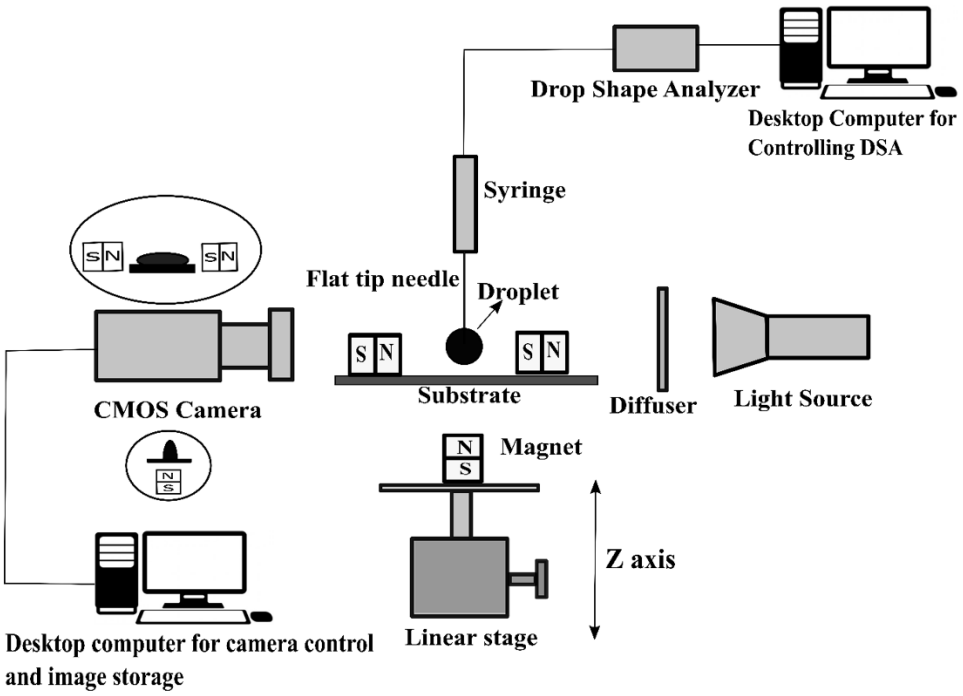

Figure 2-2 . Experimental setup (side view sketch) used to collect the droplet spreading dynamics in the presence of vertical or horizontal magnetic field. All the components are not drawn up to the scale.

2.4 Results and Discussion

The droplet spreading dynamics in the presence of a magnetic field, which is normal and parallel to the contact line of motion was investigated. Figure 2-3 shows the drop deposition and spreading of drop with the variation in vertically-oriented static magnetic field. The transient evolution of droplet morphology, i.e., spreading diameter, height and contact angle, is quantified as presented in Figure 2-3(a)-(c). The corresponding temporal snapshots are presented in the panel as Figure

2-3(d). For the discussion of droplet spreading under vertical magnetic field the considered magnetic field is limited till ~100 mT as beyond this magnetic field droplet break up takes place.

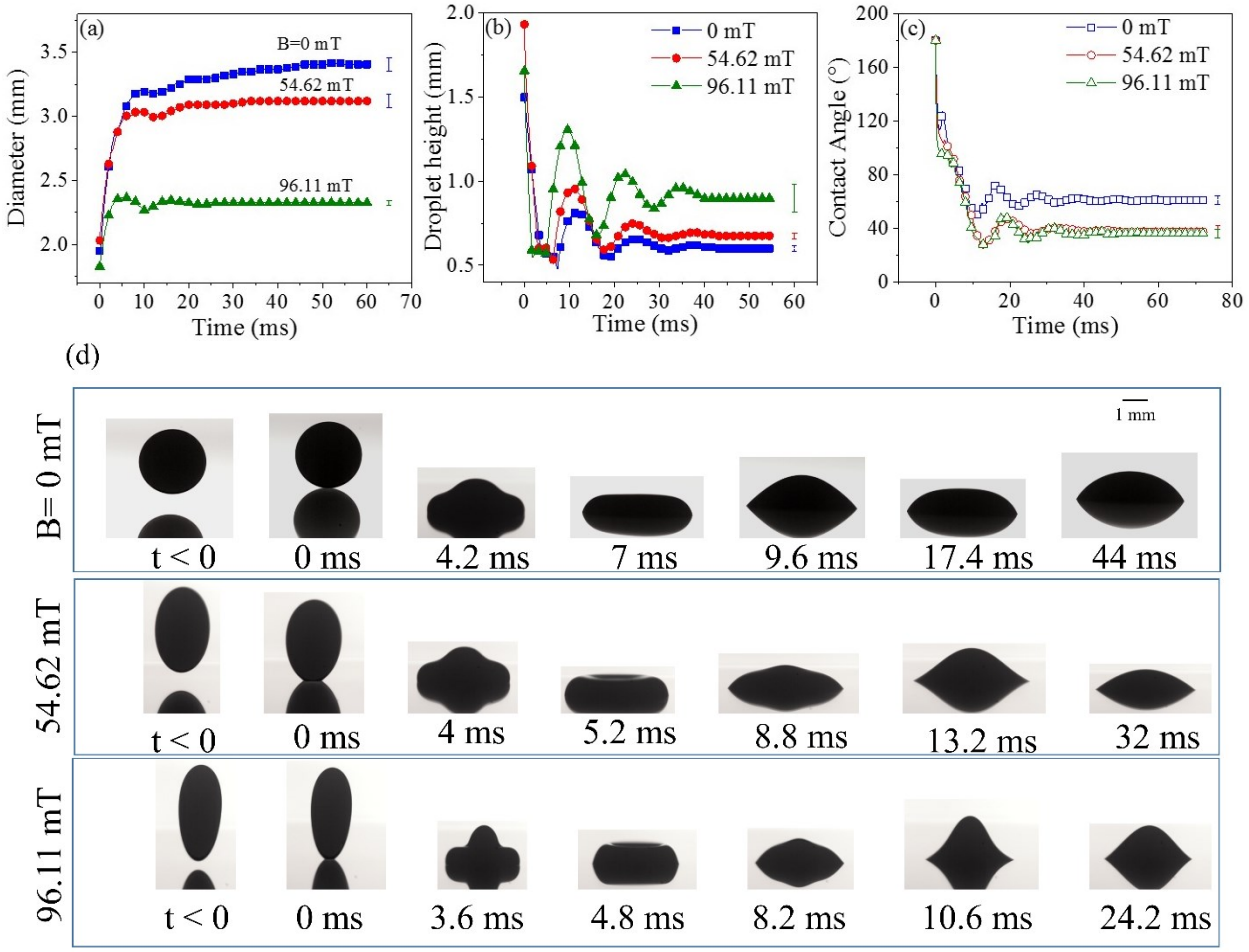

Figure 2-3. Droplet spreading dynamics under vertical magnetic field: (a) diameter (b) droplet height (c) contact angle of a ferrofluid droplet of 2 µl volume as a function of time in varying magnetic field. The drop is deposited on a solid surface under the influence of vertical magnetic field. (d) Snapshot of spreading dynamics of the same droplet for varied vertical magnetic field.

In the case of a spreading droplet, the drop instantaneously spreads with a sharp increase in diameter until the three-phase contact line was pinned. Theoretically, the base diameter of a drop should start with a point contact of a perfect 180º contact angle. Due to the rapid pressure increase at the point of impact[20] as well as the viscous nature of the liquid, the oscillating motion in the liquid-air interface with a fixed three-phase contact line can be observed[21,22]. In a similar manner,

for any observed case, in the presence or absence of magnetic field, the droplet spreading behavior is not monotonic: the sharp increase in the diameter was observed.

In the presence of a magnetic field, drops overspread marginally and attempted to retract but, due to pre-wetted surface, the maximum spreading diameter did not shrink. The oscillations or capillary waves[23] prior to attainting the equilibrium configuration were distinctly evident in the height of the drop. Further, as the magnetic field is increased, the amplitude of these oscillations also increased. These oscillations overspread the drop until viscous dissipation was triggered. When the droplet collides with a rigid surface it starts to spread rapidly until the inertial energy of the falling droplet is dissipated to form a new solid-liquid interface. Based on the surface energy of the solid surface, maximum spreading is obtained where viscosity plays an additional role by causing a sudden decrease in contact line diameter. The orientation of the applied magnetic field was in the same direction as the drop height. As a result, the increase in the drop height, with increase in the magnetic field, further changed in the equilibrium contact angle for the same droplet volume was observed. However, the magnetic field and the work of adhesion dominated the stored interfacial energy. Hence each case recoiled differently (B=0mT, 54.62mT, and 96.11mT), which altered the maximum spread and corresponding droplet shape. As at 96.11 mT, the oscillations were higher compared to 54.62 mT or the case with no magnetic field. This difference can be attributed to the vertical magnetic field where a direct relation between the height and magnetic field was witnessed. On the other hand, the inverse relationship between the spreading diameter and contact angle was observed. Thus a drop was obtained with lower contact angles with increased height, without altering the surface chemistry of the substrate.

Further analysis of Figure 2-3(b) reveals that, while attaining the equilibrium configuration, the frequency of the oscillations, remained similar regardless of magnetic field strength. However,

increase in the amplitude was evident with the increase in the magnetic field. In addition, similar patterns were seen for each of the oscillations. Despite differences in the amplitude of the peak of oscillation, all the peaks occur at the same instant. Following the conventional drop impact analysis[24, 25, 26], the spreading dynamics is dictated by the competition of several forces: falling droplet kinetic energy; surface energy; viscous dissipation; and the magnetic field. During impact, the inertial force is balanced by either the surface tension and/or the viscous dissipation. Upon impact, maximum spreading results from the competition between the kinetic energy, the surface energy and the viscous dissipation. If the kinetic energy surpasses the inherent surface energy, the drop spreads in an attempt to minimize the energy of the system. This entire process is a competition amongst inertial, viscous and capillary time scales. However, the increase in the magnetic field does not alter these time scales. Hence, we observed the same frequency in all three cases where the amplitude is varied due to the magnitude of the magnetic field. With the ferrofluid being present at the contact line, the drop failed to spread completely. The competition between interfacial forces at the three-phase contact line and the vertically-oriented magnetic field restricted the drop from spreading completely. As a result, the droplet was simply pinned with an increase in the height. However, the apparent contact angle and area were modified. The corresponding behavior for contact angles is depicted in Figure 2-3(c) and interestingly the marginal change in the equilibrium contact angle with the change in the magnetic field was observed, i.e., the contact angle change at 54.62 mT and 96.11 mT is approximately the same. The curvature radius of liquid-air interface for higher magnetic field did not follow the traditionally adapted spherical cap shape assumption. As a result, measurement of contact angles is not a trivial task with the commercially available image processing techniques. In such cases, a tangent method at the contact point was used with a single radius of curvature assumption. To demonstrate this challenge, the pictorial

representation of the droplet deformation under the influence of vertical magnetic field is presented in Figure 2-3(d). Without a magnetic field, the typical spherical shape of the drop is observed just before impact. However, in a vertical magnetic field, the spherical droplet deforms into a prolate spheroid and the aspect ratio of the drop increased with the increase in the magnetic field strength. In a higher magnetic field, the droplet elongated more along the vertical magnetic field by compensating its contact line diameter. During recoil, the increment in the dimple height of the splat shape drop can be attributed to the paramagnetic relation between the magnetic field.

As anticipated and demonstrated in Figure 2-4, in the horizontal magnetic field, the droplet shape prior to deposition was elongated in a horizontal or a radial direction. The presence of an additional driving force in the direction of spreading at the three-phase contact line suppressed the oscillations during spreading and further decreased the contact angle. Figure 2-4 elucidates the evolution of the detailed morphological shape over time under the effect of a radial magnetic field. In the presence of an additional assistant at the three-phase contact line, the interfacial forces and magnetic field assist each other to attain the equilibrium rather than compete against each other, as observed in the case of vertically oriented magnetic field. As a result, two important differences were observed compared to the vertical oriented case: first, the droplet base diameter increased monotonically without any perturbations or oscillations; secondly, despite dissimilarities in the magnetic field magnitude, the amplitude and frequency of oscillations in height was unaltered. From Figure 2-4 it is noteworthy to mention that the droplet height decreases with an increase in magnetic field, which implies that the droplets flattens along the direction of the magnetic field. The transient variation of the contact angle in different radial magnetic field is presented in Figure 2-4.

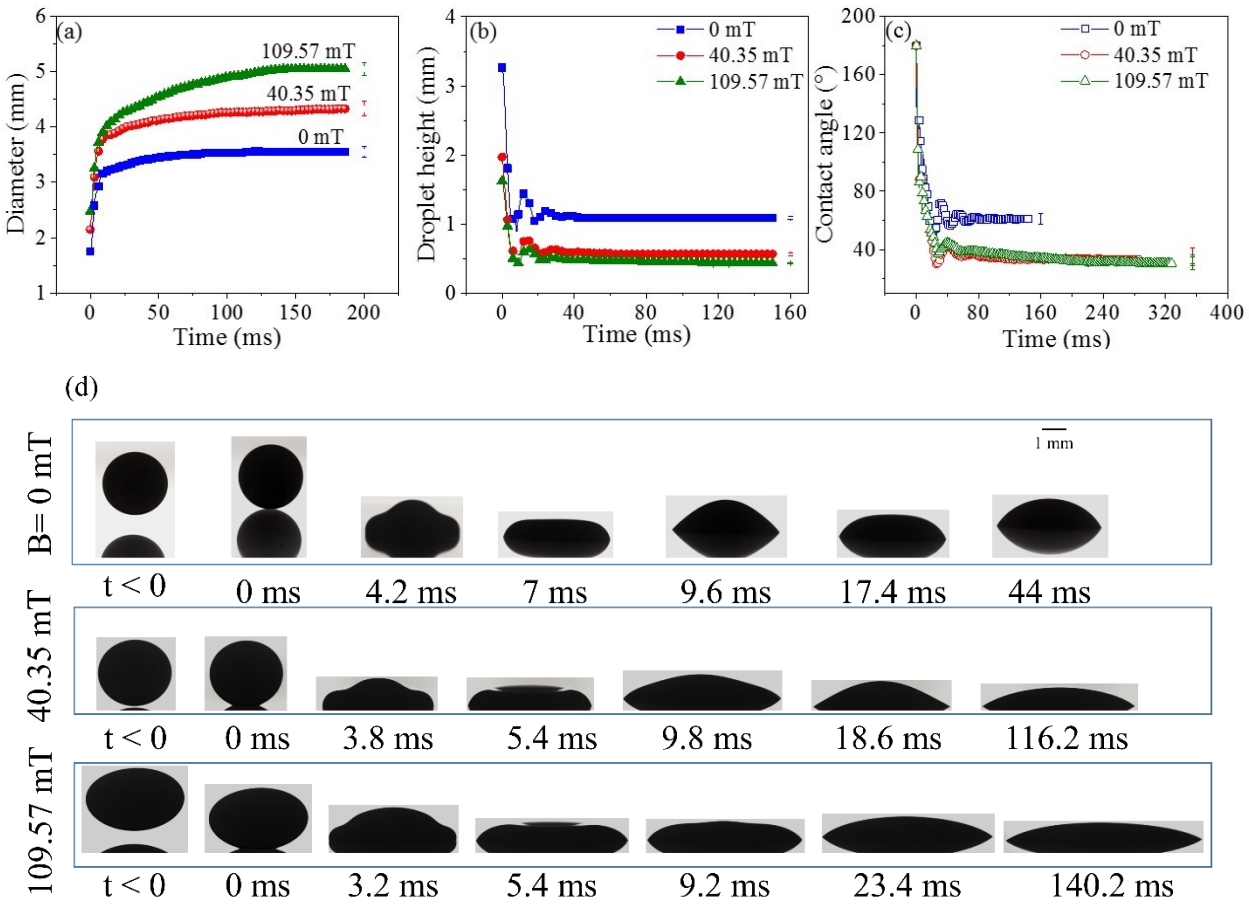

Figure 2-4. Droplet spreading dynamics under horizontal magnetic field: (a) diameter (b) droplet height (c) contact angle of a ferrofluid droplet of 2 µl volume as a function of time for different magnetic field. The drop is deposited on a solid surface under the influence of radial magnetic field. (d) Snapshot of spreading dynamics of the same droplet for varied horizontal magnetic field.

The equilibrium contact angle for the studied case was 59.5±0.5˚ without magnetic field whereas the significant decrement to 32˚ was observed due to the influence of magnetic field. Figure 2-4(d) represents the morphological evolution of a drop in the presence of a radial magnetic field. It is evident that the drop aspect ratio (droplet height to width ratio) decreases with the increase in the magnetic field. The assistance in the spreading with radial magnetic field prolongs the spreading time required to attain the equilibrium, as opposed to the vertical magnetic field case.

To draw the comparison and comment on the respective advantages and disadvantages of orientation of the magnetic field, a quantified comparison between both the cases is required. Here we attempt to compare different equilibrium or static parameters obtained with the same operating conditions except the orientation and strength of magnetic field. For a given application, it is important to identify the maximum change in the shape of the drops during the entire spreading process, starting from drop deposition. It is common practice, in drop impact studies, to compare the maximum equilibrium drop shape to the drop shape before impact [24,27 ,28]. Similarly, we compared the drop configurations, specifically the diameter and height of the drop, before and after impact. We also studied the relationship between the applied magnetic field and the change in equilibrium contact angle. Considering the equilibrium outcome from Figure 2-3 and Figure 2-4, it can be demonstrated that the equilibrium base diameter of the droplet decreased with the vertical magnetic field whereas, the opposite scenario can be obtained for a radial magnetic field. In a magnetic field, the droplet shape before the impact is influenced by the orientation of the magnetic field as observed in Figure 2-3(d) and Figure 2-4(d). On the other hand, in conventional drop impact dynamics, the drop shape before impact is always spherical. It can be concluded that the ferrofluid droplet shape resembles a prolate or oblate spheroid under the effect of vertical and radial magnetic field, respectively. It is worth analyzing whether this change in the drop shape, before the impact, increases or decreases the maximum spread after impact. Therefore, two dimensionless parameters, representing the droplet morphology, were introduced. Motivated by the drop impact literature, we borrowed the D^*_{max}, which is the ratio of the maximum equilibrium contact line diameter of a droplet upon impact to the droplet diameter before the impingement. On the other hand, due to nonaxisymmetry in the drop shape, an additional geometric parameter was introduced to ensure complete information about the drop shape. Hence, H^*_{max} was added to the

analysis, which is the ratio of maximum droplet height at the equilibrium spreading configuration to the drop height along vertical direction before impact. For a nonmagnetic case, the height and diameter before impact are the same since the drop is always spherical.

In Figure 2-5, the drop diameter is compared for vertically- and horizontally-oriented magnetic fields. The insets of Figure 2-5 represent the diameter and height before impact and the maximum base diameter and height after impact, for vertically- and horizontally-oriented cases. As the vertical magnetic field opposes the radial elongation of a drop before impact or spreading at the three-phase contact line, we noticed a decrement in the diameters before and after impact. As a result, for the horizontal or radial magnetic fields, assistance due to the magnetic field strength resulted in an increase of both diameters. Figure 2-5 is a combined representation of these two cases where D^*_{max} remains unaffected, regardless of the strength of the magnetic field. That is, the ratio of the droplet diameters remains constant before and after impact in each case. For the considered set of operating conditions, the maximum spread of the diameter was always twice that of the droplet diameter before impact. Thus, the change in the drop shape before the impact causes only a quantified increment or decrement in the maximum drop spread after impact. Similarly, the change in the drop shape in vertical direction was studied and for constant ratio of 0.3 was observed in the droplet height, as presented in Figure 2-5(b). Two inset figures inside both the figures represent the variation of diameter or height with respect to magnetic field. From both the cases presented in Figure 2-5, it can be argued that the magnetic field only affects the drop shape during the deposition and spreading. The universality in the ratio of the drop shape change suggests that the maximum spreading dynamics were completely dictated by the nonmagnetic parameters whereas the drop shape before the impact is the only parameter that governs the shape and size of the maximum spread or height of the impacting drop.

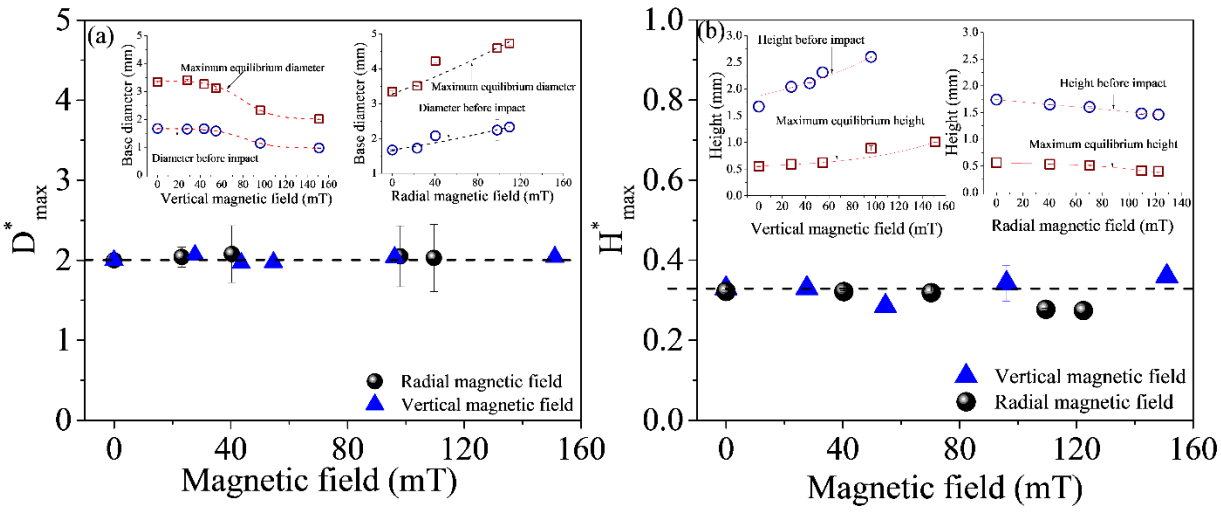

Figure 2-5. The universality of the maximum spread (D^*_{max}) and maximum height (H^*_{max}) irrespective of magnetic field strength and orientation: (a) experimental D^*_{max} as a function of magnetic field and (b) experimental H^*_{max} as a function of magnetic field. Insets in Figs. (a) and (b) depict the variation of diameter and height, respectively with respect to differently oriented magnetic field.

Both the droplet height and its diameter alter as the orientation of magnetic field is changed. With the base line expansion or reduction, the corresponding change in drop height forces the change in equilibrium contact angle. As shown in Figure 2-6(a) similar behavior (decrement in the contact angle) was observed with the increment in the magnetic field strength in either direction. Under vertical magnetic field, the static equilibrium contact angle decreased with the increment of the magnetic field though the height increased with the decrement in the baseline for a corresponding increase in the vertical magnetic field. We adhered strictly to the definition of contact angle and contact line [29] in measuring the contact angle. Hence, in the case of the vertical magnetic field, the contact angle was measured at the three-phase contact line of a cusp shape drop. At the same time,

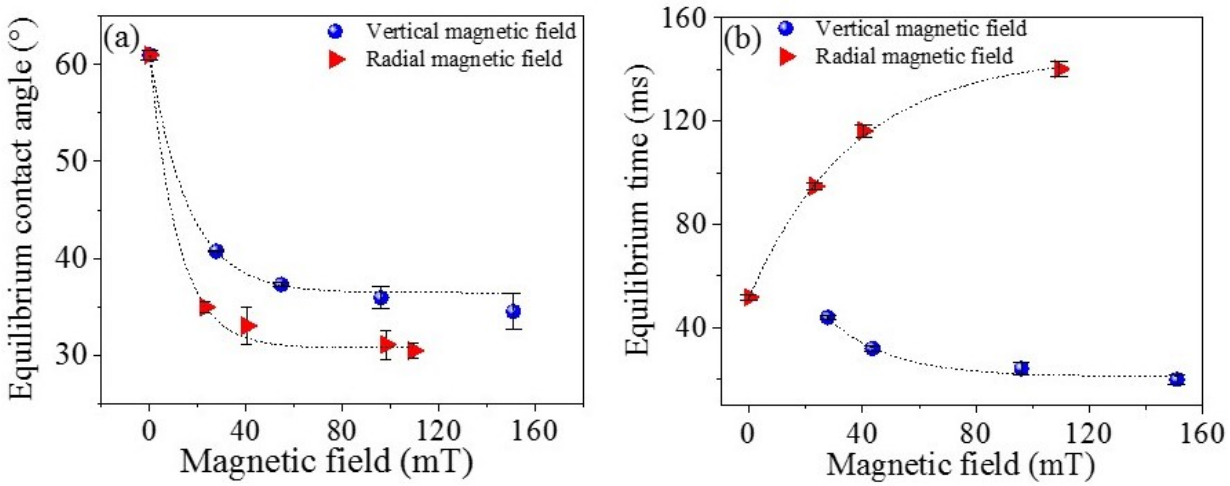

Figure 2-6. Contact angle and spreading time to attain the equilibrium under different magnetic field and direction. Contact angles show similar trends for magnetic field in either of the direction but the time required to reach the droplet at equilibrium shows opposite trends under vertical and radial magnetic field. (a) Variation of contact angle and (b) Equilibrium time, as a function of magnetic field in vertical and radial directions. Equilibrium time is the required time for the droplet to reach the stage when the droplet stops spreading and contact angle become static.

if the time required to attain the equilibrium is quantified as shown in Figure 2-6(b), the role of the direction of the magnetic field is noticeable. It is evident that the total time required to attain equilibrium droplet spreading can be controlled with the assistance of a magnetic field. For a vertical magnetic field, the time required for droplet spreading also decreased, due to the magnetic field's restrictive or opposing force. While spreading, the elongated drop, in the vertical direction was forced to spread horizontally, with a constant spreading force, i.e., surface energy of the substrate. The maximum spread decreased as the vertical magnetic field was increased and thus the time required to attain equilibrium also decreased. On the other hand, for the radial magnetic field, completely opposite behavior was observed where assistance in spreading prolongs spreading time. The radial magnetic field stretches the diameter of the droplet along the radial direction, which requires additional time to reconfigure and attain equilibrium.

From the previous discussion, it is confirmed that the ferrofluid used in this experiment shows a unique characteristics under the magnetic field. The fluid elongates along the vertical magnetic field, increasing the height and decreasing the width. On the other hand, upon extending its contact line diameter and reducing its height, the same fluid is stretched as the magnetic field strength increases in the radial direction. This whole phenomenon can be explained with the help of paramagnetism[30] , detailed quantified information of which is beyond the scope of this work . The ferrofluid used in this experiment is a colloidal suspension of magnetite particles where the carrier liquid is light hydrocarbon oil. Oil is paramagnetic in nature with positive magnetic susceptibility. The suspended ferrous particles in oil-based fluid can be considered an ensemble of individual atoms with their own magnetic moment. These atomic scale magnets are placed arbitrarily in the suspension and the inherent thermal energy is sufficient to randomize their orientation. Without the application of a magnetic field, the ferrofluid behaves as a regular suspension. However, when an external magnetic field is applied, the atomic magnetic moments reorient themselves along the field direction, resulting in a small net magnetization and positive susceptibility. As the applied field is increased, the net magnetization increases in-line with the external field, which results in a bulk motion of fluid towards the magnetic field, resulting in the deformation of the interface or bulk fluid drop.

For the range of magnetic fields, in two different directions used in this experimental study, the appropriate empirical correlations, for different observed quantified information, are given in Table 1. In order to show the agreement between the curve fitted expression and the experimental observation, a coefficient of determination is also reported in the Table 1 in parenthesis. All the fitted curves complement each other because, in every scenario, the coefficient of determination

was very close to 1. One can use these empirical correlations to quantify the drop shape for a considered range of the magnetic field without performing repetitive experiments.

Table 1. Empirical relationship for different geometrical parameter as a function of magnetic field

Parameters	**Vertical magnetic field**	**Radial magnetic field**
Equilibrium diameter	$D_{eq} = 3.34 + 0.0064B - 1.7716x10^{-4}B^2$(0.999)	$D_{eq} = 3.28 + 0.01168B + 1.844x10^{-5}B^2$ (0.894)
Droplet diameter before impact	$D_0 = -0.01203\, e^{\left(\frac{B}{25.192}\right)} + 1.686$ (0.99)	$D_0 = 1.6691 + 0.00468B + 1.313x10^{-5}B^2$ (0.913)
Equilibrium height	$H_{eq} = 0.0558\, e^{(B/68.2)} + 0.499$ (0.994)	$H_{eq} = -0.0187e^{\left(\frac{B}{50.83}\right)} + 0.5762$ (0.985)
Droplet height before impact	$H_0 = 0.555e^{\left(\frac{B}{115.31}\right)} + 1.319$ (0.925)	$H_0 = 1.7398 - 0.00215B - 1.29x10^{-6}B^2$ (0.997)
Time to reach equilibrium	$t_{eq} = 81.46e^{(-B/21.78)} + 21.15$ (0.992)	$t_{eq} = -94.07e^{\left(-\frac{B}{37.04}\right)} + 145.78$ (0.999)
Equilibrium contact angle	$\theta_{eq} = 24.56e^{(-B/15.9)} + 36.44$ (0.999)	$\theta_{eq} = 30.26e^{(-B/11.84)} + 30.75$ (0.999)

It is established from Figure 2-3 and Figure 2-4, that the drop shape prior to impact dictates the final outcome. During the process of depositing the drop, it was observed that the drop generation or detachment from the nozzle or needle is another important factor that governs the final drop

shape. For the sake of completeness, the drop deposition process, along with the drop detachment was investigated in detail.

In the present study, the drop was generated based on the drop volume tensiometry principle where the drop detaches from a needle due to its own weight[31]. This simple drop generation method cannot be achieved without breakup and satellite drop formation. The formation of daughter droplets have significant consequences in numerous applications, such as inkjet printing[32], spraying or atomization of liquids[33] , 3D printing[9]. In the case of 3D printing, these satellite droplets are the root cause of contamination[9]. Without the magnetic field the drop tends to remain spherical[34] at the tip of the needle and the detachment process is governed by competition among the viscous force, pressure difference, the interfacial tension force. The viscous force is the result of viscous stress acting on the interface and is proportional to the tip or contact area and the detachment velocity gradient[35]. The presence of a magnetic field alters the drop detachment by altering the drop shape. Assuming the viscous, gravity and interfacial forces are constant, the adhesion force between the drop and needle tip and the gravitation force govern the drop detachment. Larger capillary forces can be experienced at the beginning of the droplet formation, as the tip curvature is smaller. Capillary force is proportional to interfacial tension and it is inversely proportional to the curvature. To delineate the role of the magnetic field on drop detachment, the thread that forms during the drop detachment and the appearance of satellite drop is presented in Figure 2-7 and Figure 2-8 . Thread formation physics and its quantification is well established in the literature[31,36,37]. Thread formation is an inevitable aspect of the drop detachment process, which is attributed to the competition between the body force and interfacial stress[31, 36, 37]. During drop detachment, the thread, which is the bridge between the needle and the drop, breaks due to the development of large curvature. Immediately after this breakup at the lower end, the

new freed end of the thread tends to retract rapidly in the direction of the needle due to the interfacial tension[37,38]. The sudden change in breakup pressure and the viscous nature of the fluid frees the other end of the thread from the needle. The two free ends of the thread rapidly minimize energies by forming a satellite droplet which is completely separated from the detached primary droplet and the residual liquid at the tip of the capillary or needle. Careful observation reveals that, in a magnetic field, the detachment is similar where thread detaches first from the primary droplet rather than the needle, resulting in a satellite drop formation. However, in the presence of a vertical magnetic field, the additional vertical stretching force significantly alters the length of the thread and ultimately the recoil and satellite drop volume. However, in the higher vertical magnetic field (~55 mT) the stretching in the thread was significant enough to further break the thread and form two satellite drops. Figure 2-7 demonstrates the change in the satellite droplet volume with respect to the change in the magnetic field for the horizontal as well as for the vertical magnetic fields. With the increased strength of the vertical magnetic field, an increment in drop height and thread is depicted in the Figure 2-7. In case of the radial magnetic field, an additional force, which is not in the direction of the detachment, does not alter the drop detachment mechanism and only a marginal change in the thread length was observed as shown in Figure 2-7. Thus, we can assume that the change in the thread length is constant for the radial magnetic field since the elongation of the drop is not in the same direction as the drop detachment. The imaging ability and available sensor from the camera allowed us to determine a minimum length and width of 0.1 mm. The drop width is too small to quantify with this limitation and, as a result, the satellite droplet volume was quantified to further analyze the drop detachment.

Figure 2-8 reveals that, as the thread length is almost constant in the radial magnetic field case, the satellite drop volume also remains constant within the radial magnetic field. Interestingly, in the

case of the vertical magnetic field, beyond a critical strength, the satellite droplet volume is sufficiently high that it is dominated by gravitational force as well as the magnetic force. Beyond this critical strength of magnetic field, the satellite droplet merges with the primary droplet instead of returning to the needle. For the observed scenario and operating parameters, this critical magnetic field is around 151 mT and above this strength the travelling of the satellite drop towards the primary droplet was observed which is represented as Zone II in Figure 2-8. In case of the radial magnetic field, the satellite droplet always returns to needle since the alteration in the magnetic field is only in the radial direction and does not affect the drop detachment process significantly. Based on the performed analysis, it can be concluded that magnetic force plays a pivotal role on the droplet formation, detachment and spreading process. In the absence of the magnetic field, the initial shape of the ferrofluid drop at the tip of the needle is approximately spherical[34] due to the balance of the opposing forces of the hydrostatic pressure

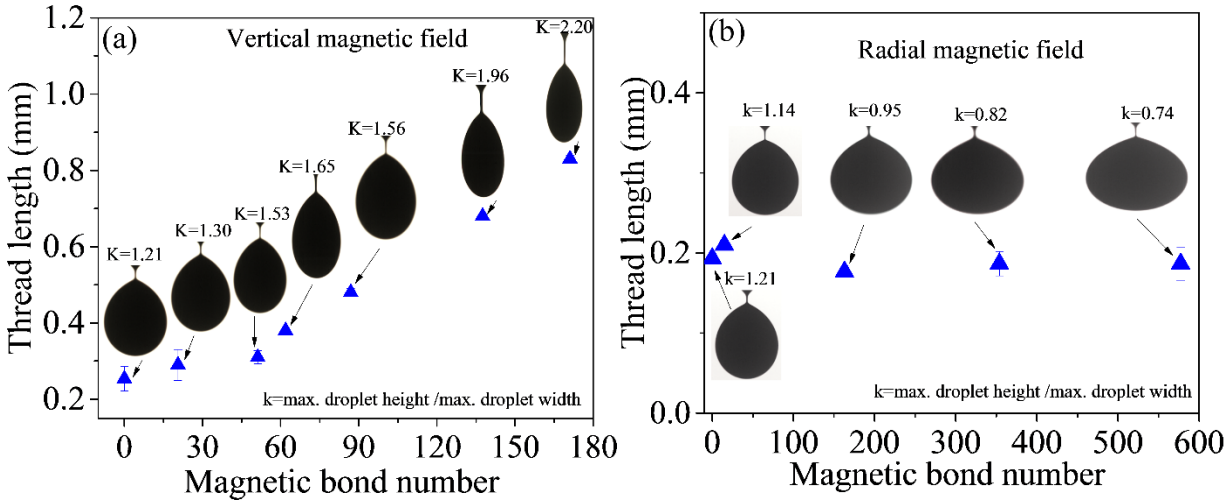

Figure 2-7 Thread length is proportional to the vertical magnetic field whereas it is constant with respect to radial magnetic field. (a) Thread length as a function of magnetic Bond number in vertical direction (b) thread length as a function of magnetic Bond number in radial direction. Here k is the aspect ratio of the droplet.

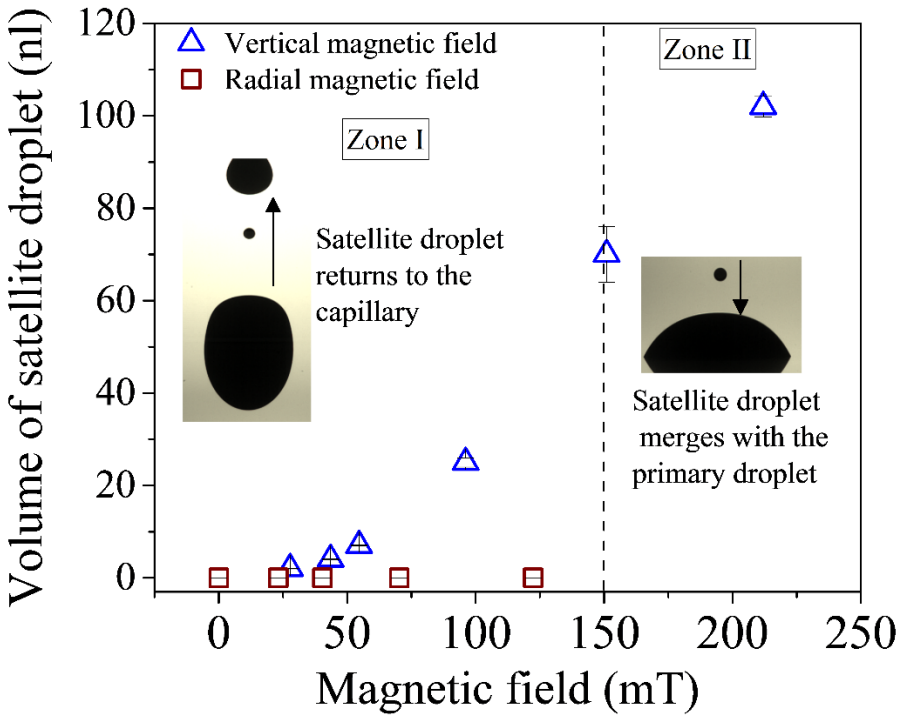

Figure 2-8. Variation in satellite droplet volume as a function of magnetic field at different orientation. Arrow sign indicates the direction in which the satellite droplet lands under the effect of vertical magnetic field. In zone I the drop goes towards the needle whereas in the satellite drop adds to the disposed drop in Zone II. Under radial magnetic field the satellite droplet always retracts back to the capillary irrespective of magnetic field strength and direction.

(ρgR), caused by gravity and the Laplace pressure (γ/R) caused by surface tension, where $\rho, g, \gamma,$ and R are the density, gravitational acceleration, surface tension and the radius of the curvature, respectively. When the needle containing paramagnetic ferrofluid is exposed to the magnetic field, a combined effect of interfacial tension, pressure difference, viscous force and magnetic stretching is imposed on the generated drop. The magnetic Bond number[35] and the magnetic susceptibility are two crucial dimensionless parameters which dictate the droplet shape and formation at the needle tip. The magnetic Bond number ($B_{om} = \frac{\mu_0 H^2 L}{\gamma}$, where μ_0, H, L and γ denote the magnetic permeability of free space, magnetic field strength, effective length and surface tension respectively) is defined as a ratio between magnetic force and interfacial tension

whereas the magnetic susceptibility is a material property which determines whether the ferrofluid will elongate or flatten along the magnetic field direction. At higher B_{om} number, the effective length of the droplet exceeds the critical capillary length. As a result, the shape of the droplet in formation is no longer a sphere as we observed in Figure 2-7.

2.5 Conclusion

This present study reports an extensive experimental investigation on the dynamic spreading of a paramagnetic ferrofluid droplet, which includes transient variation of different geometrical parameters with respect to various magnetic field strength in different directions, along with an emphasis on the formation of satellite droplets and their behavior under the effect of a magnetic field. For a considerable set of operating conditions D^*_{max} (indicating the ratio of maximum equilibrium contact line diameter of an impacting drop to the corresponding droplet dimeter before the impact) and H^*_{max} (ratio of maximum droplet height after spreading to the corresponding droplet height before the impact) remain constant regardless of magnetic field and irrespective of the direction of the magnetic field. Due to its distinctive paramagnetic nature and morphological evolution, the magnetic field has decisive control over the time required for the drop to attain its equilibrium configuration. One can observe similar observation for a given water based diamagnetic ferrofluid. The orientation of the magnetic field and the magnetic properties of the ferrofluids decide whether the droplet shape before the impact will be a prolate ellipsoid or an oblate ellipsoid. The typical spherical shape of the droplet cannot be observed under magnetic field of comparatively higher strength as the magnetic Bond number dictates the whole drop generation process. By taking advantage of high speed imaging technology, the whole satellite droplet formation process has been observed under the influence of magnetic field. It has also been discovered that, for a certain critical vertical magnetic field, the satellite droplet merges with the

deposited primary droplet whereas for radial magnetic field the satellite droplet always retracts to the needle. These findings provide us insight into the fate of satellite droplets that form upon thread breakup. All of the fundamental studies presented in this article will formulate a rational understanding to resolve some technical issues regarding, but not limited to, 3D printing with magnetic fluid where the proper manipulation of the primary droplet and elimination of the satellite droplet is desired. More experiments are underway to observe the effect of the magnetic field on ferrofluid droplets as they coalesce and solidify.

References

(1) Papell, S. S.; Otto, C. F. J. Influence of nouniform magnetic fields on ferromagntic colloidal sols. J. Chem. Inf. Model. **1968**, 53 (9), 1689–1699.

(2) Raj, K.; Moskowitz, R. Commercial applications of ferrofluids. J. Magn. Magn. Mater. **1990**, 85 (1–3), 233–245.

(3) Lübbe, A. S.; Bergemann, C.; Riess, H.; Lãbbe, A. S.; Schriever, F.; Reichardt, P.; Possinger, K.; Matthias, M.; Dã, B.; Herrinann, F.; et al. Clinical Experiences with Magnetic Drug Targeting: A Phase I Study with 4′-Epidoxorubicin in 14 Patients with Advanced Solid Tumors in 14 Patients with Advanced Solid Tumors. Cancer Res. **1996**, 56, 4686–4693.

(4) Alexiou, C.; Schmid, R.; Jurgons, R.; Bergemann, C. Targeted Tumor Therapy with " Magnetic Drug Targeting ": Therapeutic Efficacy of Ferrofluid Bound Mitoxantrone. Lect. Notes Phys. **2002**, 594, 233–251.

(5) Han-dan, L.; Wei, X.; Shi-gang, W.; Zun-ji, K. Hydrodynamic modeling of ferrofluid flow in magnetic targeting drug delivery. Appl. Math. Mech. **2008**, 29 (10), 1341–1349.

(6) Charles, S. W. Ferrofluids Magnetically Controllable Fluids and Their Applications. Ferrofluids - Magnetically Controllable Fluids and Their Applications. 2002, pp 3–18.

(7) Katsikis, G.; Cybulski, J. S.; Prakash, M. Synchronous universal droplet logic and control. Nat. Phys. **2015**, 11 (7), 588–596.

(8) Manukyan, S.; Schneider, M. Experimental investigation of wetting with magnetic fluids. Langmuir **2016**, 32 (20), 5135–5140.

(9) Visser, C. W.; Pohl, R.; Sun, C.; Römer, G.-W.; in't Veld, B.; Lohse, D. Toward 3D printing of pure metals by laser-induced forward transfer. Adv. Mater. **2015**, 27 (27), 4087–4092.

(10) Zenou, M.; Sa'ar, A.; Kotler, Z. Digital laser printing of aluminum micro-structure on thermally sensitive substrates. J. Phys. D. Appl. Phys. **2015**, 48 (20), 205303.

(11) Zenou, M.; Sa'Ar, A.; Kotler, Z. Supersonic laser-induced jetting of aluminum micro-droplets. Appl. Phys. Lett. **2015**, 106 (18).

(12) Nguyen, N.-T.; Zhu, G.; Chua, Y.-C.; Phan, V.-N.; Tan, S.-H. Magnetowetting and Sliding Motion of a Sessile Ferrofluid Droplet in the Presence of a Permanent Magnet. Langmuir **2010**, 26 (15), 12553–12559.

(13) Rigoni, C.; Pierno, M.; Mistura, G.; Talbot, D.; Massart, R.; Bacri, J. C.; Abou-Hassan, A. Static Magnetowetting of Ferrofluid Drops. Langmuir **2016**.

(14) Tenneti, S.; Subramanian, S. G.; Chakraborty, M.; Soni, G.; DasGupta, S. Magnetowetting of Ferrofluidic Thin Liquid Films. Sci. Rep. **2017**, 7 (March), 44738.

(15) Zhang, J.; Han, T.-Y.; Yang, J.-C.; Ni, M.-J. On the spreading of impacting drops under the influence of a vertical magnetic field. J. Fluid Mech **2016**, 809.

(16) Egatz-Gómez, A.; Melle, S.; García, A. A.; Lindsay, S. A.; MárquezP Domínguez-García, M.; RubioS T Picraux, M. A.; Taraci, J. L.; Clement, T.; YangMark Hayes, D. A.; Gust, D.; et al. Discrete magnetic microfluidics. Appl. Phys. Lett **2006**, 89 (34106).

(17) Nguyen, N. T.; Ng, K. M.; Huang, X. Manipulation of ferrofluid droplets using planar coils. Appl. Phys. Lett. **2006**, 89 (5), 1–4.

(18) Pipper, J.; Inoue, M.; Ng, L. F.-P.; Neuzil, P.; Zhang, Y.; Novak, L. Catching bird flu in a droplet. Nat. Med. **2007**, 13 (10), 1259–1263.

(19) Sliding, slipping and rolling: the sedimentation of a viscous drop down a gently inclined plane. J. Fluid Mech **2017**, 512, 95–131.

(20) Huang, Y. C.; Hammitt, F. G.; Yang, W. J. Hydrodynamic Phenomena during High-Speed Collision between Liquid and Rigid Plane. ASME J. Fluids Eng. **1973**, 276–294.

(21) Bird, J. C.; Mandre, S.; Stone, H. A. Short-time dynamics of partial wetting. Phys. Rev. Lett. **2008**, 100 (23), 234501.

(22) Quéré, D. Inertial capillarity, Europhysics Lett. **1997**, 39 (5), 533.

(23) Caviezel, D.; Narayanan, C.; Lakehal, D. Adherence and bouncing of liquid droplets impacting on dry surfaces. Microfluid. Nanofluidics **2008**, 5 (4), 469–478.

(24) Pasandideh-fard, M.; Qiao, Y. M.; Chandra, S.; Mostaghimi, J. Capillary effects during droplet impact on a solid surface. Cit. Phys. Fluids **1996**, 8.

(25) Chandra, S.; Avedisian, C. T. The collision of a droplet with a solid surface. Phys. Fluids A Fluid Dyn. **1990**, 2 (9), 1525.

(26) Mao, T.; Kuhn, D. C. S.; Tran, H. Spread and Rebound of Liquid Droplets upon Impact on Flat Surfaces. **1997**, 4 (9), 2169–2179.

(27) Clanet, C.; Béguin, C.; Richard, D.; Quéré, D. Maximal deformation of an impacting drop. J. Fluid Mech. **2004**, 517, 199–208.

(28) Josserand, C.; Thoroddsen, S. T. Drop Impact on a Solid Surface. Annu. Rev. Fluid Mech. **2016**, 48 (1), 365–391.

(29) De Gennes, P. G. Wetting: Statics and dynamics. Rev. Mod. Phys. **1985**.

(30) Krishnan, K. M. Fundamentals and applications of magnetic materials; Oxford University Press, 2016.

(31) Zhang, D. F.; Stone, H. A. Drop formation in viscous flows at a vertical capillary tube. Phys. Fluids **1997**, 9 (8), 2234–2242.

(32) Li, R. Droplet deposition in solid ink printing; University of Toronto, 2008.

(33) Inkpen, S. L.; Melcher, J. R. Dominant mechanisms for color differences in the mechanical and the electrostatic spraying of metallic paints. Ind. Eng. Chem. Res. **1987**, 26 (8), 1645–1653.

(34) Berthier, J.; Brakke, K. A. The Physics of Microdroplets, 1st ed.; Scrivener Publishing, 2012.

(35) Liu, J.; Yap, Y. F.; Nguyen, N.-T. Numerical study of the formation process of ferrofluid droplets. Phys. Fluids **2011**, 23.

(36) Tjahjadi, M.; Stone, H. A.; Ottino, J. M. Satellite and subsatellite formation in capillary breakup. J. Fluid Mech. **1992**, 243, 297–317.

(37) Peregrine, D. H.; Shoker, G.; Symon, A. The bifurcation of liquid bridges. J. Fluid Mech. **1990**, 212, 25–39.

(38) Zhang, X.; Basaran, O. A. Dynamics of drop formation from a capillary in the presence of an electric field. J. Fluid Mech. **1996**, 326, 239–263.

3 Maximum Spreading of a Ferrofluid Droplet under the Effect of Magnetic Field

3.1 Abstract

This chapter represents a theoretical and experimental study of the effects of vertically applied external magnetic field on the maximum spreading of ferrofluid droplets on a solid substrate. Despite numerous research works has already referred to the theoretical modelling of droplet impact scenario, the maximum spreading ratio of a droplet under the influenced of magnetic field remain unanswered. In this present study, we developed a theoretical model based on conservation of energy to predict the maximal deformation upon impact influenced by magnetic field for both diamagnetic water based ferrofluid and paramagnetic oil based ferrofluid. The physics of variation of maximum drop spread was carefully observed as a function of Weber number (We), Reynolds number (Re) and magnetic Bond number (B_{om}) ranging from 5~45, 150~400 and 150~3000, respectively. By validating the theoretical model with the experimental observations, we demonstrated that our theoretical model could successfully predict the experimental observations. Through theoretical analysis and experimental investigations a rational understanding has been formulated where we can observe all the governing non dimensional numbers (We, Re and B_{om}) assist to increase the maximum spreading of a impacting droplet.

3.2 Introduction

The maximum spreading of liquid droplet upon impact on a solid surface is not only a crucial parameter that facilitates a better understanding of several natural phenomenon but also a decisive factor in many industrial applications ranging from aerosols to pesticides[1-2]. Aerosols is generated when porous surfaces (such as , soil) erode due to the impact of rain droplet which also brings the aroma out of the earth while raining [1]. Understanding of droplet impact behavior can be applied on agricultural herbicides and insecticides sprayings where liquid sticking to the soil is important to enhance the effectiveness of the spray and decrease contamination of the soil[2]. This concept of drop impact and resulted maximum spreading is of concern for numerous technology but not limited to ; namely, spray cooling of hot surfaces[3], spray coating [4], sintering[5], thermal spray[6] and so on. The resolution and overall quality of an inkjet printing is also a function of maximum spreading diameter of an impinging ink droplet which can be manipulated as the operation demands for optimized performance [7],[8], [9]. In a crime scene domain, impact velocity of a blood droplet from the size of the bloodstain on a given surfaces predicts accurately the reconstruction of a crime scene such as position of the victim or types of wounds, flight trajectories of the blood droplets, etc.[10] . However, impingement phenomenon influenced by magnetic field is unexplored intriguing topic to study, which plays a pivotal role in 3D printing – a burgeoning area of research due to its simplicity and adaptability to numerous applications. While 3D printing in Laser induced forward transfer (LIFT) method, several droplet shape can be observed, namely; sphere, ellipsoid, disk and toroid (shape at maximum spread) which corresponds to whole droplet impact scenario[11]. The dimensions and time required forming those shapes would help to optimize the solidification

time scale and thereby freeze the droplet in any shape discussed earlier. Metal droplet spreading may limit the lateral resolution of the 3D printing because both excessive and insufficient spreading of droplet may produce distorted or porous objects [12]. Hence, in case of 3D printing with metals, it is paramount to manipulate and optimize the maximum spreading of the deposited fluid with a given constraints in mind. . The main objective of this article is to propose a theoretical model predicting a maximum spreading of ferrofluid droplet under the effect of magnetic field and it's validation with the corresponding experimental results.

Since the pioneering work of Worthington [13], the research in the field of droplet dynamics upon impact has been fueled up which leads to numerous amount of theoretical, numerical and experimental investigation in this field. One of the most important process parameters in droplet dynamics is the maximum spreading diameter, denoted as $\xi_{max} = \frac{D_{max}}{D_0}$ [14]; where D_{max} is the measured maximum spreading diameter upon impact and D_0 is the initial droplet diameter before impact . Different[14-20] numerical and theoretical models have been proposed to quantify the maximum spreading diameter [15] .Detailed studies have been conducted on maximum droplet spreading through several numerical schemes such as; finite difference[16 17 18], finite element [19] and volume of fluid method [19, 20 21 22]. Most of the theoretical modelling are developed through energy conservation between two phases, the energy before the impact and after the impact. Traditionally, to accommodate most operating parameters and thermophysical properties the governing equation, to predict maximum spread, is reported in nondimensional form. The primary forces that govern the spreading dynamics in impacting scenario are viscous, inertia, capillary and gravity. These forces are represented in terms of the nondimensional numbers such as Reynolds (Re), Capillary (Ca), Weber (We), Bond (Bo) and Ohnesorge (Oh) numbers. Different scenarios are studied for variety of ranges of these nondimensional numbers[23]. Most of the analytical solutions are focused

on the capillary regime with low impact velocity or on the viscous regime at high impact velocity[24], in short the studies with lower and higher Re numbers. The role of the inherent surface and thermal energy of the substrate is another aspect that has been studied in detailed {Chandra et al}. In their study, [15], the change in droplet shape after impact with different surface temperature is analyzed. The energy conservation model proposed in this study by Chandra et al. is a paradigm for the droplet impact modelling. Pasandideh-Fard et al.[25] attempted to extend this model for generalized droplet impact scenario and showed that capillary effects can be neglected during droplet impact if $We \gg \sqrt{Re}$. Later on, Mao et al.[26] developed a semi empirical model with a modified viscous dissipation implementation for wide range of viscosity. The development of generalized model for drop impact scenario, that can predict the maximum spread, facilitate researchers to adopt these models for cases where drop is impacting in the presence additional body or surface forces such as electric[27], acoustic[28], thermal[15]. Deng et al.[29] observed an interesting phenomenon for a charged micro droplet impacting on conducting surfaces which includes the flattening of the sessile droplets with reduced contact angle Further, a mathematical model based on energy conservation to predict the maximum spreading ratio for this case, an electrically charged droplet impact is presented by Ryu et al.[30]. It is also crucial to realize that impinging phenomenon influenced by magnetic field. During 3D printing of metal object through LIFT process researchers have already encountered with various metal droplet shape namely, sphere, ellipsoid, disk and toroid (shape at maximum spread) which corresponds to whole droplet impact scenario. The knowledge of those droplet shapes are of greater importance while solidifying droplet for metal 3D printing since manipulating droplets with different shapes ultimately facilitate to optimize the drop to drop contact area and adhesion. Therefore, investigation of maximum spreading of a magnetic fluid droplet under the influence of magnetic field is one of the priority

for understanding the basic physics of the 3-D printing of the magnetic material. Despite being abundance of modelling approaches in the field of maximum droplet interestingly the detailed theoretical modeling for ferrofluid droplet impact scenario in the presence of magnetic field where droplet is missing from the literature. However, in a most recent study, Zhang et al.[31] developed a theoretical model validated with numerical demonstrates the maximum spreading ratio of a metal droplet under the influence of magnetic field can be scaled as, $\xi_{max} \infty \frac{1}{\sqrt{N}}$, where N can be described as the ratio between the Lorentz force and the inertial force. To our best knowledge, until now this is the only theoretical model to predict impact phenomenon in the presence of a magnetic field. However, the importance of the paramagnetic/diamagnetic relationship between the droplet properties and the magnetic field is missing from the literature. Additionally, the morphological evolution of droplet under magnetic field has also been ignored to investigate. It is of greater importance too as during the fabrication of complex 3D structures through laser induced forward transfer method, the unwanted droplet spreading dictates the shape distortion i.e., both the excessive or insufficient spreading of the droplet may produce distorted or porous object [5]. It was also observed that the printing quality got reduced due to the formation of shape irregularities caused by larger droplet spreading, in case of laser induced forward transfer 3D printing method[12,32]. .

Hence, the main objective of the present study is to develop a generalized theoretical model for predicting the maximum drop spreading a ferrofluid droplet that is under the influence of magnetic field. Further, the detailed experimental studies are performed to validate the proposed theoretical modeling. The model presented here is based on the similar energy balance approached, as adopted my numerous researchers for drop impact studies, where the impact dynamics is characterized by five dimensionless parameters, such as; Reynold's number (Re), Weber number

(We), Magnetic Bond number[33] (B_{om}), magnetic susceptibility (χ) and the contact angle (θ) at the solid liquid interface. The magnetic Bond number ($B_{om} = \frac{\mu_0 H^2 L}{\gamma}$, where μ_0, H, L and γ denote the magnetic permeability of free space, magnetic field strength, effective length and surface tension respectively), which is defined as a ratio between magnetic force and interfacial tension whereas the magnetic susceptibility are magnetic susceptibility are two new parameters that adds the complexity to the analysis.

3.3 Materials and Methods

3.3.1 Ferrofluid

Ferrofluid used in this work is oil-based (EFH-1 type ferrofluid) and water based (EMG508) (purchased from Ferrotec (USA) Corp.) ferrofluids which is a colloidal suspension of magnetite particles (Fe_3O_4, 3-15% by volume) of 10nm in diameter in light hydro carbon oil (55-91 % by volume) with oil soluble dispersant (6-30% by volume). The saturation magnetization and initial magnetic susceptibility of EFH1 ferrofluid is 6mT (mili - Tesla) and 2.64, respectively whereas viscosity and density of that fluid is $6\ \text{mPa.s}$ (mili-pascal-second) and $1.21 \times 10^3\ \frac{\text{kg}}{\text{m}^3}$, whereas the saturation magnetization and initial magnetic susceptibility of EFH 1 ferrofluid is 6.6mT (mili - Tesla) and 0.88, respectively whereas viscosity and density of that fluid is $5\ \text{mPa.s}$ (mili-pascal-second) and $1.07 \times 10^3\ \frac{\text{kg}}{\text{m}^3}$. The surface tension of the EFH 1 and EMG 508 ferrofluid was found to be 24.56 ± 0.04 mN/m and 31.7 ± 0.06 mN/m, measured with a commercial force tensiometer (K-100 from KRÜSS GmbH). Considering these thermophsysical properties, the capillary length, l of the ferrofluid is ~1.5mm, which can be considered as the critical radius for critical Bond

number,$\mathrm{Bo_{cr}} = \frac{\rho g R_{cr}^2}{\gamma} = 1$ [34]. In order to maintain the Bond number below unity the diameter for the ferrofluid droplet was chosen appropriately to circumvent unwarranted effects.

3.3.2 Substrate

The substrate used in this experiment is hydrophobic in nature. A tempered glass surface (purchased from ZAGG) was used as a substrate for drop spreading with equilibrium contact angle (measured by ADVANCE, KRÜSS GmbH). The rectangular surface is 0.6 mm thick with an area of $150\text{x } 40 \ \ \mathrm{mm^2}$, which accommodates at least five droplets before being reused for another set of experiments. Prior to each set-of experiments, the substrate was cleaned with deionized (DI) water followed by anhydrous Ethyl Alcohol. .

3.3.3 Magnets

In this study, a permanent magnet (NdFeB Grade-N35) with Ni-Cu-Ni finish was used. The dimension of the magnet was 5 mm x 9.5 mm x 9.5 mm. For the sake of the theoretical prediction presented here, a homogeneous vertical magnetic field was desired. However for creating homogeneous vertical magnetic field environment it is difficult to use two or more magnets. It is because setting up two movable permanent magnets while the droplet deposition unit is between the magnets is experimentally challenging as it is not possible to keep the droplet aligned with the magnet. Therefore, we have ensured uniform vertical magnetic field with single permanent magnet by maintaining the diameter of the ferrofluid droplet much smaller than the frontal area of the magnets [35]. The magnetic field applied in this experiment was varied by changing the distance between magnet and the substrate. A movable manual linear actuator was used to move the magnets and a gaussmeter (H.S. Martin & Co.) was used to measure the magnetic field, (B –

magnetic flux density) as a function of the distance between the magnets and the bottom of the droplets. The magnetic field as a function of distance between the magnet and the substrate is presented in Figure 3-1(a). From Figure 3-1(a) it can be observed that the vertical magnetic field decays exponentially with the increased distance between the substrate and magnet.

3.3.4 Optical Setup

All the ferrofluid droplet impact scenarios were recorded with a CMOS high-speed camera (Vision research, phantom V711). In order to enlarge the droplet visualization an extended macro lenses assembly was installed with the camera Through our experimental arrangements, we attempted to maintain the similar order of frame capturing frequency and the spreading time scale . We assumed the maximum spreading speed was around 1m/s and with capillary length scale limit, the required time scale is in the order of ~10ms. Therefore, frequency of 5000 fps at 30 μs exposure time with a resolution of 800 × 800 pixels was chosen for all the experiments. The camera was mounted on a three dimensional tripod (Manfrotto, Italy) in such a way the levels of the substrate and camera sensor are aligned perfectly. The front view of the droplet was recorded with optimized magnification where more than two-third portion of sensor was occupied by the drop image. For the calibration purpose a small portion of the needle (used for the drop deposition- KRÜSS GmbH) with known diameter was made visible in the captured frame and used as a reference .We employed a backlight illumination technique by using a 150Watt, 60 Hz fiber optics light source (Type MO150, JH TECHNOLOGIES INC). However, surrounding temperature rise due to the light source was found to be minimum. A 70 mm × 70 mm square glass diffuser (Thorlab, Inc.) was used between the camera and the light source to maintain a smooth and homogeneous

illumination . For the sake of droplet quantification purpose i.e. the measurement of drop height, shape, volume and contact angle, all the captured videos were processed by in-built ADVANCE software with DSA 100E (KRÜSS GmbH) and another commercial image processing software (Image – Pro Premiere V. 9.2, MEDIA CYBERNATICS and ADVANCE, KRÜSS GmbH) .

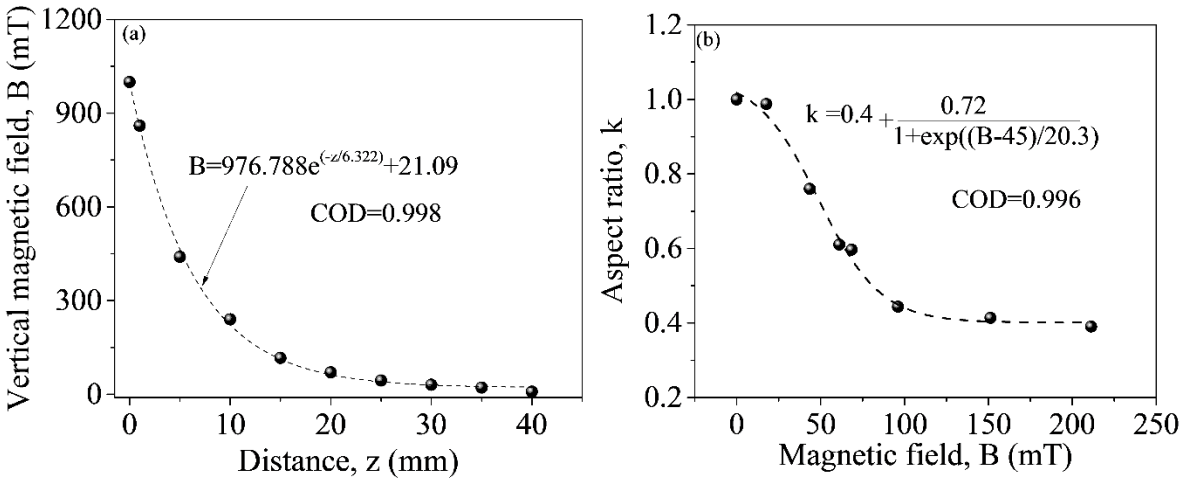

Figure 3-1. (a)Vertical magnetic field strength as a function of the distance from the surface of the magnets. For vertical magnetic field distance is measured from the top surface of the magnet to the bottom of the droplet[37]. (b) Aspect ratio of a droplet as a function of vertical magnetic field.

3.3.5 Experimental Setup

The experimental set up for the study presented in this chapter is similar to the experimental set up illustrated in Figure **2-2**.

3.4 Theoretical Analysis

A drop impact phenomenon, with energy approach, is modelled with four different stages [36], such as; (a) before impact (b) maximum spreading (c) maximum recoil (d) equilibrium which is shown

in Figure 3-2. Adopting the similar conservation of energy approach, we developed a model for the maximum spreading ratio where hydrodynamic forces are coupled with magnetic force. We assume uniform magnetic field for a given case, i.e., for horizontal as well as for vertical case. An additional energy term, due to a constant magnetic field, and corresponding change in the drop shapes[37] are two new aspect of the proposed modeling compared to the modeling proposed in the literature.

We consider a system defined by a control volume that consists of a ferrofluid droplet and the surrounding which is under the effect of a constant but homogeneous magnetic field. To justify the assumption of homogeneous magnetic field, the diameter of the ferrofluid droplet was always kept much smaller than the frontal area of the magnets[35] . The total surface energy before the impact consists of only the liquid-vapor interfacial tension (Υ_{lv}). Therefore, immediately before the impact the total energy in the system consists of kinetic energy, due to the descent of the drop, and surface energy of a distorted shape droplet. As discussed earlier, due to the influence of magnetic field the typical spherical droplet flattens or extends along the magnetic field direction based on the diamagnetic and paramagnetic behavior of the fluid and deforms into an ellipsoid – either prolate or oblate.

To obtain the maximum spreading ratio of magnetized ferrofluid droplets, the concept of the energy conservation was adopted for the process of droplet impact and the corresponding equation can be written as follows:

$$\mathrm{K.E_1} + \mathrm{S.E_1} = \mathrm{K.E_2} + \mathrm{S.E_2} + \mathrm{W_{1-2}} \qquad (1)$$

Stage a: Before impact

The kinetic energy of the droplet before impact can be written as:

$$K.E_1 = \frac{1}{12}\pi\rho AB^2 v_0^2 \qquad (2)$$

where, ρ is the density of the ferrofluid, v_0 is the velocity of the falling droplet, A and B are the lengths of major and minor axis of the ellipsoid shape drop respectively as depicted in Figure 3-2.

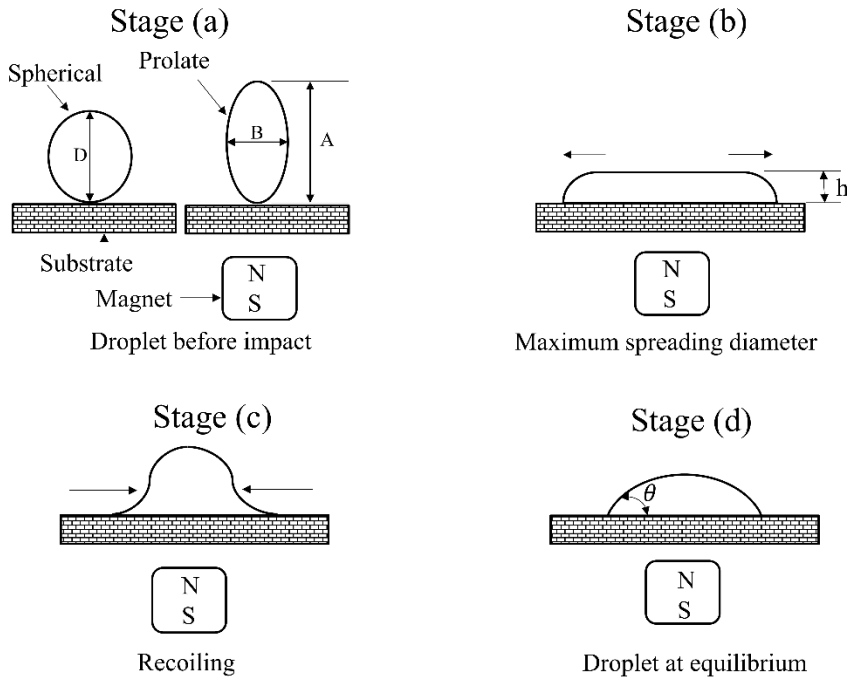

Figure 3-2. Schematic representation of sequence of droplet deformation during the analysis of drop impact under the effect of magnetic field. Stage (a) denotes the droplet before the impact, stage (b) represents the maximum spreading diameter where the drop recoiling state and equilibrium configuration is presented in stages (c) and (d). Arrow indicated the direction of movement of fluid film.

Surface energy of the droplet before impact is the product of surface area of the droplet and the liquid-vapor surface tension. As mentioned in the Figure 3-1(b), the aspect ratio of the drop shape

is function of the magnetic field and one of the input parameters for the analysis along with the other physical property inputs. The surface area of an ellipsoid can be expressed as [38],

$$S.A = \frac{2\pi B}{2}\left(\frac{A}{2}\frac{(\sin^{-1}\sqrt{1-B^2/A^2})}{\sqrt{1-\frac{B^2}{A^2}}}+\frac{B}{2}\right)\text{; for prolate spheroid (A>B)}$$

Or, (3)

$$S.A = \frac{2\pi B}{2}\left(\frac{A}{2}\frac{(\sinh^{-1}\sqrt{\frac{B^2}{A^2}-1})}{\sqrt{\frac{B^2}{A^2}-1}}+\frac{B}{2}\right)\text{; for oblate spheroid (B>A)}$$

The surface energy of the a given shape droplet before impact can be written as,

$$S.E_1 = \frac{\pi}{2}\,BA\,S\,\Upsilon_{lv} \tag{4}$$

Here, Υ_{lv} is the interfacial tension at the liquid-vapor interface and *S* is the surface area factor which depends on the shape of the droplet before impact. For prolate spheroid (A>B), $S = \frac{(\sin^{-1}\sqrt{1-B^2/A^2})}{\sqrt{1-\frac{B^2}{A^2}}} + k$ and for oblate spheroid (B>A), $S = \frac{(\sinh^{-1}\sqrt{\frac{B^2}{A^2}-1})}{\sqrt{\frac{B^2}{A^2}-1}} + k$, whereas $k = \frac{B}{A}$, is the aspect ratio of the droplet[38].

The magnetic field magnetizes the drop and adds an additional energy to the falling ferrofluid droplet which that can be expressed as[39],

$$E_M = -\frac{1}{12}\pi\frac{B_0^2\chi}{\mu_0(1+N\chi)}\,AB^2 \tag{5}$$

where, B_0, χ, μ_0 and *N* denote the magnetic field, magnetic susceptibility, magnetic permeability at free space and demagnetizing factor, respectively.

The interfacial tension between the liquid and air is also a function of the applied magnetic field and to determine the relationship between applied magnetic field and surface tension, the knowledge of the total force acting on the drop is required. Therefore, the total force acting on the droplet before the impact can be written as,

$$F = \frac{\partial(S.E_1 + E_M)}{\partial B} = A\gamma_{lv}(-\frac{\pi}{3}\frac{\chi}{1+N\chi}B_{om} + \frac{\pi}{2}S) \quad (6)$$

where, $B_{om} = \frac{B_0^2 B}{2\mu_0 \gamma_{lv}}$ is the magnetic Bond number, a dimensionless parameter which can be defined as the ratio of magnetic force to the interfacial tension. Hence, with the help of the net force acting on a magnetized ellipsoidal droplet, a concise form of a modified liquid gas interfacial tension ($\gamma_{lv}{}^{m}$), can be expressed as follows:

$$\gamma_{lv}{}^{(m)} = \gamma_{lv}(-\frac{\pi}{3}\frac{\chi}{(1+N\chi)}B_{om} + \frac{\pi}{2}S) \quad (7)$$

Considering equations (5) and (6), one can determine the net force acting on the ferrofluid droplet under the influence of magnetic field.

Stage b: During the impact

At the impact, the kinetic energy is consumed in increasing the area of the liquid vapor and generating the solid liquid interfaces in addition to the dissipation forces due to the viscous nature of the liquid. At the moment of maximum spreading the kinetic energy, $K.E_2$ of the droplet can be assumed as zero. Total surface energy at the maximum spread can be considered as the function of three interfacial forces, i.e., liquid-vapor surface energy (Υ_{lv}), solid-liquid (Υ_{sl}) interface and the solid-vapor surface energy (Υ_{sv}), [36] which results as:

$$S.E._2 = \frac{\pi}{4}B_m^2(\Upsilon_{sl} - \Upsilon_{sv}) + \left(\frac{\frac{2}{3}\pi AB^2}{B_m} + \frac{\pi}{4}B_m^2\right)\Upsilon_{lv} \quad (8)$$

As Υ_{lv} and Υ_{sv} are not readily available we can use Young's equation to get the relation between surface energies and contact angle. For a drop impact studies, in absence of magnetic field, Pasandideh Fard [14] and Furmidge[40] used dynamic contact angle whereas , Mao et al.[26] considered static contact angle. However, we chose the approach taken by Yonemoto et al.[41]; that showed better agreement with the experimental results which suggests to consider the average of dynamic angles (θ_{avg}) at the moment of maximum spread. The resulted surface energy with the maximum spread drop is,

$$S.E_2 = \left[\frac{\pi}{4}B_m^2\left(1 - \cos\theta_{avg}\right) + \frac{\frac{2}{3}\pi AB^2}{B_m}\right]\Upsilon_{lv} \quad (9)$$

The important aspect of this modeling is to determine the loss of the energy due to the viscosity of the liquid drop, i.e., the viscous dissipation, i.e., the work done in deforming the droplet against viscosity is[15],

$$W_{1-2} = \int_0^{t_c}\int_{\Omega} \phi \, d\Omega \, dt \approx \phi\Omega t_c \quad (10)$$

Where Ω is the volume of the viscous fluid, t_c is the time taken for the droplet to spread and ϕ is the viscous dissipation function. The magnitude of the ϕ is estimated by the following expression[15],

$$\phi \sim \mu\left(\frac{V_0}{L_c}\right)^2 \quad (11)$$

Where v_0 is the velocity of the falling droplet and L_c is the effective length of the droplet. Following to the traditional drop impact modeling [14] the volume of the viscous fluid can be expressed as,

$$\Omega = \frac{\frac{\pi}{2} B_m^2 B}{\sqrt{Re}} \tag{12}$$

The time t_c required for a liquid droplet to reach the maximum splat diameter can be estimated by assuming the drop spreads into a cylindrical disk of diameter $B'$and thickness h as shown in Figure.3-3. The splat thickness h after impact can be calculated by equating the volume of a ellipsoidal droplet with major and minor axis of A and B, respectively to that of a cylinder with height h and diameter B_m,

$$h = \frac{\frac{2}{3} AB^2}{B_m^2} \tag{13}$$

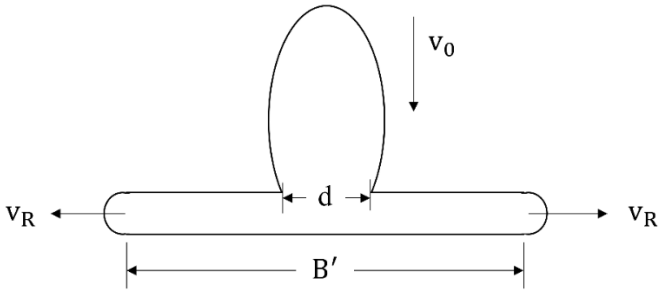

Figure 3-3. Spreading of an ellipsoidal droplet. $B'$is the length of three phase contact line diameter at any moment. v_R is the velocity at horizontal direction and v_0 is the velocity at vertical direction.

Form Figure 3-3 it is seen that when liquid flows from the drop, shaped like a truncated ellipsoid, into the film through an area of diameter d with velocity,v_0. The velocity at the edge of the splat during spreading v_R is given by conservation of mass and results in the following equation,

$$\frac{v_R}{v_0} = \frac{3}{4}\, s\, \frac{B_m^2}{AB'} \tag{14}$$

As mentioned earlier in the previous literature[14] we can assume $d \sim \frac{B'}{2}$ as the d varies form 0 to B'. Therefore, with the help of equation 14 we can get the following expression,

$$\frac{dB'}{dt} = 2v_R = \frac{3}{2} s \frac{B_m^2}{AB'} v_0 \tag{15}$$

Integration of equation 15 will give an expression for the splat diameter, B',

$$\frac{B'}{B_m} = \sqrt{3t^* ks} \tag{16}$$

Where , $t^* = \frac{tv_0}{B} = \frac{1}{3ks}$ is dimensionless time required for the droplet to reach its maximum extent $B' = B_m$. Considering this dimensionless time we can get the total time, t_c required for the droplet to reach its maximum spreading diameter, B_m which can be expressed as,

$$t_c = \frac{\frac{1}{3ks} B}{v_0} \tag{17}$$

Considering equation (10)-(17), viscous dissipation term can be written as ,

$$W_{1-2} = \frac{\pi \mu v_0 \sqrt{Re}}{24ks} B_m^2 \tag{18}$$

To obtain the maximum spreading ratio of magnetized ferrofluid droplets, the concept of the energy conservation was adopted and considering Equations (1) – (19) we can formulate the expression for the maximum spreading factor:

$$\xi_{max} = \frac{B_m}{B} = \sqrt{\frac{\frac{6s + We^*}{12k}}{\frac{1 - cos\theta_{avg}}{4} + \frac{We^*}{24ks\sqrt{Re}}}} \tag{19}$$

Where, $We^* = \frac{We}{\left(-\frac{\pi}{3(1+N\chi)}\frac{\chi}{B_{om}} + \frac{\pi}{2}S\right)}$ and can be denoted as modified or effective Weber number and Re is $\frac{\rho v_0 D}{\mu}$; where μ is the viscosity of the liquid droplet.

3.5 Results and Discussion

Figure 3-4 shows the corresponding temporal snapshots of the morphological evolution of ferrofluid droplet with different magnetic field, due to the impingement on a solid tempered glass substrate with a falling velocity of ~0.5 m/s. A droplet of volume of 2 μL was deposited with certain velocity on a perfectly flat surface and experiments were performed with the water based ferrofluid and oil based ferrofluid .Two different scenarios are presented in Figure 3-4; viz., drop impact with no magnetic field and with the vertical magnetic field of 75 mT. A droplet striking a solid surface spreads instantaneously due to the rapid pressure increase at the point of impact [42], regardless the nature of both the substrate and the liquid. We also observed the similar phenomenon

in case of both water based and oil based ferrofluid presented in Figure 3-4. The ferrofluid droplet deformed as the time advances (from left to right in Figure 3-4) and eventually the droplet gains maximum deformation state. At the maximum spreading state, the ferrofluid droplet takes the shape of a splat or flattened disc, irrespective of the magnitude of the magnetic field. However, an additional external force in the form of magnetic field significantly effects the maximum spreading dynamics and the overall shape of the droplet. During the absence of magnetic field, the maximum spreading diameter was attained between 5 to 6 ms for both the liquids. On the other hand, under the effect of vertically oriented magnetic field the maximal deformation was reached at 7 ms which is comparatively larger elapsed time than the absence of magnetic field condition.

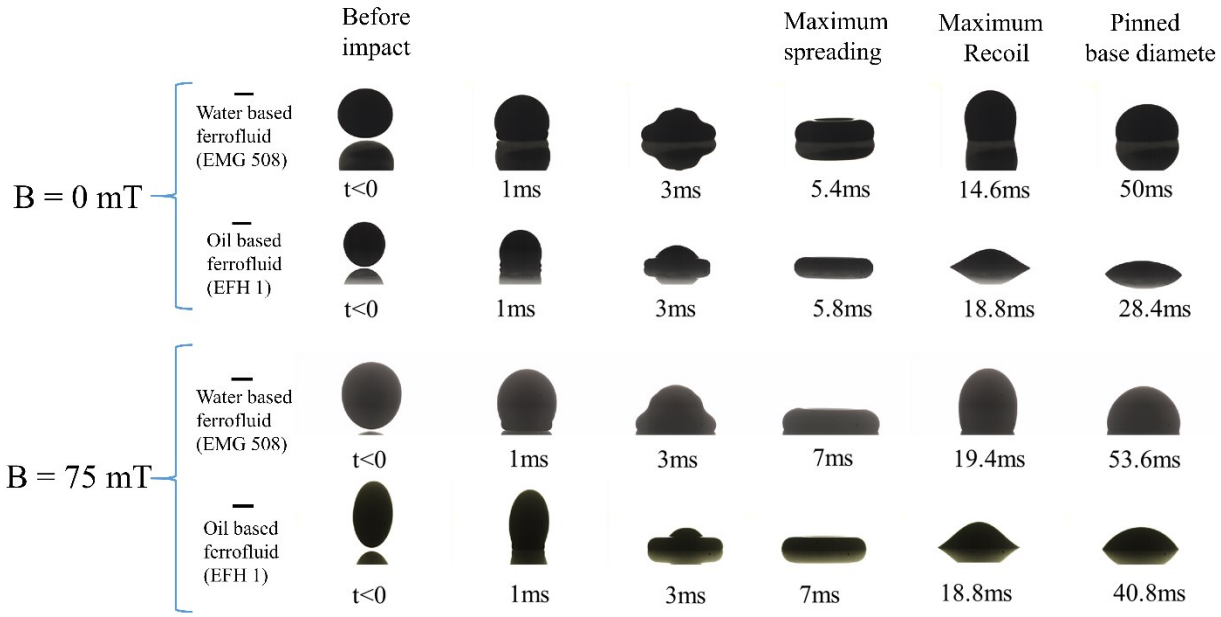

Figure 3-4. Snapshots of sequence of impacting ferrofluid droplet in absence of magnetic field and under the effect of vertical magnetic field. The magnetic field considered here is 0 mT and 75 mT. EMG 508 is a water based ferrofluid whereas EFH1 is oil based ferrofluid. Droplet before impact condition is designated by $t < 0$. The scale bar presented in the image corresponds to 1mm.

If we run a comparative analysis in terms of Figure 3-4, it is evident that for water based liquid, the droplet spreads more with magnetic compared to the no magnetic field condition. At magnetic field, $B = 0\ mT$ typical spherical shape of the droplet is observed immediately before the impact as shown in. On the other hand at B= 75 mT, the droplet deforms into a prolate ellipsoid by stretching it's height along the vertical magnetic field direction. Interestingly, at higher magnetic field (75 mT), it is clearly visible that before the impact the oil based ferrofluid was stretched longer compared to the water based ferrofluid which can be attributed to the opposite nature of the two fluids used in this experiment in terms of magnetic behavior. The water based ferrofluid is diamagnetic whereas an oil based ferrofluid is paramagnetic in nature. We will explain about this in quantitative manner at the later section of this paper where we will discuss in detail about the effect of magnetic field on the maximum spreading dynamics.

Figure 3-5 delineates the transient evolution of impinging ferrofluid droplet morphology under the effect of vertical magnetic field. Figure 3-5 (a) and Figure 3-5 (b) represents the variation of the maximum spreading ratio (ξ) i.e. D_{max}/D_0 of Water based ferrofluid and oil based ferrofluid respectively.The first contact of a drop with solid substrate with $180°$ of contact angle is considered as an initial time for the analysis. In Figure 3-5 we showed the variation of ξ of water based ferrofluid for three different magnitudes of magnetic field; *B*= 0 mT, 235 mT and 280 mT, whereas the impact velocity of the droplet was approximately ~0.5 m/s for each scenario. For water based ferrofluid, we can observe a rapid oscillating motion in the base diameter or the three phase contact line due to the rapid pressure increase at the point of impact [42] and inertial forces or viscous nature of the liquid . A sharp increase in base diameter of water based ferrofluid droplet, from the point of impact to the maximum spreading, was observed distinctively which is due to the dissipation of the inertial or kinetic energy. Further analysis of Figure 3-5 (a) reveals that with the

increasing of vertical magnetic field the base diameter and the maximum spreading ratio of a water based ferrofluid droplet is increasing with approximately similar oscillation frequencies. For B= 0 mT, 235 mT and 280 mT the maximum spreading ratio of the droplet is 1.55, 1.9 and 2, respectively. In spite of differences in magnitudes, the maximum spreading condition of water based ferrofluid is attained approximately at the same time, i.e., at ~ 5.6 ms. However, in the absence of magnetic field the maximum diameter was attained little earlier which is at 4.4 ms. The diamagnetic nature of the water based ferrofluid dictate the proportional relationship between the magnetic field (B) and maximum spreading ratio (ξ_{max}). Immediately after reaching maximum spreading configuration, the minimization of surface energy of drop results in sharp downfall of base diameter. The competition between the inherent surface energy, kinetic energy, viscous dissipation retracts back the overspread drop by shrinking its contact line diameter. The surface energy of the solid-air interface is also another factor that alters this oscillatory behavior. The time span and the magnitude of these oscillatory behaviors needs to be investigated in details in similar line of inertial capillarity studies[43,44] . The recoiling[45] and rebound criteria[26, 45, 46] in the case of impacting droplet is beyond the scope of this study since our theoretical model is restricted to predict only maximum spread of the drop. Figure 3-5 (b) is the representation of the variation of ξ while oil based ferrofluid (EFH1) was impinging on a surface under the vertical magnetic field strength of 0 mT, 52 mT and 68.5 mT with an impact velocity ~0.4 m/s. It is to be noted that, in both cases (water based and oil based) the ferrofluid properties restricts the bounding region for selecting the strength of magnetic field. The interfacial properties of the ferrofluids along with the surface energy of the solid material allows us to decide to the extent of impact velocity that can be studied without drop breakup which is beyond the scope of this study. In the case of oil based ferrofluid, the sharp increment of diameter after the impact was also observed as we noticed in the

case of water based fluid. However, the recoiling of the droplet after attaining maximum spreading diameter was with minimal oscillations and the time required to attain the equilibrium was much earlier than water based fluid as shown in Figure 3-5. Increment of maximum spreading ratio with the increasing of magnetic field was also observed in case of oil based ferrofluid, as both the base diameter or three phase contact line and initial diameter were inversely responding with the magnetic field. . For oil based ferrofluid it was also observed that at 48.5 mT and 68.5 mT the maximum spreading configuration is attained at the same time instant (~10.2 ms) whereas in the absence of magnetic field the maximum spreading was attained a bit earlier (8.4 ms).

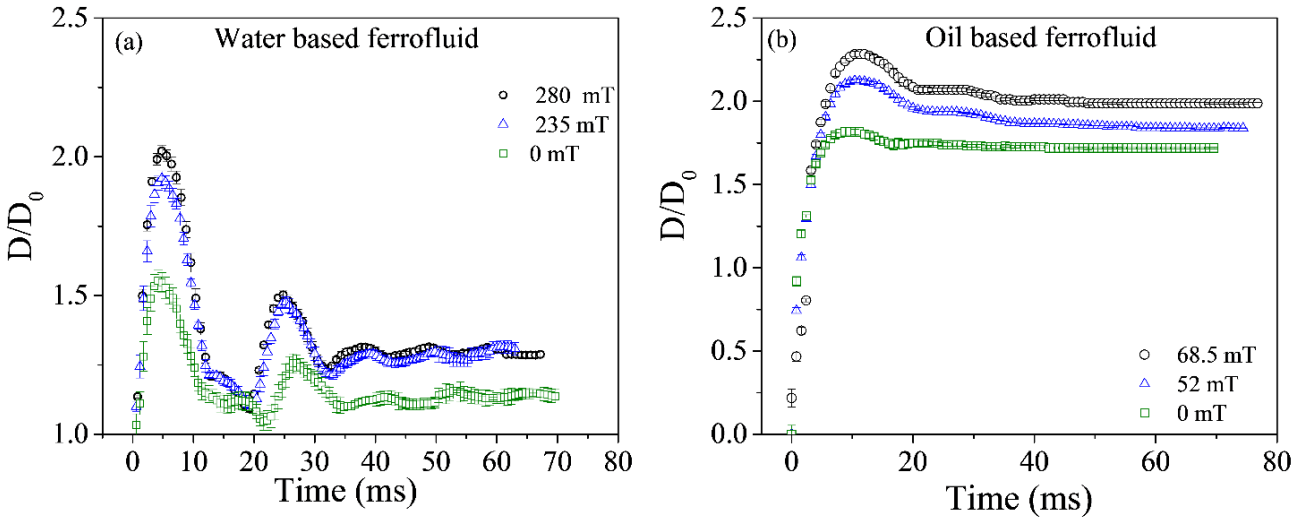

Figure 3-5 . Transient of variation of maximum spreading ratio in case of both (a) water based ferrofluid and (b) oil based ferrofluid. For both of the liquids maximum spreading ratio is increasing with the magnetic field.

In order to draw a comparison between the morphology of impinging water based and oil based ferrofluid, it can be said from Figure 3-5 that the three phase contact line diameter of water based drop showed more oscillatory behavior than the oil based ferrofluid. If we compare the kinetic energy for both of the fluids where we considered the experimental data for around 70 ms and we

found that even beyond the 70 ms the water based ferrofluid was not stop oscillating whereas the base line of the oil based ferrofluid reached equilibrium at 45 ms. The domination of viscous dissipation and the surface energy of the hydrophobic surface on highly viscous oil based ferrofluid is much greater than the low viscous water based ferrofluid , due to which the oil based ferrofluid experienced less oscillation than the water based ferrofluid. Based on the comparative analysis between the ratio of kinetic energy to surface energy and viscous time scale, it is imperative that for same kinetic energy the lower viscosity case will demonstrate higher oscillations as we observed with water based ferrofluid.

3.5.1 Effect of Weber Number

Weber number[2] is a dimensionless number, which can be defined as the ratio of the kinetic energy on impact to the surface energy of the droplet. For a droplet falling from a certain height, h with diameter before impact D_0, surface tension γ, density ρ and an impact velocity v_0, the Weber number is , $We = \frac{\rho v_0^2 D_0}{\gamma}$. From classical literature [24,36,47] of droplet impact studies, it is well known that the maximum spread increases with increasing *We* or impact velocity. In the case of the magnetic filed induced drop impact scenario, we have also noticed the similar observation as presented in Figure 3-6(a and b). Figure 3-6 illustrates the relationship between ξ_{max} and *We* for both water and oil based ferrofluids respectively where the impact is studied on a solid hydrophobic tempered glass for three different magnetic field conditions. In addition to conventional results, increment of ξ_{max} with *We*, it was also observed that for a fixed *We*, ξ_{max} was increasing with the increasing of magnetic field which is very important to note. One can argue that as magnetic Bond number, B_{om} increased, the enhancement in the drop spreading can

be achieved without altering the *We* or impact velocity. The proposed theoretical modeling for maximum spread as presented in equation 19 can also predict the similar physical trend. However, the mathematical expression represented in equation 19 over predicts the maximum spreading by ~15-40%. The over or under prediction of maximum spread form theoretical model is quiet commonly observed for numerous studies in the literature[15, 26] which is attributed to the numerous assumptions and experimental conditions such as appropriate consideration of wetting angle[14,41], assumption of laminar flow distribution inside the spreading splat[15]. In addition to that, the applied magnetic field can also alter the instantaneous contact angles as well the velocity field with the spreading drop. Hence, viscous dissipation of paramagnetic and diamagnetic ferrofluid droplets induced by vertical magnetic field is difficult to quantify correctly. To circumvent this difficulty empirical coefficients are added to the model that can closely predict the experimental observations. Based on the empirical constant or multiplication factor to a given representative term of a governing equation allows us to identify the limitation of the considered assumptions. In order to obtain such a modified model, considering the effect of magnetic field, we introduced an empirical constant in equation 19 based on the detailed sensitivity analysis. The modified expression for maximum spreading, in the presence of vertical magnetic field can be expressed as:

$$\xi_{max} = \sqrt{\frac{\frac{6s + We^*}{12k}}{\frac{1 - \cos\theta_{avg}}{4} + \frac{\alpha\, We^*}{24ksRe^{(1/2.5)}}}} \tag{20}$$

Where, α is an empirical constant with a value of 561.8 and 12.5 for water based ferrofluid and oil based ferrofluid respectively. The minor difference in the exponent of Re, in comparisons with Equation 19, can be attributed to the viscous dissipation quantification in the modeling. Different magnetic behavior of paramagnetic and diamagnetic ferrofluid inside a magnetic field results in two different empirical coefficients for α. If we carefully notice the expression for We^* and

maximum spreading drop equation 20, the B_{om} in the denominator is the representation of magnetic Bond number and for a fixed B_{om}, analysis, the change in the fluid properties must be accounted which results in the change of the empirical constant as we change the fluid properties. It is to be noted that for wide range of experimental analysis the empirical constant remains the same for a given fluid as observed for conventional drop impact studies[10,26].

Figure 3-6 (a) elucidates the comparison between presented proposed model, equation (20), and experimental results. From Figure 3-6 (a), we can strongly argue that our theory shows well agreement with our experimental results as the path followed by the experimental data and the theoretical predictions are almost in convergence with each other. The proportional relationship among $\xi_{\max}$, We and B_{om} is a strong function of magnetic behavior of water based ferrofluid as presented in Figure 3-6 (a). Water based ferrofluid is a colloidal suspension of magnetite particles where the carrier liquid is water. Water is diamagnetic in nature and suspended ferrous particles, inside the bulk water, can be considered as an ensemble of individual atoms with its own magnetic moment. Therefore, when the diamagnetic water based ferrofluid was exposed to the vertically oriented magnetic field, the atomic magnetic moment inside the fluid reoriented themselves against or opposite to applied magnetic field direction. Due to this diamagnetic nature of the water based ferrofluid, there is a proportional relationship between the maximum diameter of the droplet and vertical magnetic field strength and therefore $\xi_{\max}$ is increasing with B_{om}. The increment in the maximum spread with respect to the increase in the We is quite well understood in the literature[48,49] hence for the brevity purpose we are mainly focused on the relationship between the magnetic Bond number and maximum spread.

Figure 3-6 (b) depicts the $\xi_{\max}$ vs We relationship for oil based ferrofluid under vertical magnetic field of various strength. The carrier liquid of the oil based ferrofluid is light hydrocarbon oil which

is paramagnetic in nature. Therefore, with the application of vertical magnetic field the atomic magnetic moments inside the oil based ferrofluid reorganized themselves, similar to the water based fluid but along the field direction resulting in a small net magnetization and positive susceptibility. Due to this nature of the oil based ferrofluid droplet, the droplet is elongated along the vertical magnetic field direction by contracting its three-phase contact line diameter with the increase of vertical magnetic field. Hence, there is a inversely proportional relationship between the vertical magnetic field strength and the three phase contact line or the base diameter of the droplet before the impact[50, 51] . However, from Figure 3-6 (b) we can observe that the maximum spreading factor, ξ_{max} is increasing with the increase of magnetic Bond number which is similar to the water based ferrofluid scenario. To clarify this, we have presented two inset figures in the

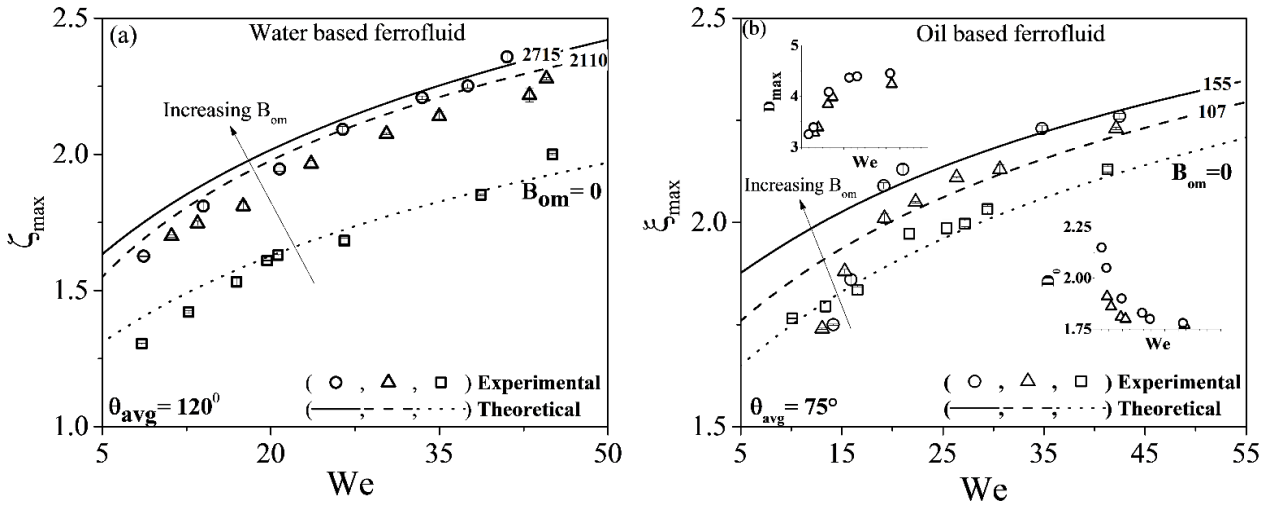

Figure 3-6 . Variation of ξ_{max} with respect to We for different magnetic Bond number for water based ferrofluid and oil based ferrofluid. (a)Experimental observation of ξ_{max} vs We at B_{om}= 0, 2110 and 2715, is represented by the symbols where results extracted from theoretical modeling represented by the lines. (b) Experimental observation of ξ_{max} vs We at B_{om}= 0, 107 and 155 is represented by the symbols where results extracted from theoretical modeling represented by the lines.

Figure 3-6 (b) which demonstrate the respective magnitudes for the drop diameter before the impact and after the impact. As discussed earlier ξ_{max} is the ratio of maximum spreading diameter D_{max} and the diameter of the droplet immediately before the impact, D_0. From the insets we can notice that the D_{max} and D_0 is increasing and decreasing, respectively with the increasing of *We*, the increment in the maximum spread dominant compared to the decrement in the drop diameter before the impact hence maximum spreading ratio always increases with the increasing of B_{om}. It is to be noted that in case of the water base the initial drop diameter, D_0 , is marginally affected by the magnetic field, therefore we did not represent the quantified information of the diameters before and after impacts for the water based ferrofluid scenario. In general, the effect of a surrounding medium in the form of a drag causes a falling drop to deform but the inherent surface tension minimizes the deformed area and attempts to attain the spherical shape. In the case of water based ferrofluid, the external magnetic field is insufficient to overcome these interfacial forces. However, in the case of oil based fluid, where the interfacial tension is lower as compared to water based ferrofluid and due to the addition of surfactant used for stabilizing the ferrofluid particles, the external magnetic field is sufficient to deform the falling drop.

3.5.2 Effects of Magnetic Bond Number

Magnetic Bond number significantly effects the overall shape of the ferrofluid droplets. As we noticed in the previous section, the application of magnetic field deforms the droplet by stretching or flattening along the direction of magnetic field. The paramagnetic or diamagnetic nature of the fluid dictates the deformation shape[37]. Therefore, the overall droplet deformation with a magnetic field can be attributed to the result of interplay between the magnetic force and the interfacial force which is the magnetic Bond number [33, 52] and it can be expressed as, $B_{om} = \frac{\mu_0 M H D_0}{2\gamma}$, where

μ_0 is the magnetic permeability in the free space, M is the magnetization of the fluid, D_0 is the characteristics length of the droplet and γ is the interfacial tension. Figure 3-7 (a-b) illustrates the theoretical and experimental relationship between the ξ_{max} and B_{om} for both water based and oil based ferrofluid. For both oil based and water based ferrofluid, we could observe an incremental relation between the experimental ξ_{max} and B_{om} which was well predicted by our theoretical model. With the increase of B_{om}, the ξ_{max} is increasing for both of the oil based and water based

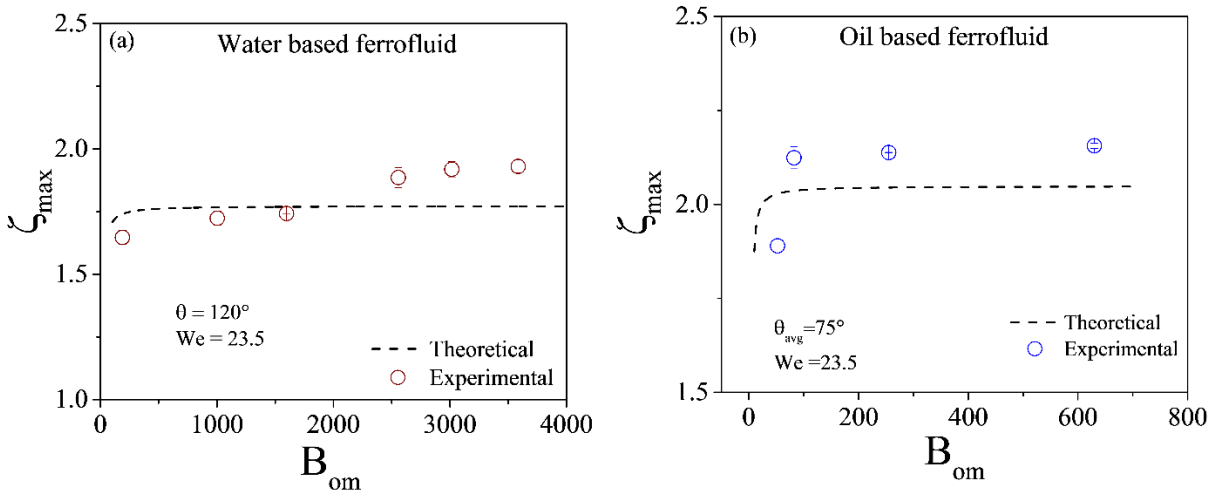

Figure 3-7. Analogy between the theoretical and experimental observation in terms ξ_{max} as a function of B_{om}. (a)Represents water based ferrofluid where the $\theta_{avg} = 120°$ and We =23.5 and (b) represents oil based ferrofluid where the $\theta_{avg} = 75°$ and We =23.5. For both the cases, the black dashed line indicates the theoretical prediction whereas the circles mark the experimental observations.

ferrofluid though they are different in nature in terms of magnetic behavior. As we observed in case of *We* sensitivity analysis, in the case of B_{om} as well, for water based ferrofluid the D_{max} increases with increase of vertical magnetic field whereas opposite scenario was observed for oil based ferrofluid. Due to the effect of B_{om}, the D_0 is decreasing for both of the fluids. It is to be noted that B_{om} is a function of the magnetic properties of the liquid and applied magnetic field, it alters the effective B_{om} this causes an additional change in the drop shape prior to the drop impact[37]. We can easily observe prolate ellipsoidal shape for both water based and oil based

ferrofluid but the increment in the maximum spread of the drop dominates over the initial drop diameter as we observed in the case of We. The maximum bounding factor for the considered range of *We* and B_{om} is the droplet break up and we would like perform all the studies for the scenario where drop does not lose its mass after the impact. The droplet break up of oil-based ferrofluid takes place at comparatively lower (160 mT) vertical magnetic field compared to the water-based ferrofluid (300 mT). Further analysis of Figure 3-7 reveals that, for a given maximum bounding range, the change in ξ_{max} is less sensitive to the B_{om} compared to the We.

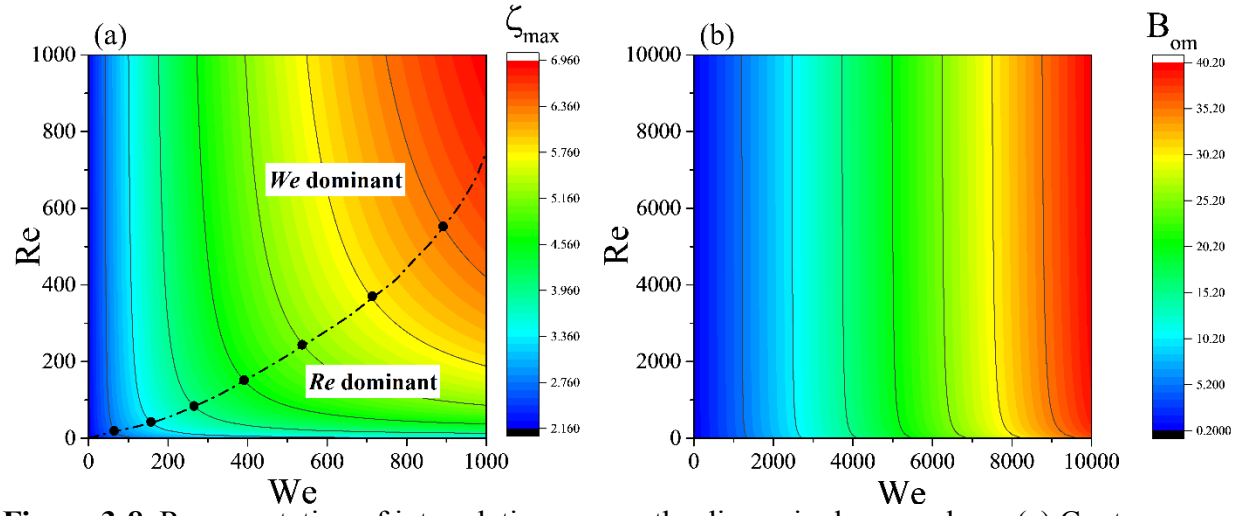

Figure 3-8. Representation of interrelation among the dimensionless numbers. (a) Contour plot showing the relation between *We, Re* and ξ_{max} at $B_{om} = 2500$. All the black dots in the figure (a) denote the inflection points which are connected by a dotted line for the representation of We dominant and Re dominant regime only. (b) Contour plot showing the relation between *We, Re* and B_{om} for attaining the $\xi_{max} = 2$.

Figure 3-7 (a) reveals that the experimental data of water based ferrofluid deviates from the theoretical predictions for magnetic Bond number greater than 2500. Higher B_{om} may cause instabilities [39] in the drop which we are unaccounted in the modeling. If we pay a closer attention to the theoretical modeling represented by equation (20) , ξ_{max} is a function of three dimensionless numbers such as, *Re* , *We* and B_{om}. It would be interesting to see the sensitivity analysis with all

three nondimensional parameters on ξ_{max} and the confidence level of the proposed theoretical model.

We can observe a proportional relationship between these dimensionless numbers from Figure 3-8 (a and b) which delineates our theoretical prediction. Figure 3-8 (a) is a contour plot showing the variation of ξ_{max} for a fixed B_{om} with respect to *We* and *Re*. The contour plot can be divided by connecting the inflection points of the fixed ξ_{max} curve, which clearly defines two regimes either dominated by *Re* or *We*. Therefore, contour plot for fixed ξ_{max} is presented in Figure 3-8 (b). Figure 3-(a) and (b) clearly indicate that for fixed *Re* or *We* the wide range of ξ_{max} can be achieved. One can perform similar analysis for with the variation with B_{om} our analysis suggests that (Figure 3-7), the ξ_{max} is less sensitive to B_{om} , hence we avoided the sensitivity analysis for the variations in the B_{om} .

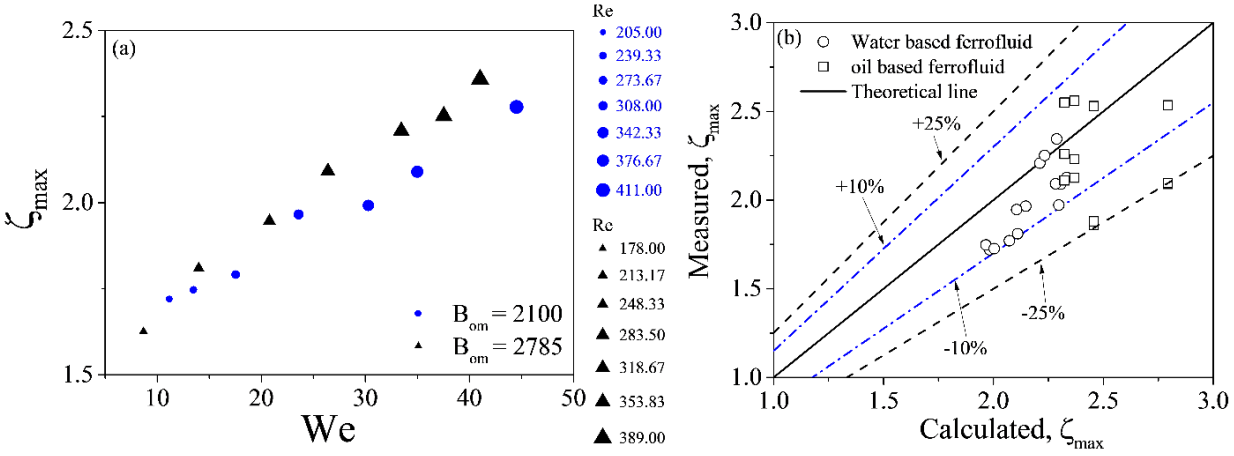

Figure 3-9. Comparison between theoretical prediction and experimental observations.(a) Experimental observation of We vs ξ_{max} for varying Re and B_{om}. The area of the circles and triangles are the representative of the magnitude of Re. (b) Comparison of the calculated maximum spread for both water based ferrofluid and oil based ferrofluid using the model in equation 20 with the experimental data in this study. For water based and oil based ferrofluid the ranges of considered magnetic Bond number is 0 ~ 2200 and 0~200 respectively.

Finally, we would like to compare all experimental results with our presented theoretical model. In Figure 3-9 (a), the combined message of the analysis is presented for the variation of ξ_{max} with respect to *We, Re* and B_{om}. It is evident from Figure 3-9(a) that ξ_{max} has a proportional relationship with *We, Re* and B_{om} as predicted by the Equation (20). In order to complete the discussion regarding the validation of theory and experiment, we also presented the comparison between experimental measurements and theoretical prediction in Figure 3-9 (b). From Figure 3-9 it can be said that the theory and experiment in case of water based ferrofluid showed better agreement, which is within 10%, than the oil based ferrofluid, which is within 25%. Considering the analysis performed, it is beyond any doubt that the proposed theoretical model can predict the physical nature of the maximum spreading of an impinging ferrofluid droplet under the effect of magnetic field. Additional efforts are warranted to find out the appropriate viscous dissipation term and drop shape factors as function of the magnetic field, which will increase the confidence level of the proposed expression.

3.6 Conclusion

This present study represents the theoretical and experimental investigations on the maximal extension of impinging ferrofluid droplets on a solid hydrophobic surface under the influence of vertically oriented magnetic field. The theoretical model accounts for the presence of inertial and viscous force, surface tension, wettability, and magnetic field where fluids with different magnetic characteristics show unique response with a magnetic field. Through theoretical and experimental investigations, it has been uncovered that the maximum droplet spreading, has proportional relationship with all the corresponding dimensionless number i.e., Weber number (*We*), Reynolds number (*Re*) and magnetic Bond number (B_{om}). Additionally, our drop impact model shows good agreement with the experimental observations with a maximum error of 10% for water based

ferrofluid and 25% for oil based ferrofluid. The study presented here has opened up the possibility to resolve some unanswered issues regarding industrial application like maximizing the drop to drop contact area and adhesion while 3D printing. Furthermore, the theoretical modelling can be extended to model the droplet rebound phenomenon under the effect of magnetic field as well as run the both theoretical and experimental study in the presence of a radial magnetic field, which would be mentioned by our future works or by some other researchers.

References

(1) Joung, Y. S.; Buie, C. R. Aerosol generation by raindrop impact on soil. *Nat. Commun.* **2015**, *6* (May 2014), 6083.

(2) Bergeron, V.; Quéré, D. Water droplets make an impact. *Phys. World* **2001**, *14* (5), 27–31.

(3) Ghodbane, M.; Holman, J. P. Experimental study of spray cooling with Freon-113. *Int. J. Heat Mass Transf.* **1991**, *34* (4–5), 1163–1174.

(4) Gutierrez-Miravete, E.; Lavernia, E. J.; Trapaga, G. M.; Szekely, J.; Grant, N. J. A mathematical model of the spray deposition process. *Metall. Trans. A* **1989**, *20* (1), 71–85.

(5) Visser, C. W.; Pohl, R.; Sun, C.; Römer, G.-W.; in't Veld, B.; Lohse, D. Toward 3D printing of pure metals by laser-induced forward transfer. *Adv. Mater.* **2015**, *27* (27), 4087–4092.

(6) McDonald, A.; Lamontagne, M.; Moreau, C.; Chandra, S. Impact of plasma-sprayed metal particles on hot and cold glass surfaces. *Thin Solid Films* **2006**, *514* (1–2), 212–222.

(7) Derby, B. Inkjet Printing of Functional and Structural Materials: Fluid Property Requirements, Feature Stability, and Resolution. *Annu. Rev. Mater. Res.* **2010**, *40* (1), 395–414.

(8) Martin, G. D.; Hoath, S. D.; Hutchings, I. M. Inkjet printing - the physics of manipulating liquid jets and drops. *J. Phys. Conf. Ser.* **2008**, *105*, 12001.

(9) Perelaer, J.; Smith, P. J.; van den Bosch, E.; van Grootel, S. S. C.; Ketelaars, P. H. J. M.; Schubert, U. S. The Spreading of Inkjet-Printed Droplets with Varying Polymer Molar Mass on a Dry Solid Substrate. *Macromol. Chem. Phys.* **2009**, *210* (6), 495–502.

(10) Laan, N.; De Bruin, K. G.; Bartolo, D.; Josserand, C.; Bonn, D. Maximum diameter of impacting liquid droplets. *Phys. Rev. Appl.* **2014**, *2* (4), 1–7.

(11) Visser, C. W.; Pohl, R.; Sun, C.; Romer, G. W.; Huis In 'T Veld, B.; Lohse, D. Toward 3D Printing of Pure Metals by Laser-Induced Forward Transfer. *Adv. Mater.* **2015**, *27* (27), 4087–4092.

(12) Zenou, M.; Sa'ar, A.; Kotler, Z. Digital laser printing of aluminum micro-structure on thermally sensitive substrates. *J. Phys. D. Appl. Phys.* **2015**, *48* (20), 205303.

(13) Worthington, A. M. A Second Paper on the Forms Assumed by Drops of Liquids Falling Vertically on a Horizontal Plate. *Proc. R. Soc. London* **1876**, *25* (171–178), 498–503.

(14) Pasandideh-fard, M.; Qiao, Y. M.; Chandra, S.; Mostaghimi, J. Capillary effects during droplet impact on a solid surface. *Cit. Phys. Fluids* **1996**, *8*.

(15) Chandra, S.; Avedisian, C. T. On the collision of a droplet with a solid surface. In *Proceedings of the Royal Society of London A: Mathematical, Physical and Engineering Sciences*; 1991; Vol. 432, pp 13–41.

(16) Harlow, F. H.; Shannon, J. P. The splash of a liquid drop. *J. Appl. Phys.* **1967**, *38* (10), 3855–3866.

(17) Tsurutani, K.; Yao, M.; Senda, J.; Fujimoto, H. Numerical analysis of the deformation process of a droplet impinging upon a wall. *JSME Int. journal. Ser. 2, Fluids Eng. heat Transf. power, Combust. Thermophys. Prop.* **1990**, *33* (3), 555–561.

(18) Watanabe, T.; Kuribayashi, I.; Honda, T.; Kanzawa, A. Deformation and solidification of a droplet on a cold substrate. *Chem. Eng. Sci.* **1992**, *47* (12), 3059–3065.

(19) Fukai, J.; Zhao, Z.; Poulikakos, D.; Megaridis, C. M.; Miyatake, O. Modeling of the deformation of a liquid droplet impinging upon a flat surface. *Phys. Fluids A Fluid Dyn.* **1993**, *5* (11), 2588–2599.

(20) Pasandideh-Fard, M.; Mostaghimi, J. *Deformation and solidification of molten particles on a substrate in thermal plasma spraying*; 1994.

(21) Trapaga, G.; Szekely, J. Mathematical modeling of the isothermal impingement of liquid droplets in spraying processes. *Metall. Mater. Trans. B* **1991**, *22* (6), 901–914.

(22) Trapaga, G.; Matthys, E. F.; Valencia, J. J.; Szekely, J. Fluid flow, heat transfer, and solidification of molten metal droplets impinging on substrates: comparison of numerical and experimental results. *Metall. Trans. B* **1992**, *23* (6), 701–718.

(23) Josserand, C.; Thoroddsen, S. T. Drop Impact on a Solid Surface. *Annu. Rev. Fluid Mech.* **2016**, *48* (1), 365–391.

(24) Clanet, C.; Béguin, C.; Richard, D.; Quéré, D. Maximal deformation of an impacting drop. *J. Fluid Mech.* **2004**, *517*, 199–208.

(25) Pasandideh-Fard, M.; Qiao, Y. M.; Chandra, S.; Mostaghimi, J. Capillary effects during droplet impact on a solid surface. *Phys. Fluids* **1996**, *8* (3), 650.

(26) Mao, T.; Kuhn, D. C. S.; Tran, H. Spread and Rebound of Liquid Droplets upon Impact on Flat Surfaces.

(27) Deng, W.; Gomez, A. The role of electric charge in microdroplets impacting on conducting surfaces. **2015**, No. January.

(28) Doel, K. van den. Physically based models for liquid sounds. *ACM Trans. Appl. Percept.* **2005**, *2* (4), 534–546.

(29) Deng, W.; Gomez, A. The role of electric charge in microdroplets impacting on conducting surfaces. *Phys. Fluids* **2010**, *22* (5), 51703.

(30) Ryu, S. U.; Lee, S. Y. Maximum spreading of electrically charged droplets impacting on dielectric substrates. *Int. J. Multiph. Flow* **2009**, *35* (1), 1–7.

(31) Zhang, J.; Han, T.-Y.; Yang, J.-C.; Ni, M.-J. On the spreading of impacting drops under the influence of a vertical magnetic field. *J. Fluid Mech* **2016**, *809*.

(32) Zenou, M.; Sa'Ar, A.; Kotler, Z. Supersonic laser-induced jetting of aluminum micro-droplets. *Appl. Phys. Lett.* **2015**, *106* (18).

(33) Liu, J.; Yap, Y. F.; Nguyen, N.-T. Numerical study of the formation process of ferrofluid droplets. *Cit. Phys. Fluids* **2011**, *23*.

(34) Sliding, slipping and rolling: the sedimentation of a viscous drop down a gently inclined plane. *J. Fluid Mech* **2017**, *512*, 95–131.

(35) Rigoni, C.; Pierno, M.; Mistura, G.; Talbot, D.; Massart, R.; Bacri, J. C.; Abou-Hassan, A. Static Magnetowetting of Ferrofluid Drops. *Langmuir* **2016**.

(36) Mao, T.; Kuhn, D. C. S.; Tran, H. Spread and Rebound of Liquid Droplets upon Impact on

Flat Surfaces. **1997**, *4* (9), 2169–2179.

(37) Ahmed, A.; Fleck, B. A.; Waghmare, P. R. Dynamics of Magnetowetting with ferrofluids. 1–29.

(38) Tee, G. J. G. Tee, "Surface area of ellipsoid segment," Dept. Math., School Math. Inform. Sci., Univ. Auckland, Auckland, New Zealand, **2005**, *1* (4), 1–25.

(39) Rosensweig, R. E. *Ferrohydrodynamics*; 1997; Vol. 1.

(40) Ford, R. E.; Furmidge, C. G. L. Impact and spreading of spray drops on foliar surfaces. *Soc Chem Ind Monogr* **1967**, *25*, 417–432.

(41) Yonemoto, Y.; Kunugi, T. Analytical consideration of liquid droplet impingement on solid surfaces. *Sci. Rep.* **2017**, *7*.

(42) Huang, Y. C.; Hammitt, F. G.; Yang, W. J. Hydrodynamic Phenomena during High-Speed Collision between Liquid and Rigid Plane. *ASME J. Fluids Eng.* **1973**, 276–294.

(43) Quéré, D. Inertial capillarity. *EPL (Europhysics Lett.)* **1997**, *39* (5), 533.

(44) Shardt, O.; Waghmare, P. R.; Derksen, J. J.; Mitra, S. K. Inertial rise in short capillary tubes. *RSC Adv.* **2014**, *4* (28), 14781–14785.

(45) Smith, M. I.; Bertola, V. Effect of polymer additives on the wetting of impacting droplets. *Phys. Rev. Lett.* **2010**, *104* (15), 1–4.

(46) Shen, Y.; Liu, S.; Zhu, C.; Tao, J.; Chen, Z.; Tao, H.; Pan, L.; Wang, G.; Wang, T. Bouncing dynamics of impact droplets on the convex superhydrophobic surfaces. *Appl. Phys. Lett.* **2017**, *110* (22), 221601.

(47) Šikalo, Š.; Tropea, C.; Marengo, M.; Ganić, E. N. Spreading of droplets on horizontal surfaces. In *New and Renewable Technologies for Sustainable Development*; Springer, 2002; pp 683–692.

(48) Comeau, D.; LaTourette, K.; Pate, J. The effect of Weber number and spread factor of a water droplet impinging on a super-hydrophobic substrate. *Appl. Math.* **2007**.

(49) Gu, Y.; Li, D. Liquid drop spreading on solid surfaces at low impact speeds. **2000**, *163*, 239–245.

(50) Timonen, J. V. I.; Latikka, M.; Leibler, L.; Ras, Robin H A; Ikkala, O. Switchable Static and Dynamic Self-Assembly of Magnetic Droplets on Superhydrophobic Surfaces. *Science (80-.).* **2009**, *325* (5939), 419–422.

(51) Manukyan, S.; Schneider, M. Experimental investigation of wetting with magnetic fluids. *Langmuir* **2016**, *32* (20), 5135–5140.

(52) Torres-D'iaz, I.; Rinaldi, C. Recent progress in ferrofluids research: novel applications of magnetically controllable and tunable fluids. *Soft Matter* **2014**, *10* (43), 8584–8602.

4 Concluding Remarks and Future Recommendations

4.1 Overview and Summary

The present thesis addressed some important questions pertaining to the impact dynamics of ferrofluid droplets under the effect of magnetic field and its application in 3D printing. For the sake of resolution of those addressing question we pursued following investigation:

- Transient variations in the morphological evolution of ferrofluid droplet spreading under the influence of magnetic field
- Comparison of spreading dynamics of ferrofluid droplet under the effect of both vertically oriented magnetic and radially oriented magnetic field
- Effect of magnetic field strength and its direction on the satellite droplet formation during the drop deposition and the trajectory of satellite drops in the process of attaining equilibrium destination
- A generalized theoretical model for the maximum spreading of an impinging ferrofluid droplet under the effect of magnetic field.
- Validation of proposed theoretical models with the experimental observations

From our analysis, it is evident that due to the distinctive magnetic behavior of ferrofluid the maximum spreading of diamagnetic water based ferrofluid is larger than the paramagnetic oil based ferrofluid. The orientation of the magnetic field and the magnetic properties of the ferrofluids decide whether the droplet shape before the impact will be a prolate ellipsoid or an

oblate ellipsoid. The typical spherical cap shape of the droplet cannot be observed under magnetic field of comparatively higher strength as the magnetic Bond number dictates the whole drop generation, deposition and spreading dynamics. In the process of detailed experimental study, a new phenomenological observation was noticed where the ratio of the drop shape parameters before an impact and after the impact remains constant regardless of the magnetic field strength and orientation. Careful analysis has been presented on the droplet breakup while the drop deposition takes place in particularly the satellite droplet formation in the presence of differently oriented magnetic fields. We discovered that for a certain critical vertical magnetic field, the satellite droplet merges with the deposited primary droplet, significantly alters the volume of deposited volume and profile contour of the drop; whereas for radial magnetic field the satellite droplet always retracted back to the needle. From the theoretical modelling and experimental observations, it is ensured that maximum spreading of a ferrofluid droplet maintains a proportional relationship with the Weber number, Reynolds number and magnetic Bond number, irrespective of magnetic nature of the fluid. All the experimental and theoretical studies presented here opens up the possibility of using ferrofluid as a potential working substance for metal 3D printing manufacturing process. In addition to this, the research outcomes will also help us to resolve some unanswered technical difficulties in in 3D printing with magnetic fluid where the manipulation of the primary droplet and elimination of the satellite droplet is desired in the droplet delivery process.

4.2 Future Works

4.2.1 Droplet Coalescence

Droplet coalescence refers to the phenomenon when two droplets merge with each other where mass transfers through a liquid bridge between two drops, which further evolve into a single drop. Droplet coalescence has been studied for several droplet configurations. Bradley and Stow[1] in their

classical work first showed a comprehensive experimental study on the coalescence of two water droplets of different sizes during free fall. Eggers[2] showed the mechanics of coalescence of two heated metal droplets dominated by surface diffusion. Eggers, Lister and Stone[3] investigated the surface tension driven coalescence of two spherical drops through both numerical and experimental analysis. Sprittles et al.[4] and Paulsen et al.[5] also discussed about the merging of two pendant droplets where two drops first touch and then merge, as the liquid neck connecting them grows from initially microscopic scales to a size comparable to the drop diameters. However, the merging of two sessile droplets is of greater importance for our study as it is one of the crucial stages for the 3D printing. Sessile droplets usually merge immediately after the contact due to the capillary driven force. Interestingly, Reigler et al.[6] also found that fusion of sessile droplets might be delayed by many seconds if the two merging droplets are of different in nature.. However, a very brief explanation of this phenomenon was given by Maxwell more than a century ago[6] . Karpitschka et al.[7] investigated the coalescence behavior of different but miscible sessile droplet and suggested two clearly different regimes for the coalescence behavior: a delayed and a fast regime. They also found that the transition between the fast and delayed coalescence behavior depends mainly on the differences in the surface tensions of the two droplets where if the difference exceeds ~3 mN/m, delayed coalescence takes place; if it is less, rapid fusion of droplet occurs. This surface tension gradients is known by the popular term named "Marangoni effects". Sánchez et al.[8] showed the contact angle dictates the symmetry and asymmetry of coalescence dynamics of two sessile droplets. However, in 3D printing it is also important to know the coalescence behavior of a droplet on a pool of liquids. Charles and Mason comprehensively studied the drop interface coalescence phenomenon, which includes the effects of density, surface tension, viscosity and surface charge on droplet merging. The total process droplet coalescence can be explained in

several stages namely; residence time, time of coalescence, rupture of the film and the ratio of secondary drop to the primary drop. For many chemical processing and manufacturing industries, additional efforts are being exerted to either prevent or promote the coalescence of drops with each other or at interfaces. One of the most important external forces that is used frequently in chemical processing is a result of the electric field. Brown and Hanson[9] first studied the effect of oscillating electric fields on coalescence where they showed that increasing the electric field strength has the effect of decreasing the number and life-times of these secondary drops and at some critical field strength, coalescence becomes instantaneous and single-staged. Through electro coalescence the full engulfment can be prevented by enforcing partial coalescence instead as well as the coalescence of two drops can also completely prevented when it is not warranted[10]. In addition, by increasing the electric field strength, the residence time of coalescence decreases [11] and the size of this secondary drop increases [12]. However, to our best knowledge only a few literatures explains about the effect of magnetic field on the coalescence of two or more magnetic liquid droplets. Ghaffari et al.[13] performed a CFD simulation to explain the equilibrium shape and coalescence of ferrofluid droplets subjected to uniform magnetic field. Sander et al.[14] demonstrated the magnetically triggered coalescence of double emulsion nanoliter droplets in a microfluidic channel. Varma et al.[15] studied the ferrofluid droplet merging on a lab on a chip platform by uniform magnetic field. However, a numerous number of unanswered questions related to coalescing of droplets under the effect of magnetic field are yet to be discussed.

Therefore, as a future work we recommended the investigation of various techniques related to coalescence behavior of sessile and pendant ferrofluid droplet under the effect of magnetic field. So far, we have studied the effect of vertically oriented magnetic field on the coalescence behavior of two oil based ferrofluid droplet. We showed a very brief but significant experimental

observation of pendant drop coalescence and sessile droplet coalescence under the vertical magnetic field. The ultimate aim of the presented experimental study is to lay the foundation of the future work which is continuation of the study performed in Chapters two and three.

4.2.2 Pendant Drop Coalescence

In pendant drop coalescence one pendant droplet from the needle is merged with already deposited sessile droplet. This type of coalescence technique is of great importance for 3D printing of column like structure. Figure 4-1 represents the sequences of snapshots of pendent drop coalescence behavior of oil-based ferrofluid. From temporal snapshots t it can be seen that in the absence of magnetic field typical coalescence behavior is observed i.e., at the beginning the two merging droplet create a singularity at their point of contact followed by gradual bridge formation between them and eventually two drops merged into a single sessile droplet.

Without any magnetic field, we manually brought the pendant droplet in the vicinity of the liquid-air interface of the sessile droplet so that the coalescence of a pendent drop with sessile drop can be observed. The coalescence triggers as soon as the contact is obtained without any delay as observed in numerous cases for pendant drop coalescence in the literature. Immediately after the point contact a rapture in the liquid film resulting in a gradual formation of a liquid bridge connecting the two droplets. However, in the presence of vertical magnetic we could observe a different coalescing scenario, for example at 76.7 mT, as shown in Figure 4-1, it can be seen that the pendant drop is elongated due to the magnetization that lead to mass transfer without any significant spreading in the sessile drop. During the coalescence, the most of the mas transfer takes

place through the bridge hence the bridge thickness is uniform without marginal necking near to the sessile drop. However, in magnetic field the coalescence process is accompanied by the

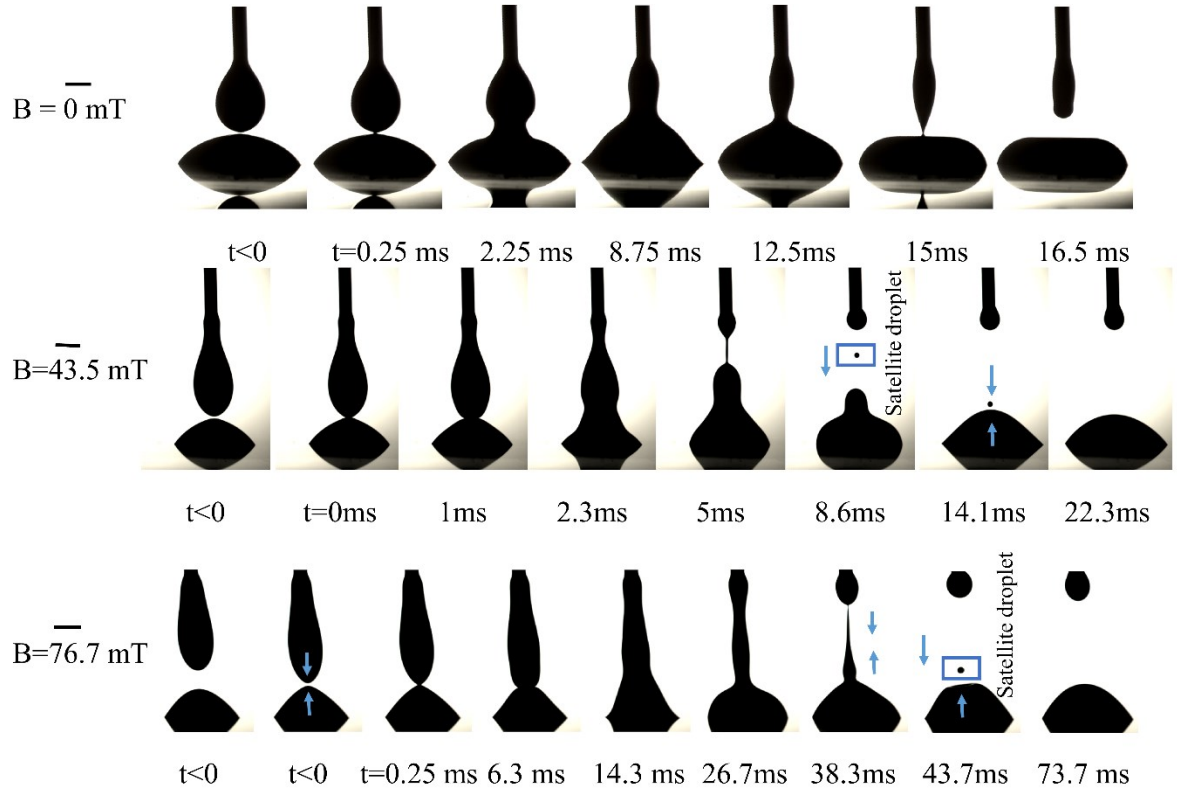

Figure 4-1. Coalescence of pendent oil based ferrofluid droplet with a sessile ferrofluid droplet under the effect of magnetic field. The blue arrow signs indicate the movement of liquid film directions whereas the small droplet inside the rectangular box is the satellite droplet formed due to the effect of magnetic field. The small bar presented at the left most of each sets of figures denotes 1mm.

formation of satellite droplet as seen form Figure 4-1 It is to be noted that the pendant droplet coalescence with sessile droplet was delayed with the increase of vertical magnetic field and the quantified delayed time is reported in Figure 4-2.

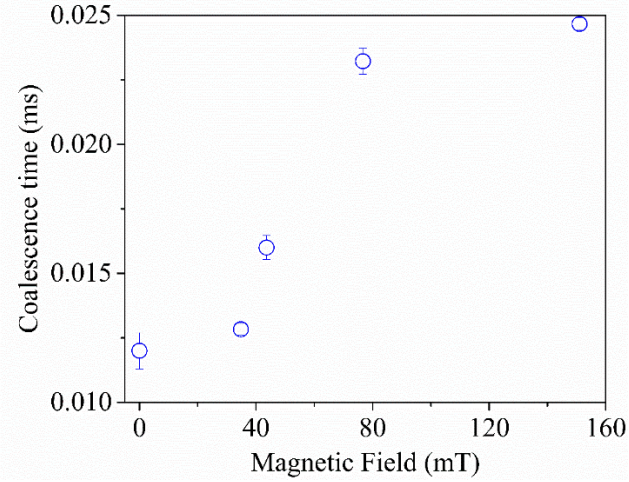

Figure 4-2. Coalescence behavior of oil based ferrofluid droplets under the effect of vertical magnetic field. Here horizontal axis represents magnetic field strength whereas the vertical axis is the representation of the span of coalescence time.

4.2.3 Sessile Drop Coalescence

Another interesting aspect of the future work is to study the coalescence between two sessile drops which is a common phenomenon that one can observe in 3-D printing process. Coalescence of oil based sessile ferrofluid droplet under the effect of vertical magnetic field is presented as one of the case studies. Figure *4-3* demonstrates the coalescence behavior of two sessile oil based ferrofluid droplet under the effect of vertical magnetic field through temporal snapshots captured at different magnetic field strengths. Two sessile droplets were deposited on a solid tempered glass substrate in the absence of magnetic field. There was no movement of either of the droplets until the magnetic field was applied. At 48.8 mT, the droplet 1, as indicated by the left most snapshot of the Figure 4-3, gets actuated by extending its height along the vertical magnetic direction. At 68.5 mT the droplet 1 started attracting droplet 2 due to which the droplet 2 was sliding towards the droplet 1 and as a result two droplets made a point contact with each other. When the magnetic field was further increased to 85.8 mT the bridge formation was triggered and even further increase, i.e., at

107.6 mT the droplet 2 pushed the droplet 1 whereas the coalescence followed by a zigzag pattern was observed at 151 mT. It is noteworthy to mention that at 265.72 mT the two coalescing drops looked like a mountain shape and at this condition the coalescence is at halt as beyond this magnetic field the droplet break up takes place. However, after removing or reducing the magnetic field strength, interestingly, the two droplets completely merged with each other by forming single sessile ferrofluid droplet. It is evident that the optimization of magnetic field is paramount to obtain the efficient coalescence and we strongly recommend a oscillatory magnetic field strength to merge two sessile oil based ferrofluid droplet for an effective mass transfer.

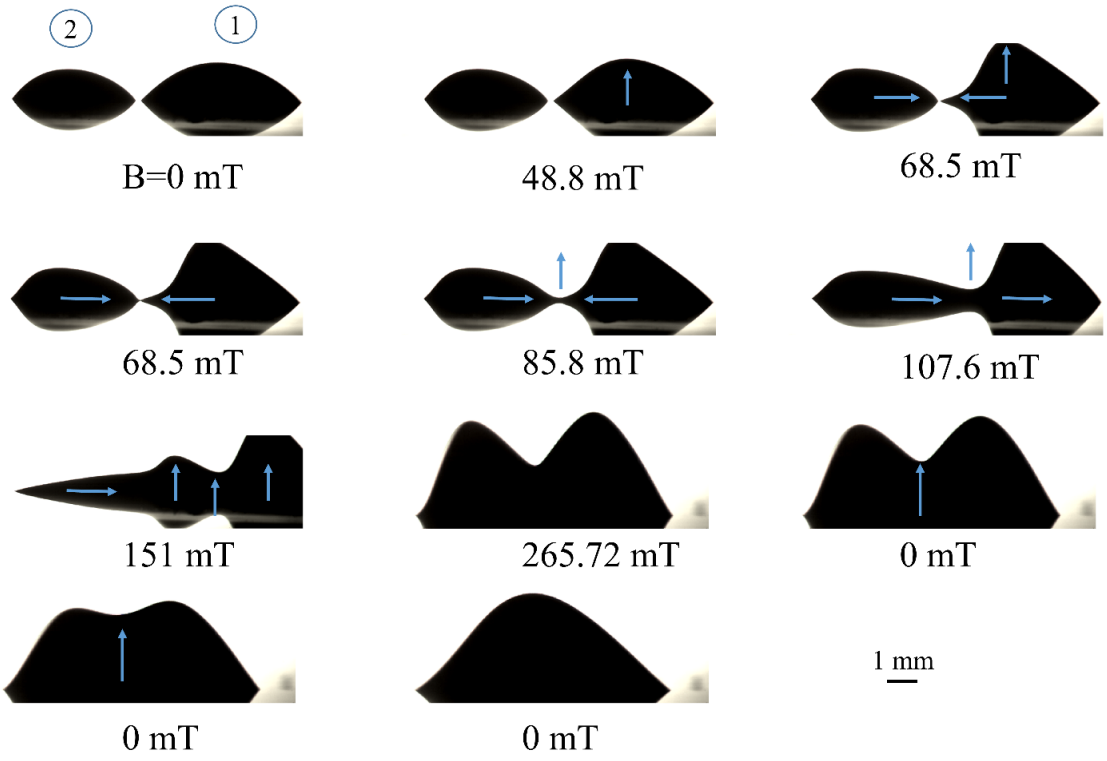

Figure 4-3. Droplet merging phenomenon for two sessile droplets of oil based ferrofluid under the effect of vertical magnetic field. The arrow signs indicate the direction of motion of the corresponding liquid film.

In addition to presented studies, a detailed quantified analysis can be performed in conjunction with the effect of vertical, radial magnetic field on the both oil based, and water based sessile ferrofluid droplet. It would also be interesting to observe the effect of oscillating magnetic force on the droplet coalescence dynamics as well as merging of two or more levitated magnetic fluid droplets, which will be continued as part of the future work.

References

(1) Bradley, S. G.; Stow, C. D. Collisions between liquid drops. Philos. Trans. R. Soc. London A Math. Phys. Eng. Sci. **1978**, 287 (1349), 635–675.

(2) Eggers, J. Coalescence of spheres by surface diffusion. Phys. Rev. Lett. **1998**, 80 (12), 2634.

(3) EGGERS, J.; LISTER, J. R.; STONE, H. A. Coalescence of liquid drops. J. Fluid Mech. **1999**, 401, 293–310.

(4) Sprittles, J. E.; Shikhmurzaev, Y. D. A parametric study of the coalescence of liquid drops in a viscous gas. J. Fluid Mech. **2014**, 753, 279–306.

(5) Paulsen, J. D.; Burton, J. C.; Nagel, S. R.; Appathurai, S.; Harris, M. T.; Basaran, O. A. The inexorable resistance of inertia determines the initial regime of drop coalescence. Proc. Natl. Acad. Sci. **2012**, 109 (18), 6857–6861.

(6) Riegler, H.; Lazar, P. Delayed coalescence behavior of droplets with completely miscible liquids. Langmuir **2008**, 24 (13), 6395–6398.

(7) Karpitschka, S.; Riegler, H. Quantitative experimental study on the transition between fast and delayed coalescence of sessile droplets with different but completely miscible liquids. Langmuir **2010**, 26 (14), 11823–11829.

(8) Hernández-Sánchez, J. F.; Lubbers, L. A.; Eddi, A.; Snoeijer, J. H. Symmetric and asymmetric coalescence of drops on a substrate. Phys. Rev. Lett. **2012**, 109 (18), 184502.

(9) Brown, A. H.; Hanson, C. The effect of oscillating electric fields on the coalescence of liquid drops. Chem. Eng. Sci. **1968**, 23 (8), 841–848.

(10) Brandenberger, H.; Nüssli, D.; Piech, V.; Widmer, F. Monodisperse particle production: A method to prevent drop coalescence using electrostatic forces. J. Electrostat. **1999**, 45 (3), 227–238.

(11) Eow, J. S.; Ghadiri, M.; Sharif, A. O.; Williams, T. J. Electrostatic enhancement of coalescence of water droplets in oil: a review of the current understanding. Chem. Eng. J. **2001**, 84 (3), 173–192.

(12) Aryafar, H.; Kavehpour, P. Electrocoalescence. Phys. Fluids **2007**, 19 (9), 91107.

(13) Ghaffari, A.; Hashemabadi, S. H.; Bazmi, M. CFD simulation of equilibrium shape and coalescence of ferrofluid droplets subjected to uniform magnetic field. Colloids Surfaces A Physicochem. Eng. Asp. **2015**, 481, 186–198.

(14) Sander, J. S.; Erb, R. M.; Denier, C.; Studart, A. R. Magnetic transport, mixing and release of cargo with tailored nanoliter droplets. Adv. Mater. **2012**, 24 (19), 2582–2587.

(15) Varma, V. B.; Ray, A.; Wang, Z. M.; Wang, Z. P.; Ramanujan, R. V. Droplet Merging on a Lab-on-a- Chip Platform by Uniform Magnetic Fields. Nat. Publ. Gr. **2016**.

Bibliography

Afkhami, S.; Tyler, A. J.; Renardy, Y.; Renardy, M.; St. Pierre, T. G.; Woodward, R. C.; Riffle, J. S. Deformation of a hydrophobic ferrofluid droplet suspended in a viscous medium under uniform magnetic fields. J. Fluid Mech. 2010, 663, 358–384.

Ahmed, A.; Fleck, B. A.; Waghmare, P. R. Dynamics of Magnetowetting with ferrofluids. 1–29, (To be submitted in Langmuir)

Alexiou, C.; Schmid, R.; Jurgons, R.; Bergemann, C. Targeted Tumor Therapy with " Magnetic Drug Targeting ": Therapeutic Efficacy of Ferrofluid Bound Mitoxantrone. Lect. Notes Phys. 2002, 594, 233–251.

Antkowiak, A.; Audoly, B.; Josserand, C.; Neukirch, S.; Rivetti, M. Instant fabrication and selection of folded structures using drop impact. Proc. Natl. Acad. Sci. 2011, 108 (26), 10400–10404.

Aryafar, H.; Kavehpour, P. Electrocoalescence. Phys. Fluids 2007, 19 (9), 91107.

Bartolo, D.; Bouamrirene, F.; Verneuil, E.; Buguin, A.; Silberzan, P.; Moulinet, S. Bouncing or sticky droplets: Impalement transitions on superhydrophobic micropatterned surfaces. EPL (Europhysics Lett. 2006, 74 (2), 299.

Bergeron, V.; Quéré, D. Water droplets make an impact. Phys. World 2001, 14 (5), 27–31.

Berthier, J.; Brakke, K. A. The Physics of Microdroplets, 1st ed.; Scrivener Publishing, 2012.

Bird, J. C.; Mandre, S.; Stone, H. A. Short-time dynamics of partial wetting. Phys. Rev. Lett. 2008, 100 (23), 234501.

Bradley, S. G.; Stow, C. D. Collisions between liquid drops. Philos. Trans. R. Soc. London A Math. Phys. Eng. Sci. 1978, 287 (1349), 635–675.

Brandenberger, H.; Nüssli, D.; Piech, V.; Widmer, F. Monodisperse particle production: A method to prevent drop coalescence using electrostatic forces. J. Electrostat. 1999, 45 (3), 227–238.

Brown, A. H.; Hanson, C. The effect of oscillating electric fields on the coalescence of liquid drops. Chem. Eng. Sci. 1968, 23 (8), 841–848.

Caviezel, D.; Narayanan, C.; Lakehal, D. Adherence and bouncing of liquid droplets impacting on dry surfaces. Microfluid. Nanofluidics 2008, 5 (4), 469–478.

Chandra, S.; Avedisian, C. T. On the collision of a droplet with a solid surface. In Proceedings of the Royal Society of London A: Mathematical, Physical and Engineering Sciences; 1991; Vol. 432, pp 13–41.

Charles, S. W. Ferrofluids Magnetically Controllable Fluids and Their Applications. Ferrofluids - Magnetically Controllable Fluids and Their Applications. 2002, pp 3–18.

Chen, C. Y.; Cheng, Z. Y. An experimental study on Rosensweig instability of a ferrofluid droplet. Phys. Fluids 2008, 20 (5).

Clanet, C.; Béguin, C.; Richard, D.; Quéré, D. Maximal deformation of an impacting drop. J. Fluid Mech. 2004, 517, 199–208.

Comeau, D.; LaTourette, K.; Pate, J. The effect of Weber number and spread factor of a water droplet impinging on a super-hydrophobic substrate. Appl. Math. 2007.

De Gennes, P. G. Wetting: Statics and dynamics. Rev. Mod. Phys. 1985.

Deng, W.; Gomez, A. The role of electric charge in microdroplets impacting on conducting surfaces. Phys. Fluids 2010, 22 (5), 51703.

Derby, B. Inkjet Printing of Functional and Structural Materials: Fluid Property Requirements, Feature Stability, and Resolution. Annu. Rev. Mater. Res. 2010, 40 (1), 395–414.

Ding, Z.; Wei, P.; Chitnis, G.; Ziaie, B. Ferrofluid-impregnated paper actuators. J. Microelectromechanical Syst. 2011, 20 (1), 59–64.

Doel, K. van den. Physically based models for liquid sounds. ACM Trans. Appl. Percept. 2005, 2 (4), 534–546.

Egatz-Gómez, A.; Melle, S.; García, A. A.; Lindsay, S. A.; MárquezP Domínguez-García, M.; RubioS T Picraux, M. A.; Taraci, J. L.; Clement, T.; YangMark Hayes, D. A.; Gust, D.; et al. Discrete magnetic microfluidics. Cit. Appl. Phys. Lett 2006, 89 (34106).

Eggers, J. Coalescence of spheres by surface diffusion. Phys. Rev. Lett. 1998, 80 (12), 2634.

EGGERS, J.; LISTER, J. R.; STONE, H. A. Coalescence of liquid drops. J. Fluid Mech. 1999, 401, 293–310.

Eow, J. S.; Ghadiri, M.; Sharif, A. O.; Williams, T. J. Electrostatic enhancement of coalescence of water droplets in oil: a review of the current understanding. Chem. Eng. J. 2001, 84 (3), 173–192.

Ford, R. E.; Furmidge, C. G. L. Impact and spreading of spray drops on foliar surfaces. Soc Chem Ind Monogr 1967, 25, 417–432.

Fukai, J.; Zhao, Z.; Poulikakos, D.; Megaridis, C. M.; Miyatake, O. Modeling of the deformation of a liquid droplet impinging upon a flat surface. Phys. Fluids A Fluid Dyn. 1993, 5 (11), 2588–2599.

Ghaffari, A.; Hashemabadi, S. H.; Bazmi, M. CFD simulation of equilibrium shape and coalescence of ferrofluid droplets subjected to uniform magnetic field. Colloids Surfaces A Physicochem. Eng. Asp. 2015, 481, 186–198.

Ghodbane, M.; Holman, J. P. Experimental study of spray cooling with Freon-113. Int. J. Heat Mass Transf. 1991, 34 (4–5), 1163–1174.

Gu, Y.; Li, D. Liquid drop spreading on solid surfaces at low impact speeds. 2000, 163, 239–245.

Gutierrez-Miravete, E.; Lavernia, E. J.; Trapaga, G. M.; Szekely, J.; Grant, N. J. A mathematical model of the spray deposition process. Metall. Trans. A 1989, 20 (1), 71–85.

Han-dan, L.; Wei, X.; Shi-gang, W.; Zun-ji, K. Hydrodynamic modeling of ferrofluid flow in magnetic targeting drug delivery. Appl. Math. Mech. 2008, 29 (10), 1341–1349.

Harlow, F. H.; Shannon, J. P. The splash of a liquid drop. J. Appl. Phys. 1967, 38 (10), 3855–3866.

Hernández-Sánchez, J. F.; Lubbers, L. A.; Eddi, A.; Snoeijer, J. H. Symmetric and asymmetric coalescence of drops on a substrate. Phys. Rev. Lett. 2012, 109 (18), 184502.

Huang, Y. C.; Hammitt, F. G.; Yang, W. J. Hydrodynamic Phenomena during High-Speed Collision between Liquid and Rigid Plane. ASME J. Fluids Eng. 1973, 276–294.

Huang, Y. C.; Hammitt, F. G.; Yang, W. J. Hydrodynamic Phenomena during High-Speed Collision between Liquid and Rigid Plane. ASME J. Fluids Eng. 1973, 276–294.

Inkpen, S. L.; Melcher, J. R. Dominant mechanisms for color differences in the mechanical and the electrostatic spraying of metallic paints. Ind. Eng. Chem. Res. 1987, 26 (8), 1645–1653.

Ji, H.; Pu, S.; Wang, X.; Yu, G.; Wang, N.; Wang, H. Magnetic field sensing based on capillary filled with magnetic fluids. Appl. Opt. 2012, 51 (27), 6528–6538.

Jiang, X. F.; Wu, Y. N.; Ma, Y.; Li, H. Z. Formation and breakup dynamics of ferrofluid drops. Chem. Eng. Res. Des. 2016, 115, 262–269.

Josserand, C.; Thoroddsen, S. T. Drop Impact on a Solid Surface. Annu. Rev. Fluid Mech. 2016, 48 (1), 365–391.

Joung, Y. S.; Buie, C. R. Aerosol generation by raindrop impact on soil. Nat. Commun. 2015, 6 (May 2014), 6083.

Karpitschka, S.; Riegler, H. Quantitative experimental study on the transition between fast and delayed coalescence of sessile droplets with different but completely miscible liquids. Langmuir 2010, 26 (14), 11823–11829.

Katsikis, G.; Cybulski, J. S.; Prakash, M. Synchronous universal droplet logic and control. Nat. Phys. 2015, 11 (7), 588–596.

Khushrushahi, S.; Zahn, M.; Hatton, T. A. Magnetic separation method for oil spill cleanup. Magnetohydrodyn. 2013, 49.

Korlie, M. S.; Mukherjee, A.; Nita, B. G.; Stevens, J. G.; Trubatch, A. D.; Yecko, P. Modeling bubbles and droplets in magnetic fluids. J. Phys. Condens. Matter 2008, 20 (20), 204143.

Korovin, V. M. On the influence of a horizontal magnetic field on the Rosensweig instability of a nonlinear magnetizable ferrofluid. Tech. Phys. 2014, 59 (11), 1577–1584.

Krishnan, K. M. Fundamentals and applications of magnetic materials; Oxford University Press, 2016.

Kwon, D. H.; Huh, H. K.; Lee, S. J. Wetting state and maximum spreading factor of microdroplets impacting on superhydrophobic textured surfaces with anisotropic arrays of pillars. Exp. Fluids 2013, 54 (7), 1576.

Laan, N.; De Bruin, K. G.; Bartolo, D.; Josserand, C.; Bonn, D. Maximum diameter of impacting liquid droplets. Phys. Rev. Appl. 2014, 2 (4), 1–7.

Li, R. Droplet deposition in solid ink printing; University of Toronto, 2008.

Liu, J.; Yap, Y. F.; Nguyen, N.-T. Numerical study of the formation process of ferrofluid droplets. Cit. Phys. Fluids 2011, 23.

Lübbe, A. S.; Bergemann, C.; Riess, H.; Lãbbe, A. S.; Schriever, F.; Reichardt, P.; Possinger, K.; Matthias, M.; Dã, B.; Herrinann, F.; et al. Clinical Experiences with Magnetic Drug Targeting: A Phase I Study with 4′-Epidoxorubicin in 14 Patients with Advanced Solid Tumors in 14 Patients with Advanced Solid Tumors. Cancer Res. 1996, 56, 4686–4693.

Mahendran, V.; Philip, J. An optical technique for fast and ultrasensitive detection of ammonia using magnetic nanofluids. Appl. Phys. Lett. 2013, 102 (6), 63107.

Maitra, T.; Tiwari, M. K.; Antonini, C.; Schoch, P.; Jung, S.; Eberle, P.; Poulikakos, D. On the nanoengineering of superhydrophobic and impalement resistant surface textures below the freezing temperature. Nano Lett. 2013, 14 (1), 172–182.

Manukyan, S.; Schneider, M. Experimental investigation of wetting with magnetic fluids. Langmuir 2016, 32 (20), 5135–5140.

Mao, T.; Kuhn, D. C. S.; Tran, H. Spread and Rebound of Liquid Droplets upon Impact on Flat Surfaces.

Martin, G. D.; Hoath, S. D.; Hutchings, I. M. Inkjet printing - the physics of manipulating liquid jets and drops. J. Phys. Conf. Ser. 2008, 105, 12001.

McDonald, A.; Lamontagne, M.; Moreau, C.; Chandra, S. Impact of plasma-sprayed metal particles on hot and cold glass surfaces. Thin Solid Films 2006, 514 (1–2), 212–222.

Nair, S. S.; Rajesh, S.; Abraham, V. S.; Anantharaman, M. R. Ferrofluid thin films as optical gaussmeters proposed for field and magnetic moment sensing. Bull. Mater. Sci. 2011, 34 (2), 245–249.

Nguyen, N. T.; Ng, K. M.; Huang, X. Manipulation of ferrofluid droplets using planar coils. Appl. Phys. Lett. 2006, 89 (5), 1–4.

Nguyen, N. T.; Zhu, G.; Chua, Y. C.; Phan, V. N.; Tan, S. H. Magnetowetting and sliding motion of a sessile ferrofluid droplet in the presence of a permanent magnet. Langmuir 2010, 26 (15), 12553–12559.

Ochonski, W. The attraction of ferrofluid bearings. Mach. Des. 2005, 77 (21), 96–102.

Odenbach, S. Microgravity experiments on thermomagnetic convection in magnetic fluids. J. Magn. Magn. Mater. 1995, 149 (1–2), 155–157.

Pal, S.; Datta, A.; Sen, S.; Mukhopdhyay, A.; Bandopadhyay, K.; Ganguly, R. Characterization of a ferrofluid-based thermomagnetic pump for microfluidic applications. J. Magn. Magn. Mater. 2011, 323 (21), 2701–2709.

Papell, S. S.; Otto, C. F. J. Influence of nouniform magnetic fields on ferromagnetic colloidal sols. J. Chem. Inf. Model. 1968, 53 (9), 1689–1699.

Pasandideh-Fard, M.; Mostaghimi, J. Deformation and solidification of molten particles on a substrate in thermal plasma spraying; 1994.

Pasandideh-Fard, M.; Qiao, Y. M.; Chandra, S.; Mostaghimi, J. Capillary effects during droplet impact on a solid surface. Phys. Fluids 1996, 8 (3), 650.

Paulsen, J. D.; Burton, J. C.; Nagel, S. R.; Appathurai, S.; Harris, M. T.; Basaran, O. A. The inexorable resistance of inertia determines the initial regime of drop coalescence. Proc. Natl. Acad. Sci. 2012, 109 (18), 6857–6861.

Peregrine, D. H.; Shoker, G.; Symon, A. The bifurcation of liquid bridges. J. Fluid Mech. 1990, 212, 25–39.

Perelaer, J.; Smith, P. J.; van den Bosch, E.; van Grootel, S. S. C.; Ketelaars, P. H. J. M.; Schubert, U. S. The Spreading of Inkjet-Printed Droplets with Varying Polymer Molar Mass on a Dry Solid Substrate. Macromol. Chem. Phys. 2009, 210 (6), 495–502.

Pipper, J.; Inoue, M.; Ng, L. F.-P.; Neuzil, P.; Zhang, Y.; Novak, L. Catching bird flu in a droplet. Nat. Med. 2007, 13 (10), 1259–1263.

Piroird, K.; Clanet, C.; Lorenceau, É.; Quéré, D. Drops impacting inclined fibers. J. Colloid Interface Sci. 2009, 334 (1), 70–74.

Quéré, D. Inertial capillarity, Europhysics Lett. 1997, 39 (5), 533.

Raj, K.; Moskowitz, R. Commercial applications of ferrofluids. J. Magn. Magn. Mater. 1990, 85 (1–3), 233–245.

Renardy, Y.; Popinet, S.; Duchemin, L.; Renardy, M.; Zaleski, S.; Josserand, C.; Drumright-Clarke, M. A.; Richard, D.; Clanet, C.; Quéré, D. Pyramidal and toroidal water drops after impact on a solid surface. J. Fluid Mech. 2003, 484, 69–83.

Riegler, H.; Lazar, P. Delayed coalescence behavior of droplets with completely miscible liquids. Langmuir 2008, 24 (13), 6395–6398.

Rigoni, C.; Pierno, M.; Mistura, G.; Talbot, D.; Massart, R.; Bacri, J. C.; Abou-Hassan, A. Static Magnetowetting of Ferrofluid Drops. Langmuir 2016.

Rosensweig, R. E. Ferrohydrodynamics; 1997; Vol. 1.

Ryu, S. U.; Lee, S. Y. Maximum spreading of electrically charged droplets impacting on dielectric substrates. Int. J. Multiph. Flow 2009, 35 (1), 1–7.

Sander, J. S.; Erb, R. M.; Denier, C.; Studart, A. R. Magnetic transport, mixing and release of cargo with tailored nanoliter droplets. Adv. Mater. 2012, 24 (19), 2582–2587.

Schlaich, J.; Bergermann, R.; Schiel, W.; Weinrebe, G. Design of Commercial Solar Updraft Tower Systems – Utilization of Solar Induced Convective Flows for Power Generation. 49 (711), 1–9.

Shardt, O.; Waghmare, P. R.; Derksen, J. J.; Mitra, S. K. Inertial rise in short capillary tubes. RSC Adv. 2014, 4 (28), 14781–14785.

Shen, Y.; Liu, S.; Zhu, C.; Tao, J.; Chen, Z.; Tao, H.; Pan, L.; Wang, G.; Wang, T. Bouncing dynamics of impact droplets on the convex superhydrophobic surfaces. Appl. Phys. Lett. 2017, 110 (22), 221601.

Šikalo, Š.; Tropea, C.; Marengo, M.; Ganić, E. N. Spreading of droplets on horizontal surfaces. In New and Renewable Technologies for Sustainable Development; Springer, 2002; pp 683–692.

Sliding, slipping and rolling: the sedimentation of a viscous drop down a gently inclined plane. J. Fluid Mech 2017, 512, 95–131.

Smith, M. I.; Bertola, V. Effect of polymer additives on the wetting of impacting droplets. Phys. Rev. Lett. 2010, 104 (15), 1–4.

Speight, J. G. "A Review of Magnetic Fluids Guidebook: Properties and Applications" By VE Fertman Hemisphere Publishing Corporation Bristol, PA 19007-1598 1990, xi+ 146 pp. Fuel Sci. Technol. Int. 1991, 9 (3), 399.

Sprittles, J. E.; Shikhmurzaev, Y. D. A parametric study of the coalescence of liquid drops in a viscous gas. J. Fluid Mech. 2014, 753, 279–306.

Tee, G. J. G. Tee, "Surface area of ellipsoid segment," Dept. Math., School Math. Inform. Sci., Univ. Auckland, Auckland, New Zealand, 2005, 1 (4), 1–25.

Tenneti, S.; Subramanian, S. G.; Chakraborty, M.; Soni, G.; Das Gupta, S. Magnetowetting of Ferrofluidic Thin Liquid Films. Sci. Rep. 2017, 7 (March), 44738.

Timonen, J. V. I.; Latikka, M.; Leibler, L.; Ras, Robin H A; Ikkala, O. Switchable Static and Dynamic Self-Assembly of Magnetic Droplets on Superhydrophobic Surfaces. Science (80-.). 2009, 325 (5939), 419–422.

Tjahjadi, M.; Stone, H. A.; Ottino, J. M. Satellite and sub-satellite formation in capillary breakup. J. Fluid Mech. 1992, 243, 297–317.

Torres-D'iaz, I.; Rinaldi, C. Recent progress in ferrofluids research: novel applications of magnetically controllable and tunable fluids. Soft Matter 2014, 10 (43), 8584–8602.

Trapaga, G.; Matthys, E. F.; Valencia, J. J.; Szekely, J. Fluid flow, heat transfer, and solidification of molten metal droplets impinging on substrates: comparison of numerical and experimental results. Metall. Trans. B 1992, 23 (6), 701–718.

Trapaga, G.; Szekely, J. Mathematical modeling of the isothermal impingement of liquid droplets in spraying processes. Metall. Mater. Trans. B 1991, 22 (6), 901–914.

Tsurutani, K.; Yao, M.; Senda, J.; Fujimoto, H. Numerical analysis of the deformation process of a droplet impinging upon a wall. JSME Int. journal. Ser. 2, Fluids Eng. heat Transf. power, Combust. Thermophys. Prop. 1990, 33 (3), 555–561.

Varma, V. B.; Ray, A.; Wang, Z. M.; Wang, Z. P.; Ramanujan, R. V. Droplet Merging on a Lab-on-a- Chip Platform by Uniform Magnetic Fields. Nat. Publ. Gr. 2016.

Visser, C. W.; Pohl, R.; Sun, C.; Römer, G.-W.; in't Veld, B.; Lohse, D. Toward 3D printing of pure metals by laser-induced forward transfer. Adv. Mater. 2015, 27 (27), 4087–4092.

Watanabe, T.; Kuribayashi, I.; Honda, T.; Kanzawa, A. Deformation and solidification of a droplet on a cold substrate. Chem. Eng. Sci. 1992, 47 (12), 3059–3065.

Watanabe, T.; Kuribayashi, I.; Honda, T.; Kanzawa, A. Deformation and solidification of a droplet on a cold substrate. Chem. Eng. Sci. 1992, 47 (12), 3059–3065.

Worthington, A. M. A Second Paper on the Forms Assumed by Drops of Liquids Falling Vertically on a Horizontal Plate. Proc. R. Soc. London 1876, 25 (171–178), 498–503.

Yonemoto, Y.; Kunugi, T. Analytical consideration of liquid droplet impingement on solid surfaces. Sci. Rep. 2017, 7.

Zenou, M.; Sa'ar, A.; Kotler, Z. Digital laser printing of aluminum micro-structure on thermally sensitive substrates. J. Phys. D. Appl. Phys. 2015, 48 (20), 205303.

Zenou, M.; Sa'Ar, A.; Kotler, Z. Supersonic laser-induced jetting of aluminum micro-droplets. Appl. Phys. Lett. 2015, 106 (18).

Zhang, D. F.; Stone, H. A. Drop formation in viscous flows at a vertical capillary tube. Phys. Fluids 1997, 9 (8), 2234–2242.

Zhang, J.; Han, T.-Y.; Yang, J.-C.; Ni, M.-J. On the spreading of impacting drops under the influence of a vertical magnetic field. J. Fluid Mech 2016, 809.

Zhang, X.; Basaran, O. A. Dynamics of drop formation from a capillary in the presence of an electric field. J. Fluid Mech. 1996, 326, 239–263.

Zhu, G. P.; Nguyen, N. T.; Ramanujan, R. V.; Huang, X. Y. Nonlinear deformation of a ferrofluid droplet in a uniform magnetic field. Langmuir 2011.